Experimental and Nonlinear Finite Element Analysis of Double Skin Beam-Column Joints

Tariq Ali Thaker

Submitted in accordance with the requirements for the degree of
Doctor of Philosophy

The University of Leeds
School of Civil Engineering

The candidate confirms that the work submitted is his own, and that appropriate credit has been given within the thesis where reference has been made to the work of others.

Acknowledgements

I would like to express my appreciation and thanks to my supervisors Professor Philip Purnell, Professor John Forth, and Dr Yong Sheng for their guidance and support throughout the period of the research.

I would like to express my gratitude to the Ministry of Higher Education and to the Iraqi Cultural Attaché for the scholarship and their support.

I would also like to thank Marcia Martell, Peter Flatt, Steve Holmes, Marvin Williams and Robert for providing help and support in the concrete lab, School of Civil Engineering, University of Leeds.

Finally, I am grateful to my parents, my brothers and sisters, my family, and my friends everywhere.

Abstract

The Double Skin Composite (DSC) or Steel-Concrete-Steel (SCS) elements (beams, slabs and columns) have been subjected to intensive studies during the last three decades. Member beam, column and slab have been studied under monotonic, cyclic and fatigue loading, and there are also a few studies on impact loading to assess the structural response of such constructions.

Validating connectivity between the DSC beam and DSC columns is behind the usage of such constructional systems since all the present studies focus on individual members. The main objective of this thesis was to introduce the Double Skin Composite (DSC) beam-column joint as a new structural element. Experimental investigation and Nonlinear Finite Element Modelling (FEM) of the structural behaviour of the DSC joint subjected to monotonic and quasi-static loading was introduced.

Five DSC joints have been tested to assess the efficiency of the DSC beam-column joint in its basic design and to identify the most efficient strengthening method. Further, six DSC beam-column joints were tested to study the effect of steel fibre (SF) and the effect of high-strength concrete (HSC) on the behaviour of the joint under monotonic loading and under cyclic loading.

The general FE Package ABAQUS 6.10 was used to model the nonlinear behaviour of the DSC joint. The Concrete Damage Plasticity Model (CDPM) was used to model the concrete in tension and compression, and the steel elements of the composite were modelled using the elastic-plastic model. The model was validated against the experimental result and showed good agreement in predicting the maximum load and the general behaviour with a deviation of 10% or less.

The examined strengthening methods showed improvement in the ultimate load capacity of between 517% and 871%. SFC and HSC provided the best performance in increasing the ultimate load and moving the location of the plastic hinge away from the face of the column.

The validated FE model was used to conduct a parametric study to investigate the effect of the concrete compressive strength, shear stud connector spacing to steel plate thickness ratio, and the stud diameter to steel plate thickness ratio. The parametric study findings were in good agreement with experimental observations such as that the concrete compressive strength had a significant effect on the joint shear resistance and ultimate load.

Table of Contents

List of Figures

List of Photos

List of Tables

Notations

A_r	Cross-section area of bar reinforcement
A_s	area of shear studs
A_{sc}	area of steel plate in compression
A_{st}	area of steel plate in tension
A_{sw}	area of shear reinforcement in the joint
C_c	Compressive force in the concrete
E_{it}	Initial tangent modulus of elasticity.
E_0	initial stiffness elastic matrix
E_s	Modulus of elasticity of steel
F_c	compression force in the concrete
G_f	fracture energy
I_{cr}	moment of inertia of the cracked section
I_g	Gross moment of inertia
I_{uc}	moment of inertia of the cracked section
K_{sc}	Shear stiffness of compression plate studs
K_{st}	Shear stiffness of tension plate studs
L	length of the beam
L_b	distance to the point of contraflexure in the beam from the column face
L_c	distance between the points of contraflexure in the upper and lower columns
L_f	Length of steel fibres
L_r	Effective bond length of bar reinforcement
$M_{b,ult}$	Ultimate moment capacity
M_b	moment in the beam
M_{col}	moment in the column resisted by concrete at the top and bottom of the beam
$M_{cr,\,c}$	Cracking moment resisted by concrete
N_{cuRd}	Design axial resistance of uncracked concrete
$N_{f,calc}$	Calculated number of cycles
$N'_{f,calc}$	Modified calculated number of cycles

$N_{\sigma B}$	Number of cycles to produce failure at the connection caused by bar tension
$N_{\sigma p}$	Number of cycles to produce tensile failure
$N_{\tau B}$	Number of cycles to produce failure at the connection caused by bar shear
N_t	forces of the tension plate
N_{tRd}	Design axial resistance of tension plate
P_{cRd}	Design shear resistance of compression plate stud connector
P_d	shear strength of the stud connector
P_{Rk}	Characteristic shear resistance of stud connector
P_R	shear resistance of the stud connectors
Q	Longitudinal shear force
Q_u	Ultimate shear strength of shear connector
S_t	Longitudinal spacing of tension plate studs
$M_{cr,\,s}$	Cracking moment resisted by steel
M_{pl}	plastic moment
N	Number of cycles to cause failure
N_c	forces of the compression plate
N_{cRd}	Design axial resistance of compression plate
N_{rRd}	Design axial resistance of bar reinforcement
T_b	Tensile force in the tension reinforcement
T_{syd}	design yield capacity of the joint shear reinforcement
V	vertical shear force
V_c	shear resistance of the concrete core
V_{col}	Shear in the column
V_f	Volume fraction
V_j	Shear in joint
W_{cr}	maximum crack opening displacement
W_f	weight percentage of steel fibres
W_t	crack opening displacement
b	section width
b_e	Effective width of the column
d	Stud diameter

d_a	maximum aggregate size
d_f	Diameter of the fibre
d_b	beam effective depth
d_c	damage in compression
d_t	damage in tension
f_{cm}	Compressive mean
f_i	predefined field variable
f_r	modulus of rupture
f_{rb}	Bond strength of bar reinforcement
f_u	ultimate tensile strength
f_{yB}	yield stress of bar
f_{yP}	yield stress of plate
f_{ysc}	Yield stress of steel compression plate
f_{ysr}	Yield stress of bar reinforcement
f_{yst}	Yield stress of steel tension plate
f_c	concrete compressive strength
f_{ck}	compressive cylinder strength of the concrete
f_{cm}	Mean value of concrete compressive strength
f_{cu}	compressive cube strength
f_s	stress in the steel at cracking
f_t	maximum tensile strength
f_{tu}	residual tensile strength
f_{yd}	design yield stress in the shear reinforcement
h	Column height
h_c	Height of concrete
h_r	Depth of bar reinforcement below compression plate
k_c	Width reduction factors for compression
k_x	Elastic local buckling coefficient in the x direction
k_{x0}	Buckling coefficient in the x direction in the absence of shear stresses
k_{xy0}	Shear buckling coefficient in the absence of biaxial compression
l_f	Length of the fibre
n	Knee factor approximation

n_c	number of stud connectors welded to the top plate
n_t	number of stud connectors welded to the bottom plate
n_o	number of studs across the width
s_x	longitudinal spacing of bar connectors
s_y	transverse spacing of bar connectors
v_j	Stress in the joint
y_t	Distance between the extreme fibre intention to the neutral axis
s	Stud spacing
s_x	Stud spacing in x direction
t	Plate thickness
t_t	Thickness of top plate
$v_{c,ult}$	Ultimate shear capacity
x	neutral axis depth
α_E	modular ratio
β	reduction factor accounts for the effect of the joint
γ	Uniaxial strength factor
γ_{352}	factor depends on the location of the joint
γ_a	Partial material safety factor for steel
γ_c	Partial factor for concrete
γ_v	Partial material safety factor for stud connectors
δ	Longitudinal slip
ε_0	strain at peak stress
$\varepsilon_{c,cr}$	cracking strain of the concrete
ε_{nom}	nominal strain
$\dot{\varepsilon}_t^{\sim pl}$	equivalent plastic strain rate
$\varepsilon_t^{\sim pl}$	equivalent plastic strain
ε_{true}^{pl}	true plastic strain
ξ	Shape factor of strength interaction curves
η	orientation factor to take into account random distribution of fibres in the three dimensions’
θ	Temperature
κ	reduction factor

ρ	Flexural beam reinforcement ratio
ρ_{max}	Maximum flexural beam reinforcement ratio
σ_c	uniaxial compressive stress
σ_{nom}	nominal (measured) stress
σ_s	steel stress calculated using the cracked section
σ_{sr}	steel stress at first crack
σ_t	uniaxial tensile stress
σ_{true}	true stress
σ_x	Applied edge stress in x direction
σ_{xu}	Ultimate strength of plate in biaxial compression in x direction
σ_{xu0}	Ultimate strength of a plate in x direction under biaxial compression only
σ_{yu}	Ultimate strength of plate in biaxial compression in y direction
σ_c	compressive stress
σ_{pf}	compressive strength of fibrous concrete
σ_y	yield stress of the plate
τ_{Rd}	Design shear resistance of concrete
τ_d	bond stress
τ_{uC}	transverse shear resistance of double skin composite beams
τ_{xyu}	Ultimate shear strength of a plate
τ_{xyu0}	Ultimate strength of a plate under pure shear only
ϕ_{cr}	the curvature of the cracked section
ϕ_r	Circumference of bar reinforcement

Abbreviations

AWS	American Welding Society
CDP	Concrete Damage Plasticity
DSC	Double Skin Composite
HSC	High-Strength Concrete
LVDT	Linear Variable Differential Transformer
NC	Normal Concrete
NWC	Normal Weight Concrete
OPC	Ordinary Portland Cement
RC	Reinforced Concrete
SCS	Steel–Concrete–Steel
SF	Steel Fibre
SG	Strain Gauge

Chapter 1 Introduction

1.1 Introduction

The term composite structural elements can imply the use of steel and concrete built together to produce a single unit. The idea behind this is to achieve the best performance relative to the performance of these materials when used separately.

Many aspects have been taken into account when comparing the benefits of composite structures with conventional reinforced concrete and steel structures (Johnson, 2008; Oehlers and Bradford, 2013). These aspects can be classified into two main categories. The first category is the structural behaviour and the second category is the economic considerations. With regard to the former, composite structures can be used in longer spans with smaller cross-section dimensions, as full advantage is taken of each material's strength, i.e. the high tensile strength of steel and the high compressive strength of concrete. The economic view can be summarised as follows:

- Assembly of the composite structures is a rapid process and this will reduce the cost in two ways. The first way is by reducing supervision and management of the project and the second way is by speeding up the completion time, thereby achieving cost benefits earlier.
- Most of the structural parts can be prefabricated.
- Fewer deliveries of materials are needed.
- Because of the small cross-sections, smaller foundations will be needed and hence there will be more room or more storeys as a result.
- Quality control and accuracy will be at the maximum level with less human involvement because of the machinery prefabrication process.
- Services can be installed more easily and faster.
- Sustainability considerations can be addressed through the reuse of steel parts.

Steel-concrete-steel composite construction was first suggested by Solomon et al. (1976) using two plates on the faces of the beam and glued to the concrete core using epoxy. Later, steel-concrete-steel was presented as an

alternative construction system for submerged tube tunnel schemes, with shear connectors to provide the bond between the concrete core and the skin plates (Tomlinson and Tomlinson, 1990).

Steel-concrete-steel primarily consists of a concrete core sandwiched between two steel plates with shear stud connectors welded to the steel plates and embedded in the concrete core, as shown in Figure 1-1(a).

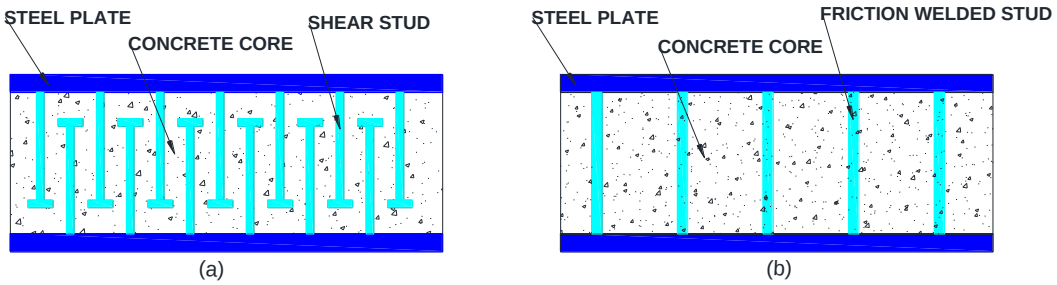

Figure 1-1: (a) Steel-concrete-steel composite construction (b) Bi-Steel

These steel plates serve as a permanent formwork in addition to their main function as reinforcement and can provide waterproofing surfaces in marine structures; moreover, the sandwiched concrete will be protected against spall and severe perforation under dynamic loads. Economic advantages may arise from the elimination of reinforcing detailing, because there is no need for such a process with plates, especially since factory manufacturing is now available for bi-steel. In bi-steel constructions, shear stud connectors are welded simultaneously to both faces using a friction-welding technique (see Figure 1-1(b)). The effects of plate thickness and shear stud connectors' diameter as well as different types of concrete have been subjected to extensive studies, as presented in Chapter two of this thesis. High performance in most of the structural properties has been reported when examining such a system.

The key factor controlling the behaviour of the system is the degree of interaction between the steel skins and the concrete core, which in turn depends upon the efficiency of shear connectors in transferring forces developed during loading. Shear connectors can be divided into two main categories:

- Rigid connectors

- Flexible connectors

Differences between these two types are the stiffness (load-slip behaviour) and failure modes. Rigid connectors cause higher stress concentration and more catastrophic (sudden) failure modes, while the flexible connectors allow for deformation and redistribution of stresses. Considerable types of shear connectors are available for use in composite structures, as is shown in Figure 1-2 (Oehlers and Bradford, 2013).

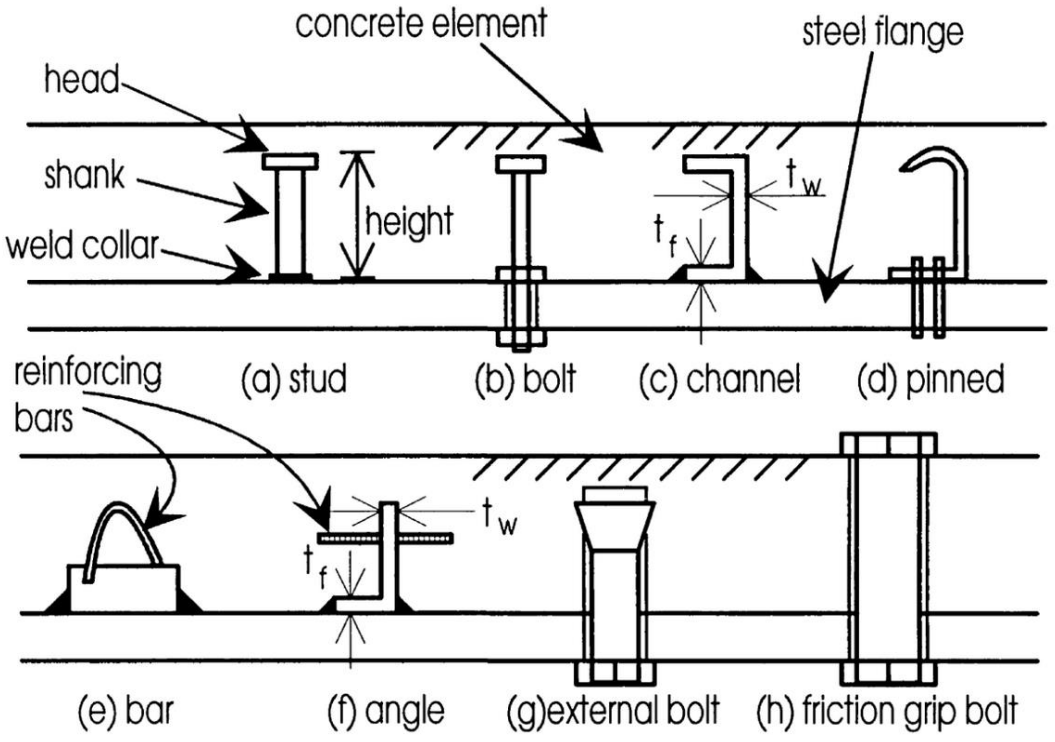

Figure 1-2: Shear connector types used in composite constructions (Oehlers and Bradford, 2013)

In the steel–concrete-steel composite constructions, different types (headed studs, channels, J-hooked, T-channel, etc.) of shear connectors are used and different methods are presented to increase the roughness of the internal face of the skin plates. (See for example Yan et al. (2014) and Figure 1-3 below.)

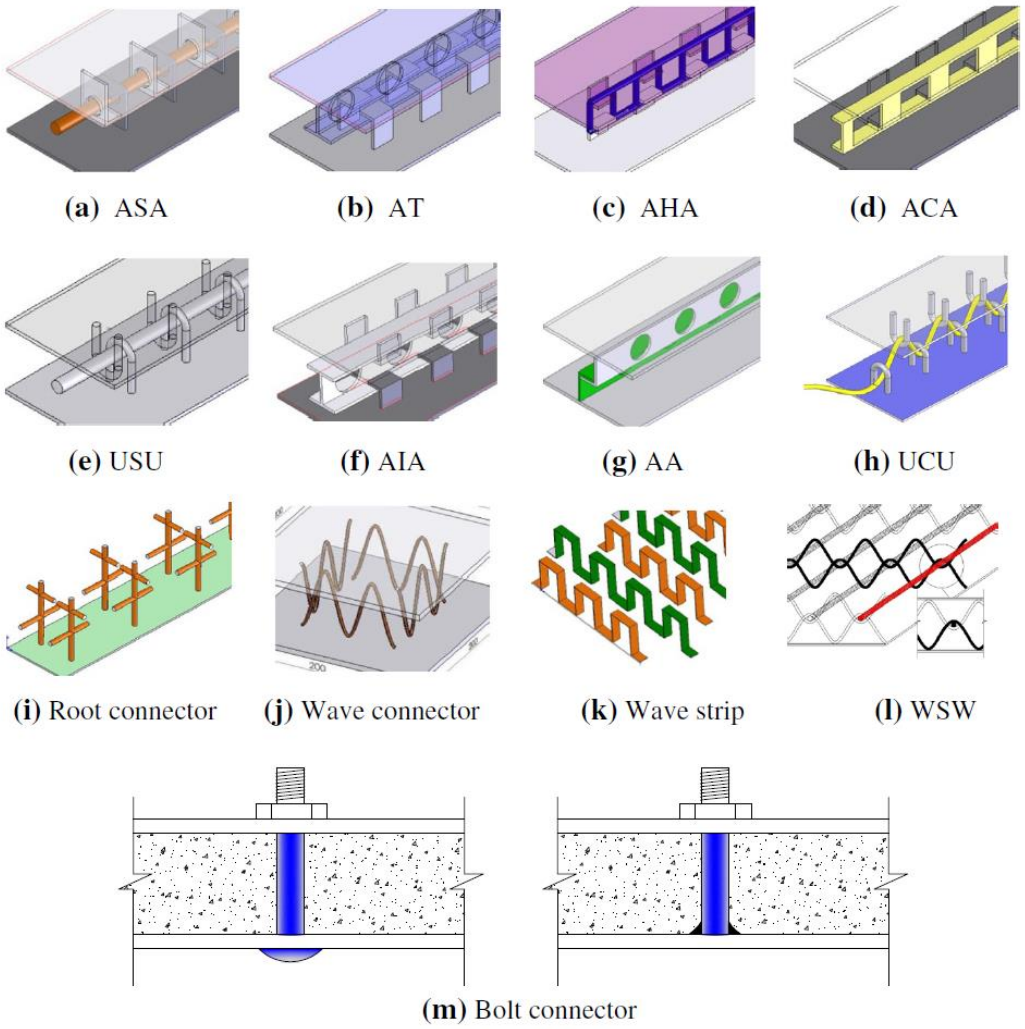

Figure 1-3: Shear connectors used in SCS constructions (Yan et al., 2014)

During the past three decades, many studies have been presented to provide an understanding of the structural performance of double skin flexural members but no attempt has been reported about the double skin beam-column joints. The beam-column joints, to some extent, are considered the most critical part of a structure. The complexity comes from the nature of forces that can be developed in the joint and because it has an essential effect on the overall response of the structure. According to the available previous studies, double skin composite members have shown good structural performance. Therefore, detailed experimental and numerical assessment of double skin beam-column joints is necessary in order to develop design guidelines for practical applications.

This thesis presents the first study of the Steel-Concrete-Steel (SCS) beam-column joints, which can be considered as a foundation for further studies to clearly understand the behaviour of the joints under different loading conditions. An experimental investigation and finite element modelling (using ABAQUS 6.10) of double skin composite beam-column joints is presented in order to examine their suitability and efficiency.

1.2 Examples of Existing Structures

An example of existing structures where the bi-steel has been used successfully is the Highline Bridge at Corus's Scunthorpe steelworks. The deck of the bridge and its piers, which are made of bi-steel panels, form the main parts of the bridge, which is used to carry raw materials to the blast furnaces. The total length of the bridge is 75 m (16 m/span) and it took 11 days to construct (Bowerman et al., 2002). Another key application is the construction of a blast wall for an underground car park (Central London Office Building). The bi-steel walls were 66% thinner than the reinforced concrete walls required to separate the car park from the service region of the structure, as referenced in Bowerman, Coyle and Chapman (2002). Other projects in which bi-steel is used can be found in http://www.tatasteelconstruction.com/.

1.3 Aim and Objectives of the Study

The main aim of the study is to investigate the behaviour of SCS composite beam-column joints under static and quasi-static loads. The objectives are classified under three parts.

Part-1: To produce experimentally the most suitable and efficient double skin composite beam-column joint, which includes the following sub-steps:

- Test a double skin beam-column joint with its basic design, i.e. a concrete core sandwiched between two steel plates using shear connectors to provide the required interaction between the concrete core and the steel skin.
- Modify the basic design in order to reach the most efficient design in terms of strength. Three modifications are made, which are: to add

horizontal and vertical steel bars in the connection, to weld the bar to the top and bottom of the beam plate, and to extend the beam plate to join the column plates.

- To compare the performance and behaviour of the modified beam-column joint based on strength and simplicity of the manufacturing process to be used in part two.

Part-2: This part involves three investigations using the joint chosen in part one: to study the behaviour of the SCS beam-column joint with a steel fibrous concrete core, to investigate the behaviour of the SCS beam-column joint with a high-strength concrete core and to investigate the SCS beam column joints subjected to cyclic loading.

Part-3: To validate a finite element model using the experimental data obtained in parts one and two above. The validated model is used for investigating the effect of concrete compressive strength, the shear stud spacing to steel plate thickness ratio, and the shear stud diameter to steel plate thickness ratio.

1.4 Research Significance

The key research focus is to investigate the possibility of using double skin composite joints as an alternative to conventional reinforced concrete. The new joint is relatively more expensive but has a higher strength relative to ordinary joints. The joint will be assessed for strength relative to the reinforced concrete beam-column joint. This proposed beam-column joint can be produced in a factory which provides better quality control and construction speed. However, further experimental tests are necessary to develop performance-based design guidelines for these proposed beam-column joints.

1.5 Thesis Layout

This thesis consists of eight chapters, as follows:

Chapter one: presents an introduction to composite structures and steel-concrete-steel constructions, examples of the current applications of steel-concrete-steel structures, and the objectives of the study.

Chapter two: contains the literature review on steel-concrete-steel constructions and its importance to the current study.

Chapter three: includes a description of all the materials used in the experimental programme and their properties.

Chapter four: presents a full description and discussion of the experimental tests.

Chapter five: presents the details of the finite element modelling of the steel-concrete-steel composite joints as well as the validation of the model against the experimental test results.

Chapter six: puts forward an analytical solution for the steel-concrete-steel beam-column joint using formulas suggested by others. A comparison between the experimental, analytical and finite element results is also presented.

Chapter seven: presents a parametric study to identify the effect of key factors on the behaviour of the steel-concrete-steel composite joint.

Chapter eight: presents the conclusions drawn from the present study as well as recommendations for future studies.

Chapter 2 Literature Review

2.1 Introduction

Since 1989, a considerable research effort has been made to investigate the behaviour of Steel–Concrete–Steel (SCS), also known as Double Skin Composite (DSC) constructions, which has concentrated on beams. In this section, the main observations from the previous studies will be presented in the following topics:

- Shear Resistance and Stud Connectors
- Fatigue
- Concrete Steel Interaction and Steel Plate Surface
- Modelling
- Failure Modes
- General Behaviour

Before introducing the previously mentioned topics, it is important to explain the components and the technical terms relating to the double skin composite construction, which will help the reader to follow and understand the presented literature.

Figure 2-1 shows the side view of a double skin composite beam that consists of a concrete core sandwiched between two steel plates. The interaction between the concrete and the steel plates, or in other words the composite action, is achieved by using shear connectors. The term long studs refers to studs welded to the plate and which are the right length to touch or to be close enough to the other plate. In the previous studies, all the tested beams and slabs were simply supported, which caused compression stress on the upper face and tension stress on the bottom side; therefore, the compression plate refers to the top plate and the tension plate refers to the bottom plate. Also, it is very common to use the terms top plate connectors and bottom plate connectors, which refer to the shear connectors welded to the top plate and to the bottom plate, respectively.

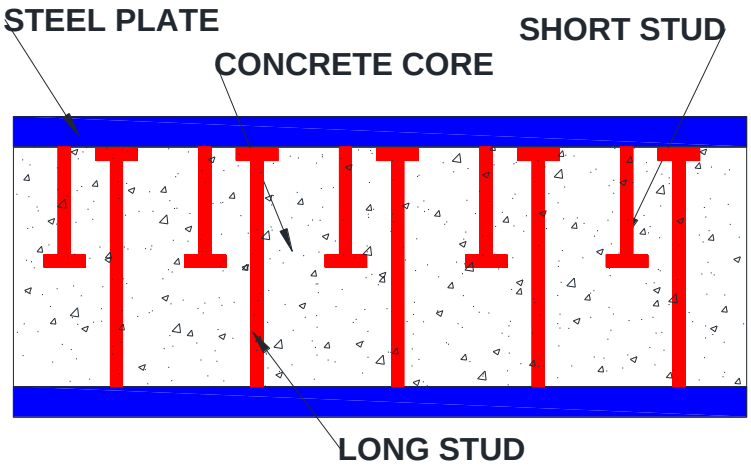

Figure 2-1: Side view of SCS beam

2.2 Shear Resistance and Stud Connectors

In DSC beams without a long stud, the vertical shear capacity will be controlled by (Oduyemi and Wright, 1989):

- Compressive strength of the concrete core
- Tension steel plate thickness
- Shear span to effective depth ratio
- Interaction degree between the bottom steel plate and the concrete core

Wright et al. (1991b) performed 11 full-scale experimental tests on DSC elements subjected to bending and a combination of bending plus an axial load to validate the theoretical work, and then presented design guidance notes. Because of the role of shear stud connectors as a crack inducer, which in turn reduces the shear strength of the concrete core, it is recommended to reduce the shear strength of concrete given in Table 3-9 of BS 8110 by 20%. Also, it is recommended to use a long stud spaced at not more than 75% of the element depth.

The author believes that the sizes of the beams used were relatively small (the beam size was 150mm x 150mm and had a span of 1.5 m to 2.3 m) and they do not reflect the behaviour of the real size. Furthermore, the two-point load test isolates the moment region but not the shear region.

Two coupled differential equations were presented by Wright and Oduyemi (1991) to model the partial interaction in double skin composite beams. The flexibility of shear connector studs, cracking of concrete and cross effect of steel plates were taken into account. The analytical results were verified by pilot tests and a full-scale tests presented by (Johnson, 1981; Roberts, 1985; Narayanan et al., 1987). Top plate connector stiffness had an insignificant effect (assuming full interaction behaviour of the bottom plate) on mid-span deflection, whereas bottom connection stiffness showed much greater influence.

Roberts et al. (1996) compared the experimental results with the shear resistance calculated from equations proposed by Narayanan et al. (1994) which were found to be very conservative. Also, it was found that a stud spacing to plate thickness ratio of 40 was satisfactory for practical considerations.

An experimental and numerical study was carried out by Clubley et al. (2003) on the strength of shear studs subjected to a pushout load. The investigation comprised 6 mm, 8 mm and 10 mm steel plates set apart at 200 mm, 400 mm and 700 mm with shear connector studs of 25 mm in diameter spaced at 200 mm in both directions. From experimental observation, two failure modes were identified that are controlled by the plate thickness: ductile failure, with tearing of the plate around the weld accompanied by a large local deformation in plates that had a thickness of 10 mm or less, while plates that were 12 mm (or more) thick had a brittle failure of the weld with little deformation in the plate. Finite element (ANSYS package software) was used to perform the numerical analysis, and an eight-node with three degrees of freedom and isoparametric elements called SOLID45 were used for steel plates. Figure 2-2 shows a comparison between experimental and numerical results of load-relative slip for different stud spacing with an 8 mm plate thickness.

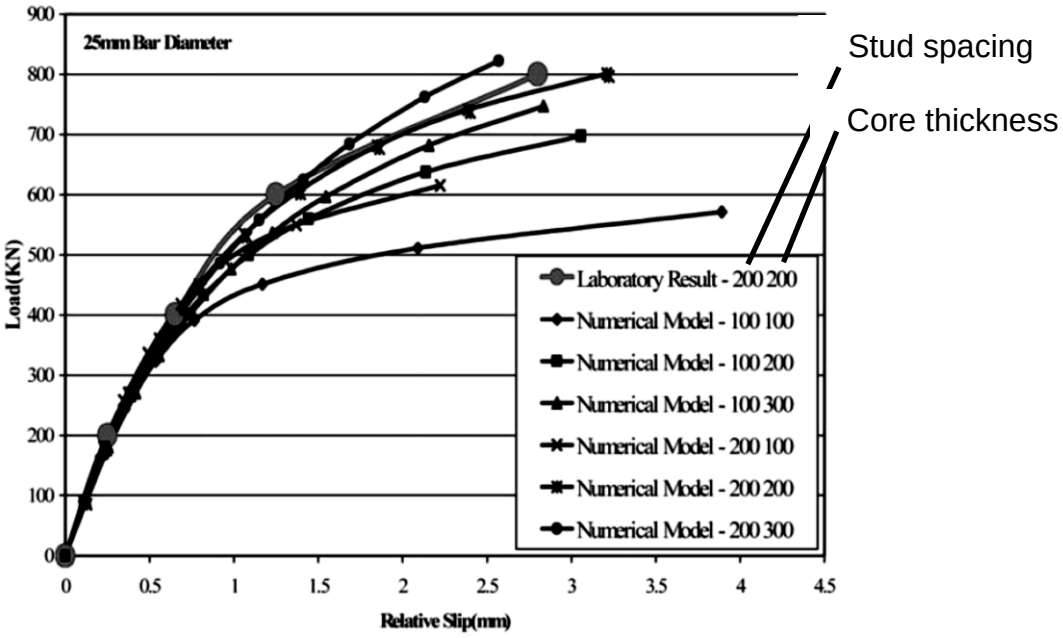

Figure 2-2: Relative slip-load curves for different stud spacings (Clubley et al., 2003)

From the numerical results, it can be observed that the slip had increased and the load capacity had decreased with increasing shear connector spacing.

Xie et al. (2005) presented the results of experimental tests and numerical analysis using a finite element (ABAQUS software package) of bi-steel with 200 mm cubic concrete samples sandwiched between steel plates 6, 8, 10, 12 and 15 mm thick to study the shear strength and stiffness based on push tests.

From the experimental results and the equation proposed by the authors, it was observed that the shear strength was not affected by the plate thickness when t≥10 mm and d=25mm. Failure modes observed in the experimental tests were:

- Tearing of the plate
- Shear through the bar section which gave the maximum strength
- Interface failure

In the numerical analysis, three-dimensional solid elements (C3D8 and C3D6) were used to model the components of the tested units. The contact pair approach was used to model the contact between the steel (plates and studs) and concrete as well as to consider the friction effects at the contact surfaces.

The distribution of the longitudinal stresses in the plate due to shear forces in the bar is shown in Figure 2-3.

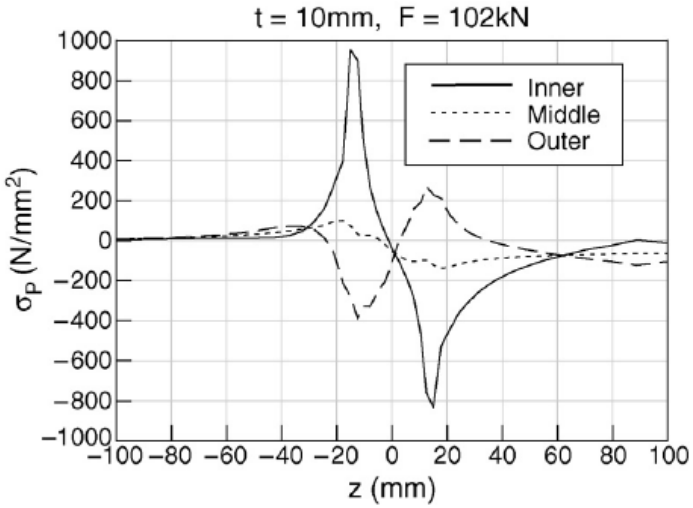

Figure 2-3: Longitudinal stress distribution in the plate due to shear forces in the bar (Xie et al., 2005)

It can be seen that *"A large local tensile stress exists around part of the boundary of the bar connector on the inner surface"* Xie et al. (2005). Figure 2-4 shows the variation of the principal and longitudinal stresses with the plate thickness that decreases almost linearly with increasing plate thickness.

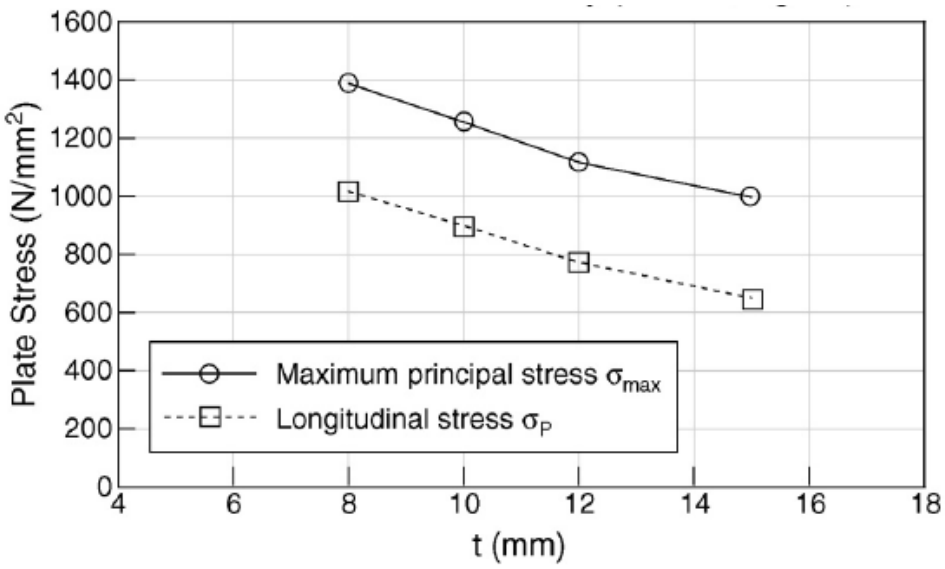

Figure 2-4: Stress variation in the plate (Xie et al., 2005)

From the experimental results, it was concluded that the ultimate strength in the shear increased to about 25% when plate thickness increased from 6 mm to 10 mm but there was no effect on the shear strength for further increments.

An analytical study on the effects of the shear connectors' alignment in DSC beams was presented by Leekitwattana et al. (2010). A bi-directional corrugated strip was proposed as an alternative for shear connectors, as shown in Figure 2-5. From the analysis presented, the conclusion was that there was a possibility of increasing shear strength using the proposed shear connectors' alignment.

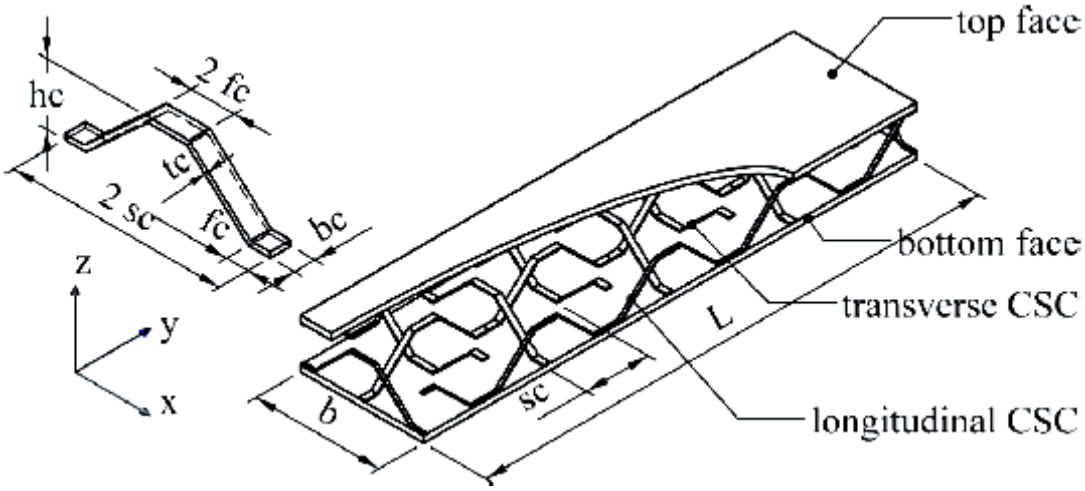

Figure 2-5: Corrugated-strip arrangement (Leekitwattana et al., 2010)

In summary, the shear strength of the double skin composite members is a function of the concrete core properties, the thickness of the top plate, and the interaction degree between the bottom steel plate and the concrete core. Maximum spacing between long studs is recommended to be no more than 0.75 of the member depth. The stud spacing to plate thickness ratio of 40 was found to be satisfactory for practical consideration.

For shear studs subjected to push-out load, two failure modes were identified: a ductile failure accompanied by a large local deformation in the plate when the plate has a thickness of 10 mm or less, whilst, for plate thickness of 12 mm or more, the failure was brittle with a little deformation in the plate.

The shear strength of studs with a diameter of 25 mm is not affected by plates having a thickness of 10 mm or more.

2.3 Fatigue

Roberts and Dogan (1998) presented an experimental and theoretical study of shear stud connectors attached to the tension plate under the fatigue load. Figure 2-6 shows the variation of the shear force range in the connectors. The results for the tested beams and push shear fatigue tests compared with Euro Code 3 and tests by King et al. are shown in Figure 2-7. The main conclusion drawn from the study was that the EC3 (Eurocode3, 1993) provides a satisfactory basis for fatigue assessment of the welded stud in steel-concrete-steel sandwich beams.

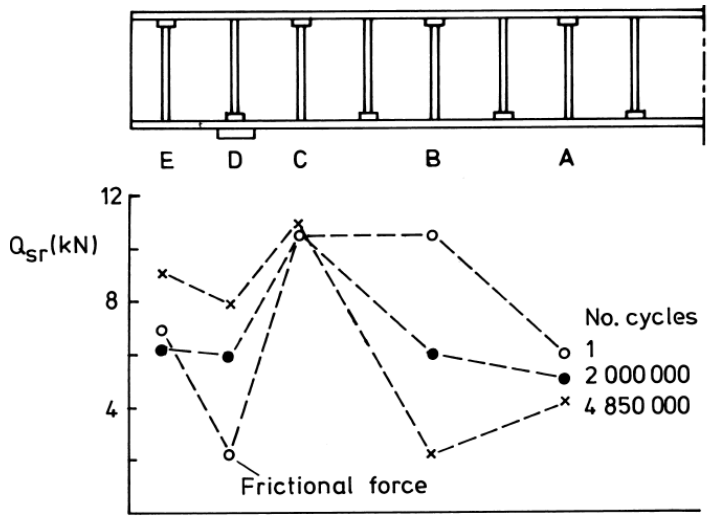

Figure 2-6: Variation of the shear force in connectors (Roberts and Dogan, 1998)

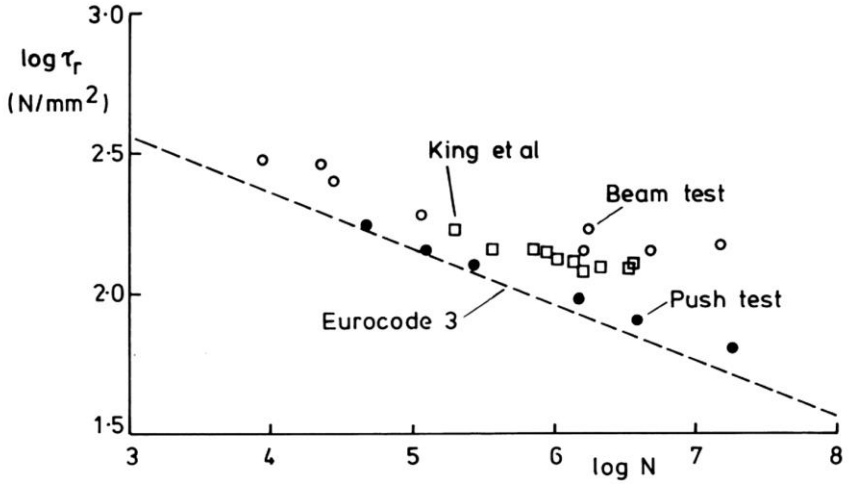

Figure 2-7: Beam and push-out test comparison with EC3 and King et al. (Roberts and Dogan, 1998)

Experimental investigation of the fatigue performance of DSC beams with a lightweight concrete core and J-hook connectors was performed by Dai and Liew (2010). Figure 2-8 shows the variation of strains on steel plates of beams cast with plain concrete (PL) (which was used as a reference) and fibrous lightweight concrete (FL).

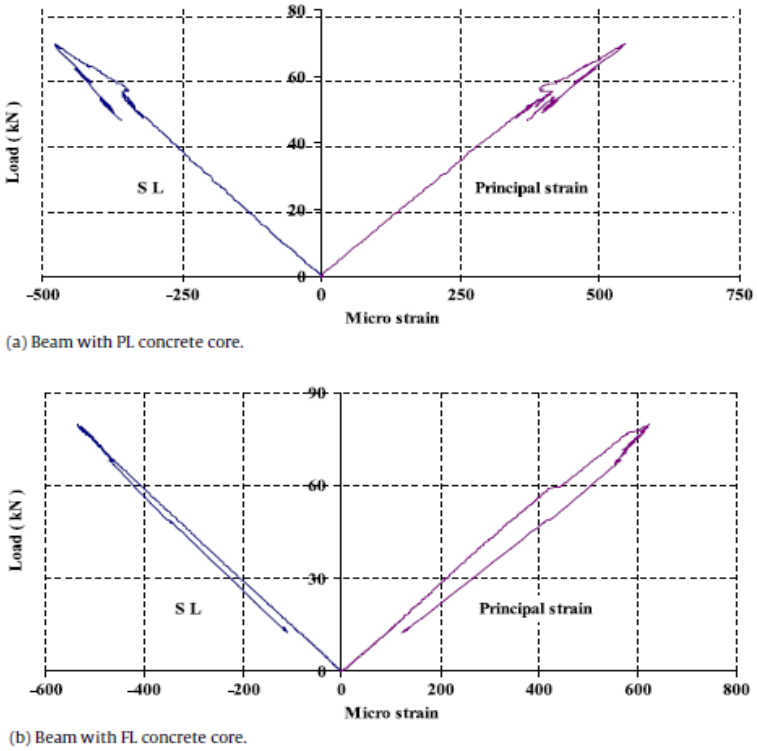

Figure 2-8: Variation of strain on plate faces (Dai and Liew, 2010)

Figure 2-9 shows the load-central deflection response of beams subjected to a static load (s1 and s2 contain a fibre-lightweight aggregate concrete core and sp contains a plain-lightweight aggregate concrete core). For both concrete core types, the behaviour was linear up to the crack formation stage. It was reported that the addition of fibres enhanced beam behaviour through:

- Prevention of the formation of large cracks other than near the loading point
- Increasing the load-carrying capacity and ductility
- Delaying the propagation of cracks

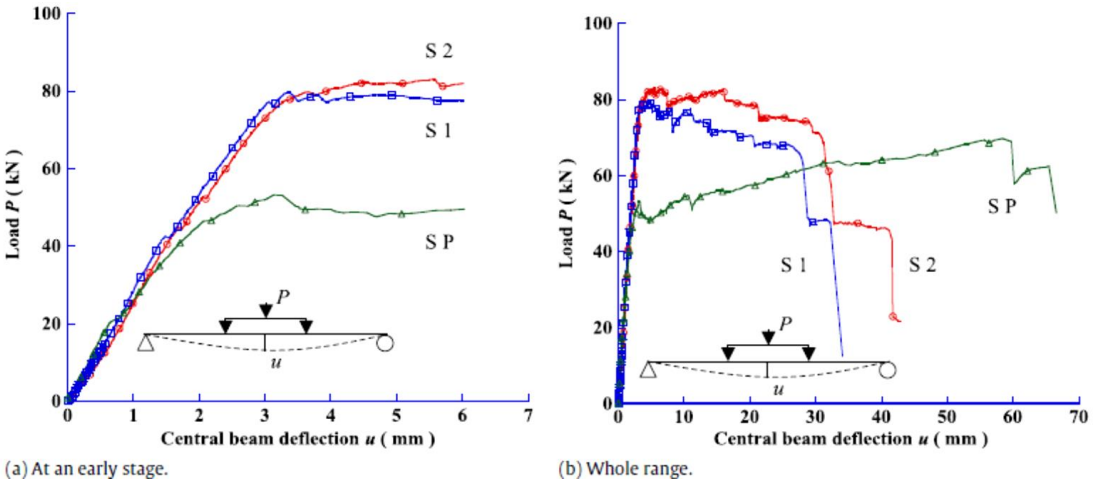

Figure 2-9: Load central deflection of SCS beams (Dai and Liew, 2010)

Fatigue and static tests were presented by Foundoukos et al. (2007). Bi-steel components and 18 beams were used to investigate their behaviour under cyclic loading as well as that of identical beams tested under static loading. Fatigue tests were carried out on a plate-stud connection under:

- Unloaded stud with a plate in tension
- Stud in shear with a plate in tension
- Stud in shear with a plate in compression
- Push-out test

From the test of the stud-plate connection, the following observations were recorded:

- Toe of the weld was the place of the crack initiation which led to the failure
- Most specimens tested under the ‘pure bar shear pull test’ failed by the same mechanism as specimens tested under the plate in tension with an unloaded bar
- Fatigue life of the stud in the shear was not affected by the plate’s thickness

As cited by Foundoukos et al. (2007), *“the current design method assumes that the beam life is given by the smaller of the plate tension life and the bar shear life”*. They proposed a correction to the equation of calculating the fatigue life based on a limited number of tests (18 tests), which is considered

insufficient to propose an equation or to suggest a modification to an existing equation.

From testing the beams under the fatigue load, it was observed that no double fracture occurred, whereas several such failure patterns existed in the embedded shear tests.

2.4 Concrete Steel Interaction and Steel Plate Surface

Subedi and Coyle (2002b) studied experimentally the effect of the inner surface on the interaction between the concrete core and the steel plates, which affects the composite behaviour of the DSC beams. Eight different surfaces were used: plain, roughened, Durbar, Expamet (thick expanded metal mesh), square bars, vertical sine wave, horizontal sine wave and air-shot studs. Figure 2-10 shows the load-displacement curves for the SCS beams that have the above surfaces and cast using C40 concrete. Based on the maximum load capacity, it is obvious that the 5 mm square bar and Expamet gave the best performance in comparison with the other types.

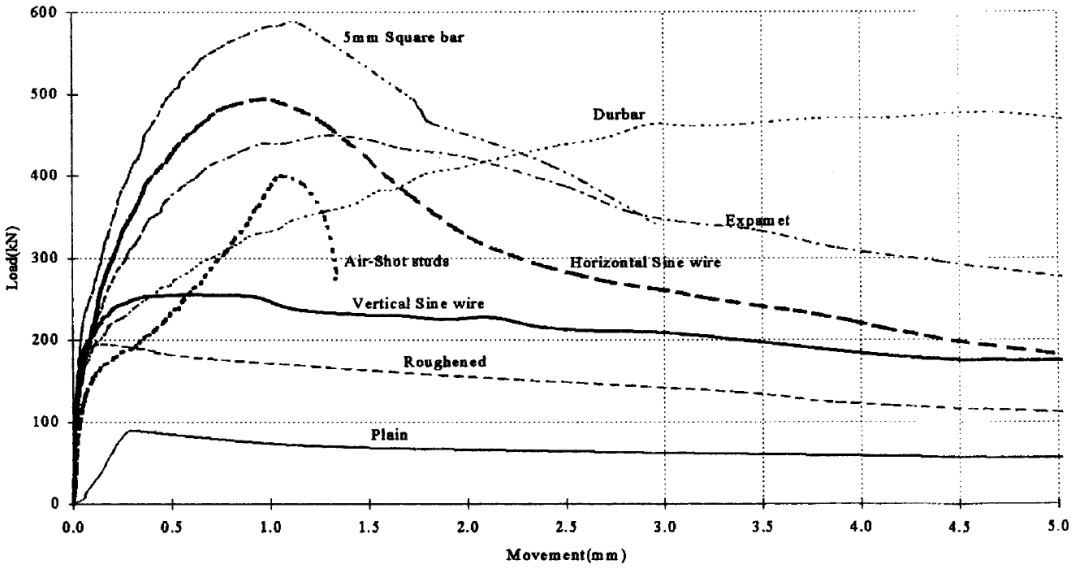

Figure 2-10: Load–deflection curves for SCS beam with concrete C40 (Subedi and Coyle, 2002b)

Subedi (2003) described an extension to the study presented in Subedi and Coyle (2002b) on the full composite action of DSC beams. As already described, the earlier study tested eight different surfaces; three of these were chosen for the extended study: Durbar, Expamet (thick expanded metal mesh)

and wavy wire, as well as a plain surface which was used as a control for comparison purposes. The experimental programme included 32 beams with three different concrete strengths (C40, C80 and C150). Expamet and wavy wire showed fully composite behaviour with good improvements to the serviceability and ultimate load stages compared with the control beams. A comparison with previous studies that had investigated unsurfaced plates (Oduyemi and Wright, 1989; Wright et al., 1991b) regarding the failure modes was undertaken and can be summarised as follows:

- For DSC beams with the same plate thickness at the top and bottom, a flexural failure which was initiated by buckling of the compression plate and concrete crushing no longer existed with surfaced plates.
- Increased vertical shear resistance was observed but without a change in the mechanism of failure.
- A significant increase in horizontal shear resistance (slip resistance) was also observed but without any changes in the mechanism of failure.

2.5 Modelling

Shanmugam et al. (2002) used FEM (ABAQUS software package version 5.7/5.8) to model DSC slabs and the results were verified by experimental tests. The steel plates were modelled using shell elements of four-node reduced integration with five integration points and with a large strain formulation. An elastic-perfectly plastic model was used for steel in both tension and compression. Buckling was not taken into account through the modelling because node-to-node connectivity did not allow for such effects. Shear stud connectors were modelled indirectly through the analysis by adjusting the parameters of the shear stress of the concrete core.

Good agreement between experimental test results and finite element analysis (ABAQUS) was reported in spite of the approximation used (plate transformation and indirect modelling of shear stud connectors). Table 2-1 shows a sample of the comparison between the experimental results and FEM based on the maximum load capacity. However, using only the maximum load

capacity as a basis for comparison provides insufficient information on the relative responses.

Table 2-1: Comparison of FE with the experimental results (Shanmugam et al., 2002)

Specimen name	Ultimate load P_u (kN)		$\frac{(P_u)_{ABAQ}}{(P_u)_{EXPT.}}$
	$(P_U)_{EXPT.}$	$(P_u)_{ABAQ}$	
DSCS1	760	786	1.03
DSCS2	687	681	0.99
DSCS3	687	697	1.01
DSCS4	720	790	1.10
DSCS5	770	740	0.96
DSCS6	889	908	1.02
DSCS7	976	1096	1.12
DSCS8	956	894	0.94
DSCS9	1151	1153	1.00
DSCS10	1072	1212	1.13
DSCS11	1181	1239	1.05
DSCS12	1266	1299	1.03

Clubley et al. (2003) took into account the non-linear effect of materials and geometry, based on the work presented by (Clubley et al., 2003; Moy et al., 1998) and used a finite element to study the local behaviour of the DSC panel under push-out loading. In their calibrated model, a smeared and discrete contact between concrete and steel technique was used. A detailed description of the effect of plate thickness on the shear strength of the DSC member using the numerical analysis was presented, and the main observations can be summarised as follows:

- In thin plates, panel resistance to the applied load continued until tearing of the weld circumference occurred.

- Plate thickness played the main role in determining the failure mode:

  - With t≤ 10 mm, concrete crushed around the stud, a plastic hinge formed within the interface of the plate, and the shear stud connector and the shear strength of the DSC panel were governed by plate strength.
  - With t≥ 12 mm, constant stress distribution through thickness located at the friction weld and brittle failure occurred by the weld fracture.

- A plastic hinge formed at the junction of the shear connector and the steel plate with thin plates (t<6mm).

Liang et al. (2004) investigated the effects of a combination of in-plane shear stresses with bi-axial stresses on the buckling strength of plates in DSC panels. This study was performed using a finite element code (STRAND7) with an eight-node plate/shell element and Von Mises yield criteria for non-linear analysis. From the finite element analysis, the observations drawn can be summarised as follows:

- As the bi-axial compressive stresses increase, the critical shear buckling capacity decreases.
- From the non-linear finite element analysis, the ultimate strength of a plate subjected to combined load states decreased with increasing width to thickness ratio.

A finite element analysis (using ABAQUS software package) of bi-steel beams was presented by Foundoukos and Chapman (2008). The beams were modelled using two-dimensional, plane stress, reduced integration elements called CPS4R. Figure 2-11 shows the effects of tension plate thickness to concrete depth ratio on the transverse shear resistance.

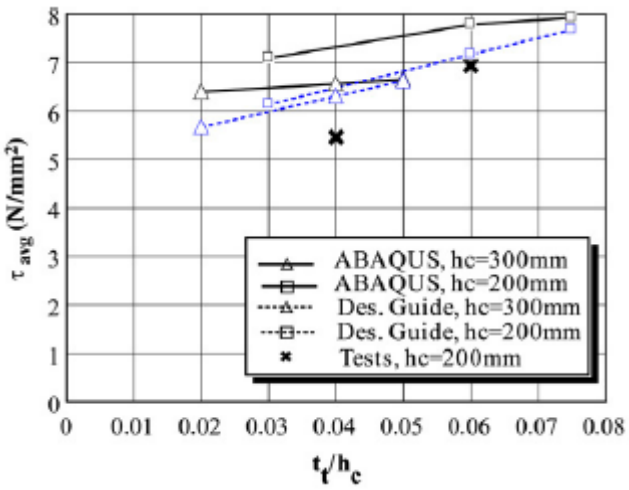

Figure 2-11: Variation of transverse shear resistance with t_t/h_c (Foundoukos and Chapman, 2008)

Tensile force in the stud was observed to be higher at the bottom end and decreased towards the top end. This was attributed to the cracking of the

concrete core. From the finite element analysis, it was observed that the maximum slip occurred close to the mid-span up to $P_u/2$ but after $P_u/2$ the maximum slip occurred at the end of the beam, which was also observed in some tested beams. This behaviour was thought to be as a result of diagonal cracking of the concrete core. Figure 2-12 summarises the effect of stud spacing to concrete depth ratio on the shear stress in the studs.

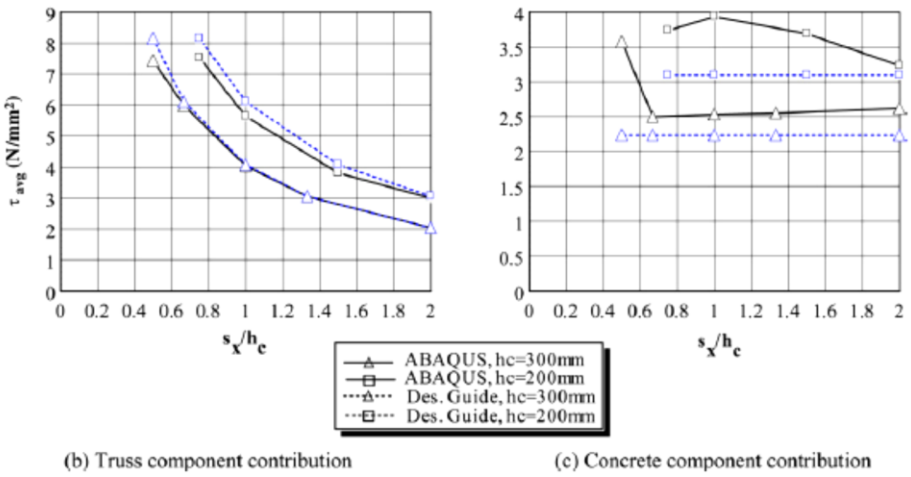

Figure 2-12: Effect of S_x/h_c (Foundoukos and Chapman, 2008)

The cracking pattern predicted by the finite element was symmetrical around the mid-span, whereas it was not the case in many cases for the beams tested experimentally. The predicted load at which cracks occurred was accurate for the mid-span but it was less than that of the test results in other locations.

Figure 2-13 illustrates the effect of concrete core depth on the transverse shear strength capacity while all other parameters were kept constant and there was a shear stud spacing to concrete depth of 1.

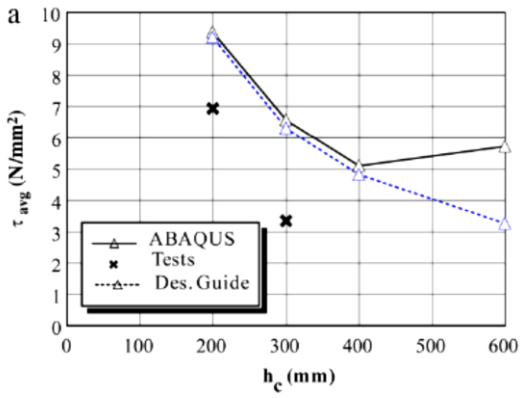

Figure 2-13: Concrete core depth (h_c) effect on the transverse shear (Foundoukos and Chapman, 2008)

A three-dimensional finite element analysis using ABAQUS was presented by Yan (2014) to study the behaviour of double skin composite beams with J-hook connectors under a quasi-static load. The model was validated using experimental tests. A Concrete Damage Plasticity model was used to model the concrete core and elastic–plastic with strain hardening of the bi-linear model was used for the steel. The central deflection was used to validate the finite element model presented, which showed good agreement between the experimental results and the model results.

2.6 Failure Modes

An experimental investigation of the behaviour of bi-steel beams when subjected to static load was carried out by Xie et al. (2007). Plate thicknesses used in the tests were 6 mm, 8 mm and 12 mm. As shown in Figure 2-14 and Figure 2-15, failure modes observed during the tests were:

- Bar shear
- Tension plate failure (identified by very high strains in the plate but rupture did not occur)
- Concrete shear
- Bar tension

Figure 2-14: Beam failure modes under static load (Xie et al., 2007)

Figure 2-15: Failure modes in shear connectors (Xie et al., 2007)

An experimental and theoretical investigation was conducted by Liew and Sohel (2009) to study the flexural and shear behaviour of DSC beams with J-hook connectors having different types of concrete core and subjected to a static point load. Figure 2-16 shows the failure modes observed through the tests:

- Tension plate yield
- Vertical shear failure
- Shear connector failure
- Slip failure (bond failure)

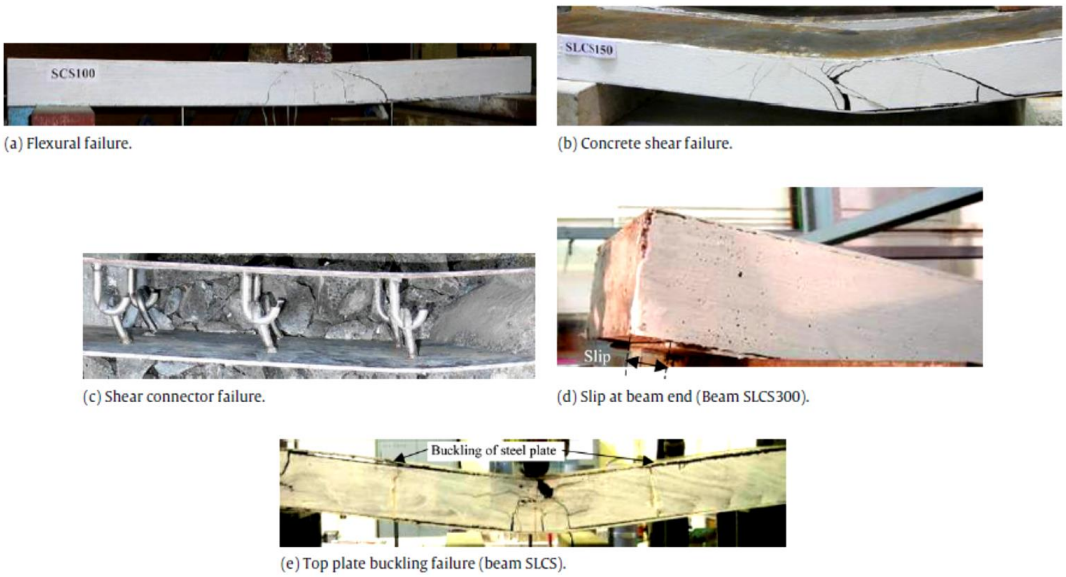

Figure 2-16: Mode of failure in beams (Liew and Sohel, 2009)

Figure 2-17 shows the effect of fibre addition where the presence of fibres prevented the brittle failure of beams, and an increase in the deflection range (up to 60 mm to 70 mm) did not result in any sudden failure in J-hook connectors. Flexural crack formation started at the maximum tensile stress region (mid-span) at about 50% of the peak load and, as the load increased, the flexural cracks increased, accompanied by shear cracks, but these cracks had no effect on the load-deflection behaviour up to 70% of the peak load.

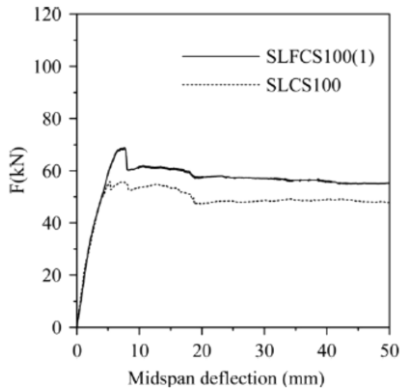

Figure 2-17: Effect of steel fibres on central deflection
(Liew and Sohel, 2009)

2.7 General Behaviour

Oduyemi and Wright (1989) investigated the effect of plate thickness on the behaviour of DSC beams experimentally using steel skin with 2, 3, 4 and 6 mm thicknesses. They suggested limiting the shear connectors' spacing to steel plate thickness ratio (s/t) to 30, according to experimental measurements and analytical analysis using Euler's elastic buckling stress.

A significant decrease in the bottom steel plate strains as well as increasing the end slip was observed when the bottom connection amount decreased. The cracking pattern was found to be affected by the spacing of the bottom studs, where the studs were considered to act as inducers for crack initiation. When the bottom stud connectors reached their strength capacity, a sudden separation between the steel plate and the concrete core occurred, followed by immediate failure. The presence of long studs is vital since they play an important role in preventing vertical shear failure.

The general behaviour of SCS sandwich slabs showed a full interaction response and no slip between the steel plates and concrete core was

observed (Liew and Sohel, 2010). Figure 2-18 shows the behaviour of a simply supported SCS sandwich slabs subjected to static load. There were obvious differences between the behaviour of the normal-weight concrete core and that of the lightweight concrete.

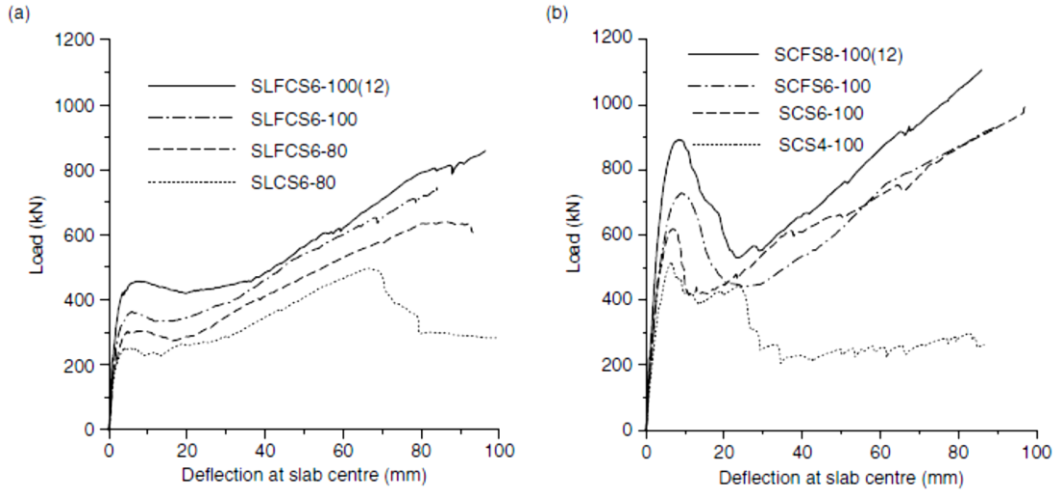

Figure 2-18: (a) SCSS slabs with LWC; (b) SCSS slabs with NWC (Liew and Sohel, 2010)

According to Dai and Liew (2010), with fatigue tests on double skin composite beams there was a permanent deflection after each unloading stage, which was attributed to the accumulative cracks in the concrete core, stud deformation, and debonding between the steel and concrete core, which in turn led to progressive degradation in beam stiffness. It was concluded that the amount of energy dissipated depends on the maximum applied load and load range.

Wright and Oduyemi (1991) conducted an experimental scale-model test programme to study the behaviour of beams, beam-columns and columns. Their main observations can be summarised as follows:

- In beams, the failure mode was not affected by low-strength concrete.
- Column tests, considering the shear stud spacing to steel plate thickness ratio, suggested that stocky plates should be used between the studs to overcome the problem of buckling.
- Beam-column tests indicated that increasing the thickness of either the tension or compression plate increased the capacity of the section; this is

strongly related to the ability of the shear stud connectors and the concrete core to carry the additional generated forces.

Figure 2-19 shows the effect of varying the number of shear stud connectors per unit length. Varying the number of top connectors had no significant effect on the failure load; however, that is not the case for the ductility. Varying the number of bottom connectors showed a noticeable effect on the capacity and ductility of the beam. It was recommended that long studs should be used and attached to the tension plate. In column tests, a pull-out depends on the length of the shear stud connectors and the strength of the concrete. The effect of reducing the amount of shear connectors attached to the tension plate increased the slip, while, in compression, this was not the case.

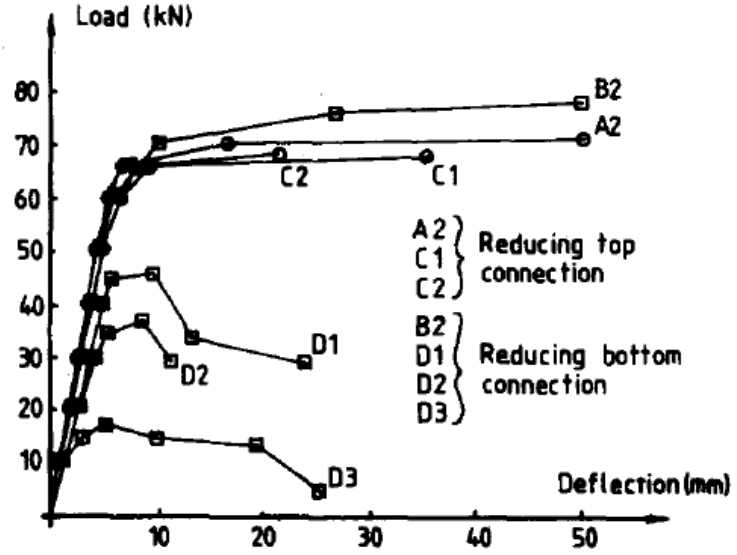

Figure 2-19: Effect of connection variation (Wright and Oduyemi, 1991)

McKinley and Boswell (2002) provided detailed analytical solutions for the elastic and plastic load-deflection behaviour of bi-steel beams and the results were compared with the tests of 16 large-scale simply supported DSC beams (bi-steel) subjected to three-point loading hold by McKinley (1999). Bending stiffness of the steel plates was ignored in calculating the position of the neutral axis as the error from this assumption is less than 1%, which depends on the distance between the steel plates centroids to steel plate thickness ratio (in bi-steel the typical ratio ranges from 16.7 to 100). The comparison between the experimental results and the analytical results determined the moment capacity agreed with a standard deviation of 4.25%.

The experimental results and finite element analysis by Foundoukos and Chapman (2008) showed that the truss model overestimates the tensile force and this force depends on the diagonal cracking.

The analytical method to calculate deflection and slip of simply supported DSC beams presented by Dogan and Roberts (2010) takes into account the effects of the degree of interaction. The results of partial and full interaction analytical theories compared with experimental results are reported elsewhere. The friction between the steel plates and the concrete core was observed to have a significant effect.

2.8 Practical Considerations

It would be difficult to produce an application for the suggested DSC beam-column joint based on the early stages of the current study because the main aim of this study is to validate the applicability of this joint type. Moreover, the current study deals with exterior joints and more research is required for the interior and corner joints shown in Figure 2-20 (a and b).

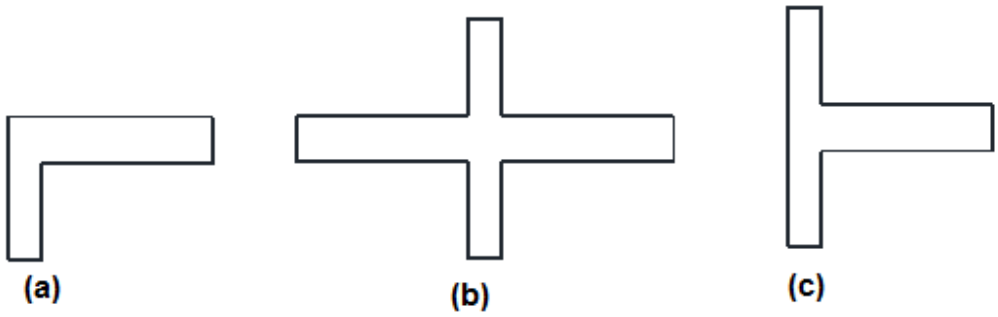

Figure 2-20: a- Corner Joint b- Interior Joint c- Exterior Joint

Construction of framed DSC structures can be performed using three different methods: cast in place, precast and a mix of cast in place and precast methods. The author suggests using the first and second methods for construction of the DSC system as is laid out in sections 2.8.1 and 2.8.2. Moreover, the suggested construction methods are for 2-D portal frames and the lateral stability will be provided by the floor system. Furthermore, lateral

stability can be increased using side rails and/or by using walls (or bracing) between columns out of plane of the portal frame.

Tying the floor system to the portal can be introduced in different methods, such as welding, bolting or pre-prepared male/female connectors welded onto the beam tops.

2.8.1 Cast in Place

This method involves a few steps: foundation casting, placement of the DSC frame, placement of formwork on the sides of the beams and the sides of the columns, and pouring of concrete. Here, the concrete will be poured through the columns and the concrete mix should be designed so it flows easily through the beams. Voids must be made in the top of the beams' formwork to allow for the air to escape (Figure 2-21). Concrete setting time will play an important role in the speed of construction and should be taken into account in the formwork design.

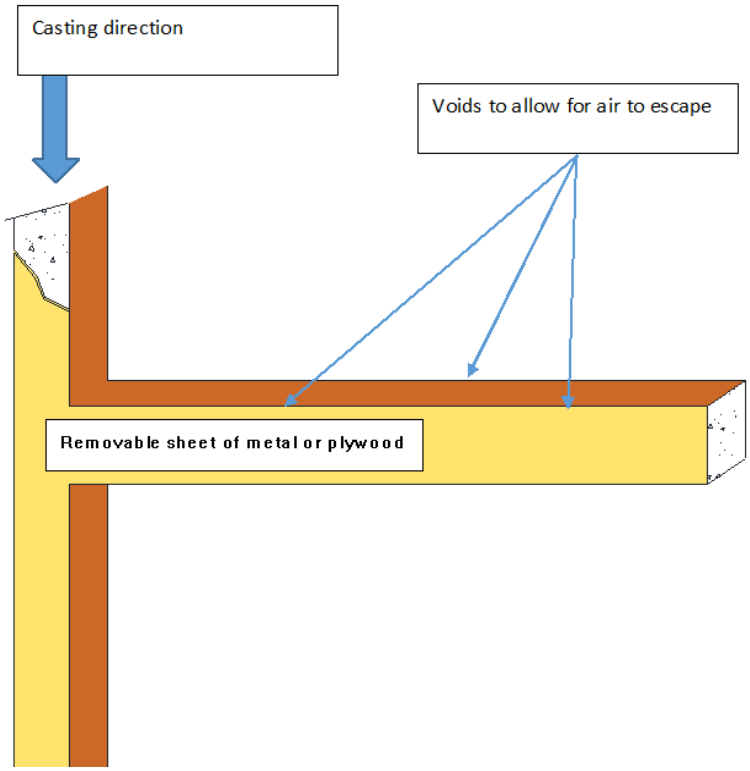

Figure 2-21: Construction of DSC System using Cast in Site Method

2.8.2 Precast Construction

Many advantages can be introduced by using this method, such as quality control, speed of construction, accuracy, etc., as known from the prefabricated systems usage Rackham et al. (2009). The main problems raised using this system are the lifting and the connections between elements. The usage of DSC constructions can reduce the size of sections and the usage of Light Weight Concrete (LWC) can reduce the weight of the individual elements. Connections should be designed at the contra-flexure regions of the frame to ensure shear force transferral and there will be no need to maintain continuity of the steel plates (Figure 2-22).

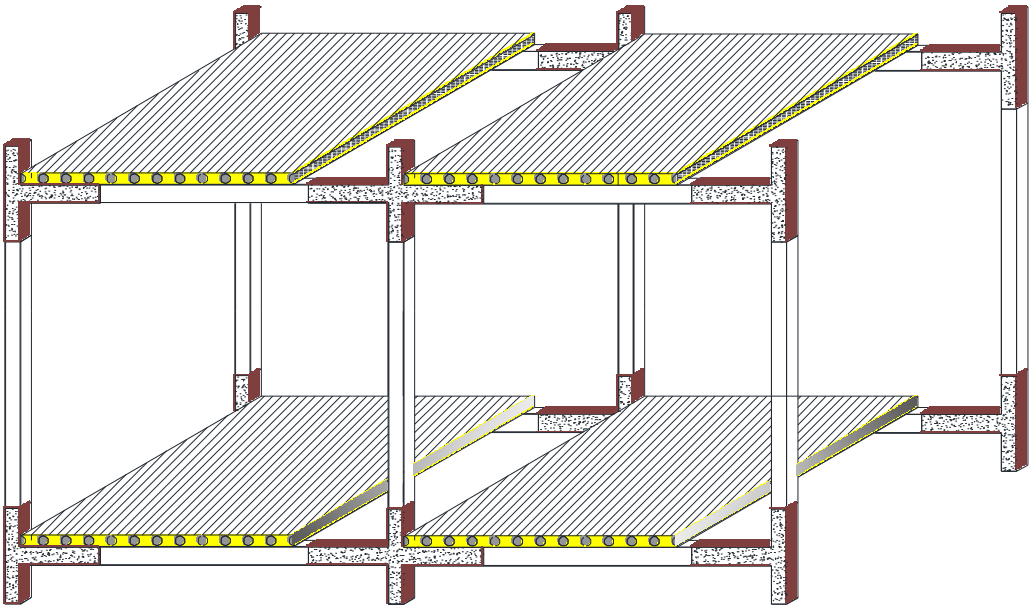

Figure 2-22: Construction of SCS system using precast elements

2.9 Summary

This chapter has presented a review of the previous studies about steel-concrete-steel (also called Double Skin Composite) members and was divided into subsections to describe the main observations recorded about the behaviour of this type of construction.

Table 2-2 outlines most of the previous studies that have been presented in the previous sections of this chapter, along with their aims and some data about the member types, loading and dimensions. It can be seen that most of these studies were conducted on beams under static load and a secondary study was presented by Wright et al. (1991a) on the behaviour of columns. In addition to the limited studies on members other than beams, it can be noticed that the main loading type used in the experimental studies was bending, with a few studies on bending also including axial load, fatigue and low-velocity impact. Also, some numerical studies were presented in order to analyse the SCS constructions with some approximation, for example, the model presented by Shanmugam et al. (2002) did not physically include the shear studs. This approximation means there was no way of investigating the behaviour of the shear connector itself or the surrounding concrete.

Steel plate thickness, stud spacing, stud size, and the addition of steel fibres were studied and their role in enhancing the SCS constructions' performance was well explained. Despite the high strength achieved by using SCS constructions, serviceability issues (wide crack widths) were reported but no attempts have been made or introduced to solve such an important matter.

Failure modes identified in the DSC beams and slabs were tearing or yielding of the tension plate, bar shear, bar tension, concrete shear and slip (bond) failure.

Analytical equations were presented to calculate the shear strength, ultimate moment capacity, and deflection of the double skin composite members as well as bi-steel members based on the theories relating to the reinforced concrete beams with some modifications.

According to the author's knowledge, there is no published work on double skin composite beam-column joints. In the current study, the behaviour of double skin beam-column joints will be investigated experimentally and numerically. This study is important for the following reasons:

- There are no previous studies on the double skin beam-column joints.
- Understanding the structural performance of the double skin composite beam-column joints will help in the development of the double skin

composite system through filling the knowledge gap in an integrated double skin skeletal system (beams, columns and beam-column joints).

- The present study will provide a good basis for more studies, for example, on the performance of such joints under transverse loads, seismic loads, and torsion capacity.
- Numerical modelling of the system will help to provide understanding of the behaviour of the double skin composite beam–column joint.

It is important to list some fields where there is currently a shortage of or no available data:

a- Structural performance of the DSC subjected to torsion
b- Structural performance of the DSC under blast loads
c- Structural performance of the DSC under seismic loads
d- Structural performance of the DSC under cyclic loads
e- Fire resistance of the system

The subsequent chapters will present the structural behaviour of double skin composite beam-column joints under monotonic and quasi-static loading experimentally and numerically using General Finite Element Package ABAQUS CAE 6.10.

2.9.1 Reflections on the Literature Review

Although there are no previous studies on DSC beam-column joints, the available studies about beams and columns can be used to support the current study in two different ways. Firstly, based on the presented literature review of the previous studies, the recommended limitations on steel plate thickness, stud diameter, and stud spacing are considered to prepare the initial design of the double skin composite joint.

The analytical methods available to analyse the double skin composite beams are considered in order to produce an analysis of the beam-column joint, as is shown in Chapter six. The recommended finite element modelling regarding the material modelling and element type is also considered.

Secondly, the behaviour of the beam and the column during loading stages can be compared to previous studies, such as in relation to cracking initiation

and development, maximum load and failure pattern. Moreover, a comparison can also be shown concerning the behaviour of the DSC beam-column joint when using another type of material in the core, such as steel fibres.

The parametric studies presented previously had taken into account the effect of different parameters that affect the performance of the double skin composite constructions. Two of these parameters are considered experimentally in the current study (concrete compressive strength and effect of steel fibres) and one is included in the numerical parametric study. These parameters were:

- Compression steel plate thickness
- Tensile steel plate thickness
- Stud spacing in the compression zone
- Stud spacing in the tension zone
- Concrete compressive strength
- Effect of steel fibrous concrete
- Shear stud connector types
- Shear stud diameters to plate thickness ratio
- Effect of the interaction between the steel plate and the concrete core to replace the stud connectors

Table 2-2: Summary of previous studies on steel-concrete-steel

No	Reference	Outcome	Member(s)	Loading	Dimensions
1.	(Tomlinson and Tomlinson, 1990) Shell composite construction for shallow-draft immersed tube tunnels. Immersed Tunnel Techniques	Suggested a design method for a dual skin composite and also described the non-linear FE program developed to model its behaviour	Rectangular tube tunnel		N.A
2.	(Oduyemi and Wright, 1989) An experimental investigation into the behaviour of double skin sandwich beams	Described an experimental work carried out at the model scale on DSCB's which are subjected to static bending only	18 model beams	Static bending (2-point load)	150x150x1500 6 mm mild Pl 6 mm stud
3.	(Wright et al., 1991a) The experimental behaviour of double skin composite elements	Described scale-model tests on beam, column and beam-column specimens	53 scale-model beams, column and beam-column specimens (1/3 full scale)	2-point load Concentric + eccentric Axial + bending M	150mm square 1.5-2.3m length 2-6 mm Pl thick 6 mm stud
4.	(Wright et al., 1991b) The design of double skin composite elements	Described design development and experimental studies "eq. + descript"	11 full-scale beams	Ref. Line load Offset point load Concentric axial	Ref. Thick=600 mm Pl t=6 or 8 mm Stud = 13 or 16
5.	(Wright and Oduyemi, 1991) Partial interaction analysis of double skin composite beams	Presented closed form solution for the analysis of ss DSC beams	beams		

No	Reference	Outcome	Member(s)	Loading	Dimensions
6.	(Roberts et al., 1996) Testing and analysis of steel-concrete-steel sandwich beams	Details of tests - check design rules	beams	Quasi-static load 2- or 4-point load (deflection control)	Hc= 150 W = 400 Tt= 8 Tc= 4 or 8 mm L=1500-3000(+200) Ten. stud= 10 mm ,150 Comp. stud = 6 mm, 65
7.	(Bowerman and Pryer, 1997) Bi-Steel: A new steel-concrete-steel composite construction system for cores and super-frames	To bring this material to the attention of those designing tall buildings in the belief that bi-steel offers structural engineers and constructors new opportunities for cost saving			
8.	(Roberts and Dogan, 1998) Fatigue of welded stud shear connectors in steel–concrete–steel sandwich beams	Tests to investigate fatigue strength of welded studs attached to T Pl	9 beams (ss)	Central concentrated	B= 200 Hc= 150 Tt=tc= 8 L= 1700 (1400) Stud= 10, 150
9.	(Subedi and Coyle, 2002b) Improving the strength of fully composite steel-concrete-steel beam elements by increased surface roughness—an experimental study	Presented preliminary test results using 8 different surface preparations	32 beams	1-point load	B= 160-320 Hc =160-268 L=1500-4000
10.	(Subedi and Coyle, 2002a) Advances In Steel-Concrete-Steel Composite Design. Concrete Floors And Slabs	Discussed the development of the interface-resisting surfaces	32 beams		W = 160 – 320 mm D= 160 – 268 mm L= 1500 - 4000

No	Reference	Outcome	Member(s)	Loading	Dimensions
11.	(McKinley and Boswell, 2002) Behaviour of double skin composite construction	Outlined a programme of research into the elastic and plastic behaviour of a series of DSC beams – with analytical solutions	16 large-scale ss beams	3-point bending	W= 1000 L= 3000 s/t=16.67 to 50 Hc= 200 T= 8, 10, 12
12.	(Shanmugam et al., 2002) Finite element modelling of double skin composite slabs	FE modelling of the ultimate load behaviour of DSC slabs (ABAQUS) - with experimental	12 ss slabs	concentrated	1500x1500x100 T= 4.6-5.9 Stud= 13, 80 Top s/t= 33-49 Bott s/t=17-38
13.	(Bowerman et al., 2002) An innovative steel/concrete construction system	This paper introduced bi-steel, reviewing its development and illustrating its typical application			
14.	(Clubley et al., 2003) Shear strength of steel–concrete–steel composite panels. Part I—testing and numerical modelling	Discussed the experimental and numerical analysis of the shear strength of each friction weld subject to push-out load (ANSYS)	12 specimens	Push-out	T= 6, 8, 10 mm Hc= 200-700 S= 25, 200
15.	(Clubley et al., 2003) Shear strength of steel–concrete–steel composite panels. Part I—testing and numerical modelling	Reported work that examined in detail the localised behaviour that affects panel shear strength. Stress distribution on the shear connector surface and through the plate thickness (ANSYS)			
16.	(Sohel et al., 2003) Experimental investigation of low-velocity impact characteristics of steel-concrete-steel sandwich beams	Investigation, quantitative and qualitative study on the effects of low-velocity hard impact on SCSS beams	45 beams	Impact (Drop weight) 43 kg from 1.5 m v=4.66 m/s 31 kg from 3.5 m v=6.5 m/s	W= 100, H= 50 L= 1200, T= 5 Shear connectors= 25x3x100@ 0-300
17.	(Liang et al., 2003) Local and post-local buckling of double skin composite panels	Investigated the local and post-local buckling behaviour of biaxially compressed plates restrained by shear connectors and concrete			B= 500 T= 10

No	Reference	Outcome	Member(s)	Loading	Dimensions
		in DSC panels by using the FE modelling technique (STRAND7)			
18.	(Xie et al., 2005) Experimental and numerical investigation on the shear behaviour of friction-welded bar–plate connections embedded in concrete	Presented experimental and numerical studies on the static behaviour of the friction-welded connections with the bar loaded in shear (ABAQUS)	24 specimens	(Static) Push-out	200 mm cubic concrete core T= 6, 10, 12, 15
19.	(Xie and Chapman, 2006) Developments in sandwich construction	Outlined research undertaken to establish design method for bi-steel beams under static and fatigue loading	36 beams Ref.	Ref.	Ref.
20.	(Zhao and Han, 2006) Double skin composite construction	Described (reviewed) behaviour of Concrete Filled Double Skin Tubes (CFDST) subjected to static and dynamic loads			
21.	(Xie et al., 2007) Static tests on steel–concrete–steel sandwich beams	Studied bi-steel beams under static load	18 beams	Static 2x100 tone – uniform across the beam	B= 400 Hc=200-300 T=6, 8, 12
22.	(Foundoukos et al., 2007) Fatigue tests on steel–concrete–steel sandwich components and beams	Described the fatigue tests conducted on bi-steel components and beams	18 beams	Central load	Hc= 400 T= 6,8,10,12 L= 1200-2400
23.	(Xie et al., 2007) Static tests on steel–concrete–steel sandwich beams	Presented summary of research about bi-steel subjected to static and fatigue loading	beams	Static and fatigue	D= 200-400 L= 1200-2400 W= 200-400 T= 6-12 s=200-300
24.	(Foundoukos and Chapman, 2008) Finite element analysis of steel–concrete–steel sandwich beams	ABAQUS			

No	Reference	Outcome	Member(s)	Loading	Dimensions
25.	(Liew and Sohel, 2009) Lightweight steel–concrete–steel sandwich system with J-hook connectors	Investigated the performance of SCS beams – ultra-lightweight – fibre – analytical	12 beams	Static point load	D= 80, L= 1200 W= 200-300 T= 4 j-hook= 10,16 s= 80-300 LWC=1400 kg/m3
26.	(Liew et al., 2009) Impact tests on steel–concrete–steel sandwich beams with lightweight concrete core	Studied the impact performance of SCSS beams consisting of a LWC core-------- J-hook		Dropping free weight 64 kg – h= 4m V= 8.14 m/s	D= 80, l= 1100 W= 200-300 T= 4 S= 100-300
27.	(Eom et al., 2009) Behaviour of double skin composite wall subjected to in-plane cyclic loading	Investigated the structural capacity of DSC walls – the seismic resistance of the walls including the load-carrying capacity and ductility was evaluated	3 isolated walls 2 coupled walls	Cyclic load	T= 10, 5.9
28.	(Liew and Sohel, 2010) Structural Performance of Steel-Concrete-Steel Sandwich Composite Structures	Investigated the flexural and impact performance of SCSS structures comprising a lightweight concrete core ... different types of shear connectors ..... plastic analysis	12 beams and 8 (2-way) slabs	Static and dynamic Central point	Hc= 80 L= 1000 W= 200-300 T= 4 J-hook= 10 or 16 1000x1000 slabs
29.	(Leekitwattana et al., 2010) An alternative design of steel-concrete-steel sandwich beam	Presented an alternative construction of SCSSB in which the new conceptual design of aligning the shear connector in the inclined direction is proposed			
30.	(Dai and Liew, 2010) Fatigue performance of lightweight steel–concrete–steel sandwich systems	Investigated the static and fatigue strength behaviour of a composite sandwich system, which consists of an LWC core ... interconnected by J-hook connectors. .... fibres --- analytical solution.....	12 beams	Static and fatigue 2-point load	L= 1200 W= 250 H= 92 Stud= 10, 100
31.	(Dogan and Roberts, 2010) Comparing experimental deformations of steel-	Compared experimental deformation results of SCSSB with full and partial interaction theories (exper. from Dogan's PhD thesis)	Ss beams	Point load	L= 1400 w= 200 Hc = 150 T= 8

No	Reference	Outcome	Member(s)	Loading	Dimensions
	concrete-steel sandwich beams with full and partial interaction theories				S= 200
32.	(Sohel and Richard Liew, 2011) Experimental investigation of low-velocity impact characteristics of steel-concrete-steel sandwich beams	Studying slabs containing J-hook connectors under static load – LWC and SFC	8 slabs	Central load	Hc= 80-100 L= 1200x1200 W= 200-300 T= 4-8 J-hook= 10 - 12
33.	(Dogan and Roberts, 2012) Fatigue performance and stiffness variation of stud connectors in steel–concrete–steel sandwich systems	Studying fatigue of push-shear specimens	6 specimens	50% of the max. shear capacity then 6 cycle/sec	Concrete blocks= 175x600x600 Steel section= RHS-8 Headed studs=10/ l= 150
34.	(Yan, 2014) Finite element analysis on steel–concrete–steel sandwich beams	Modelling SCS of previous studies using ABAQUS			
35.	(Yan et al., 2014) Experimental and analytical study on ultimate strength behaviour of steel–concrete–steel sandwich composite beam structures	Experimental and analytical study on SCS beams with different types of concrete, connectors and geometry	22 beams		Hc=50-100 W=100-250 T=4-12 Stud=10-13 S=100-300
Key: Hc: concrete core depth, W: width of the beam, T: steel plate thickness, L: span, S: stud spacing, V: velocity, Note: all dimensions are in mm.					

Chapter 3 The Experimental Programme

3.1 Introduction

The experimental programme mainly consists of three stages:

The first stage involves casting a conventional reinforced concrete joint to be used as a control specimen to monitor the general behavioural trend. This includes testing DSC beam-column joints in its basic design.

Based on the results of stage one, modifications to the basic design are introduced for further investigation in stage two.

Stage three presents some parametric studies depending on the results of stage two. All the details of these stages are presented in the methodology section. Moreover, all the geometrical and material properties of the experimental programme are presented in the remaining sections of this chapter.

3.2 Methodology

The attractive points in the double skin composite constructions are their simple geometry, construction speed and some other factors that are related to their structural behaviour, as reported by previous studies.

The current research started by testing a conventional reinforced concrete joint to monitor the general behaviour of the Double Skin Composite (DSC) beam-column joint. The first test was performed on the DSC joint in its basic design (referred to as DSC-Basic Design).

Based on the results of this test, the main problem raised was lack of anchorage for the tensile plate; therefore, it was decided to introduce the following three different methods to provide anchorage for the tension plate.

1. Add a normal steel reinforcement cage.
2. Weld steel bars to the plates.
3. Extend the beam plates to meet the back plate of the column.

Depending on the structural performance, manufacturing process, and cost, the Double Skin Composite joint with welded bars was chosen to study:

1. The effect of Steel Fibre on the behaviour of the composite joint.
2. The effect of High-Strength Concrete on the behaviour of the composite joint.
3. Efficiency of the Double Skin Composite beam-column joint under cyclic loading.

The flow chart shown in Figure 3-1 presents the summary of the development of the current study.

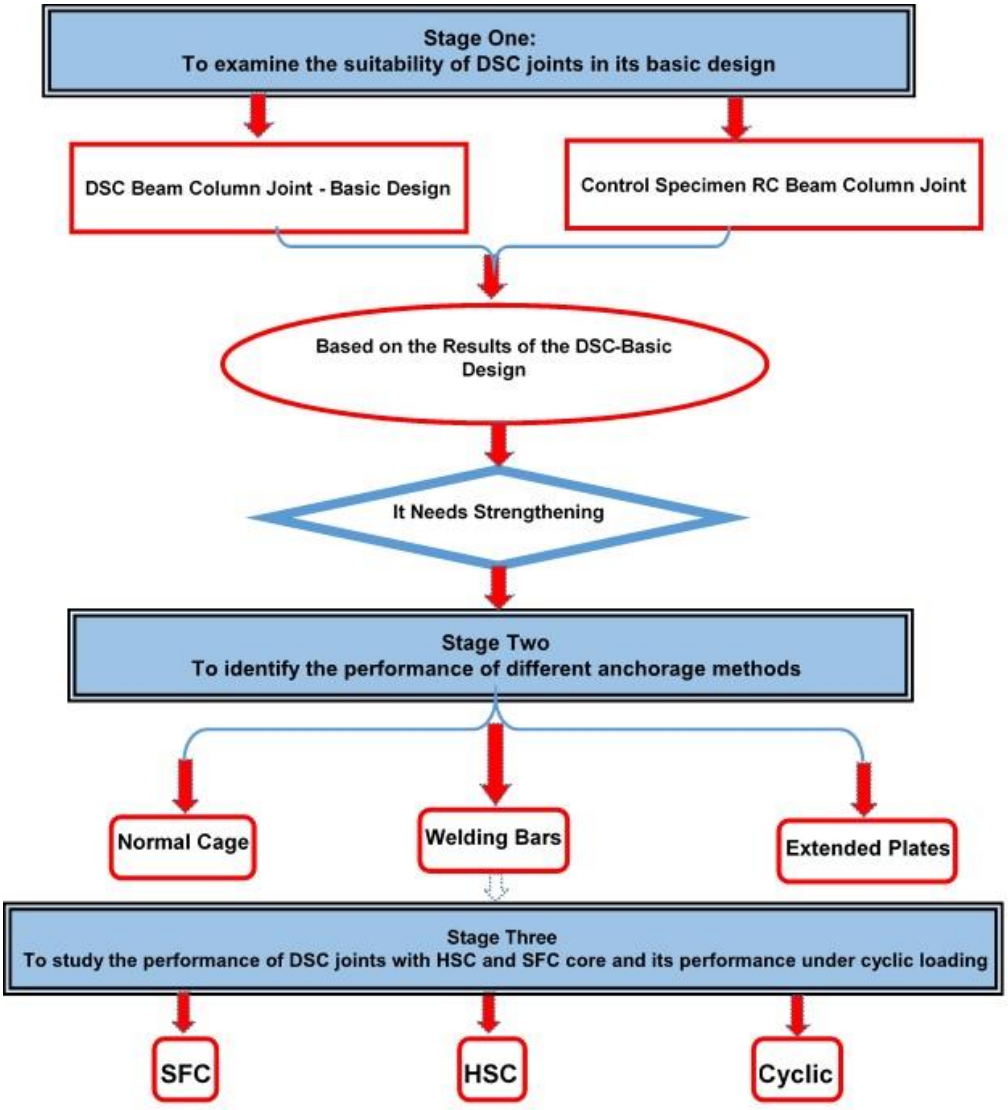

Figure 3-1: Development of the experimental programme

Table 3-1 summarises the test programme and shows the purpose of each test.

Table 3-1: Summary of experimental test purposes

Test	Purpose of the Test
RC Joint	To be used as a reference for the general behaviour of the DSC joint.
DSC-No Modification	To examine the efficiency of the DSC joint in its basic design. Furthermore, to identify the problems and to develop corresponding solutions and ideas.
DSC-Normal Cage	To study the effect of conventional reinforcement on the anchorage efficiency.
DSC-Ext Pl	To study the effect of conventional reinforcement on the anchorage efficiency.
DSC- Weld	To study the effect of extending the steel plate on the anchorage efficiency.
DSC- SF-1%	To identify the effect of steel fibres on the DSC joint's behaviour.
DSC- SF-0.25	
DSC- HSC	To examine the effect of increasing concrete compressive strength.
DSC-Cyclic	To study the efficiency of the DSC joint under a cyclic loading.

The reinforced concrete beam-column joint was designed with a low flexural beam reinforcement ratio $\rho = 0.25\rho_{max}$ according to the ACI 318 code in order to ensure the failure of the beam in flexure. The joint was tested under monotonic loading to represent the reference joint for the double skin composite joint by having similar dimensions in each joint, support the conditions and loading scheme. Beam details are $b = 200mm, h = 300mm,$ and $clear\ span = 1250mm$ and the column details are $b = 200mm, h = 250mm,$ and $column\ height = 1500mm$.

The Double Skin Composite beam-column joints of the basic design consisted of a steel plate of thickness $= 8mm$ and concrete core of $284mm$ in the beam and $234mm$ in the column with J-hook shear studs of $10mm$ in diameter welded to the inside face of the plates and spaced at $100mm.$ Recommended

(Narayanan et al., 1994) values of the stud spacing to plate thickness ratio $(s/t \leq 40)$ and stud diameters to plate thickness ratio $(1.0 \leq d/t \leq 2.5)$ were used.

The materials' basic properties – such as concrete compressive strength, concrete tensile strength, steel bar properties and steel plate properties – were measured according to the EC requirements.

Deflection in the beam and steel plate strains were measured at different locations, and crack initiation and development was monitored in order to evaluate the response of the joint and to collect sufficient information for the finite element modelling. The loading point was located at $100mm$ from the free end of the beam. Assessment of the response of the double skin composite joint is based on the load deflection and failure mechanism in order to introduce the alternative design ideas.

3.3 The RC Joint under Monotonic Loading

A reinforced concrete assembly was cast using normal weight (NWC) with a 28 days' compressive strength of 40 N/mm^2. Figure 3-2 shows the beam-column joint detail; the cross-section dimensions of the beam are 200x300 mm and 200x250 for the column. The column height is 1500 mm and the beam span is 1250 mm. The beam was reinforced with 3B12 mm for longitudinal reinforcement, top and bottom, as well as B8 mm links spaced at 100 mm c/c. The column's longitudinal reinforcement is 4B16 mm and B8 mm links are spaced at 100 mm c/c.

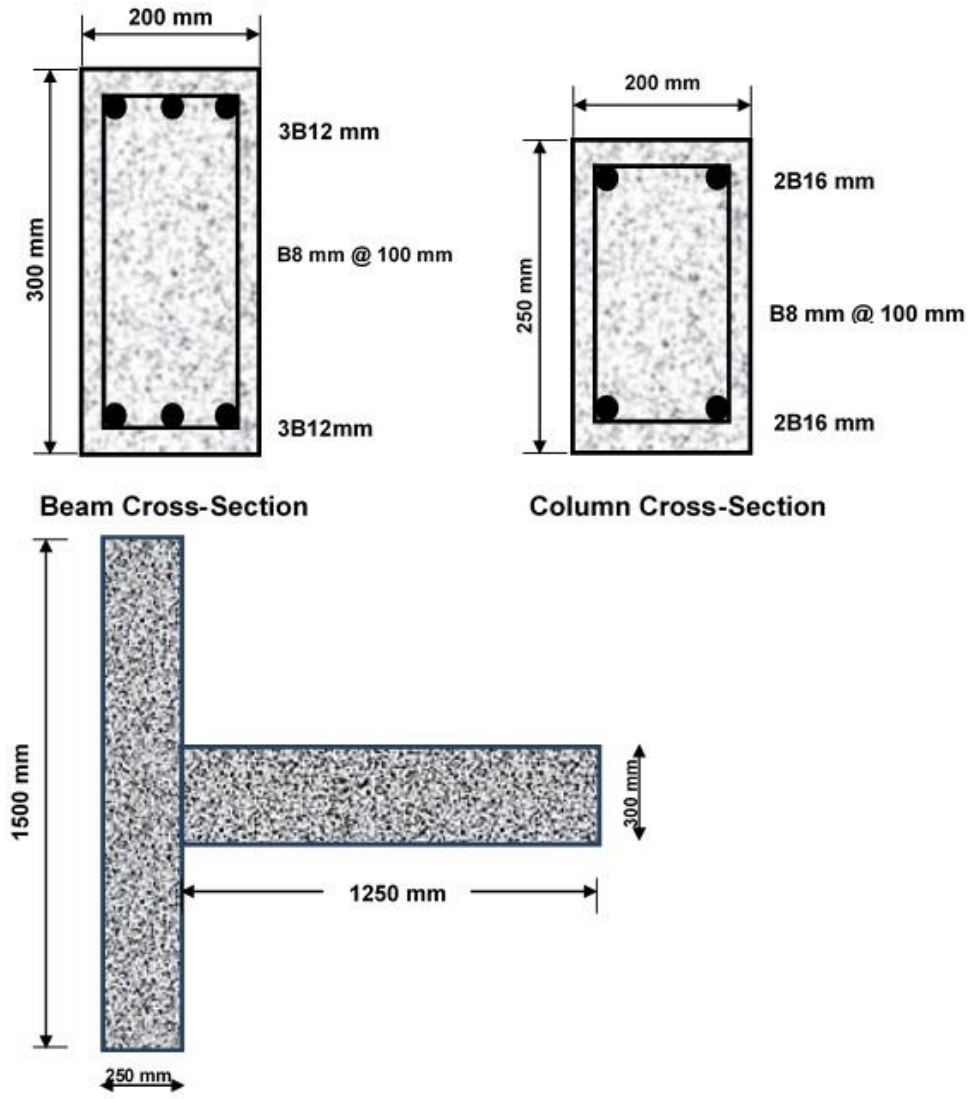

Figure 3-2: Reinforced concrete beam-column joint

3.4 Double Skin Composite Joint – Basic Design

As shown in Figure 3-3 and Photo 3-1, the double skin composite joint consists of steel plates of 8 mm in thickness on the top and bottom faces of the beam and on the front and back faces of the column. J-hook connectors of 10 mm diameter are welded onto the inside faces of the plates spaced at 100 mm in two rows in the longitudinal direction of both the beam and the column. These J-hook connectors are interconnected and embedded in the concrete to produce the composite action. Concrete is poured inside the plates that formed a mould and this is considered one of the benefits of the double skin members.

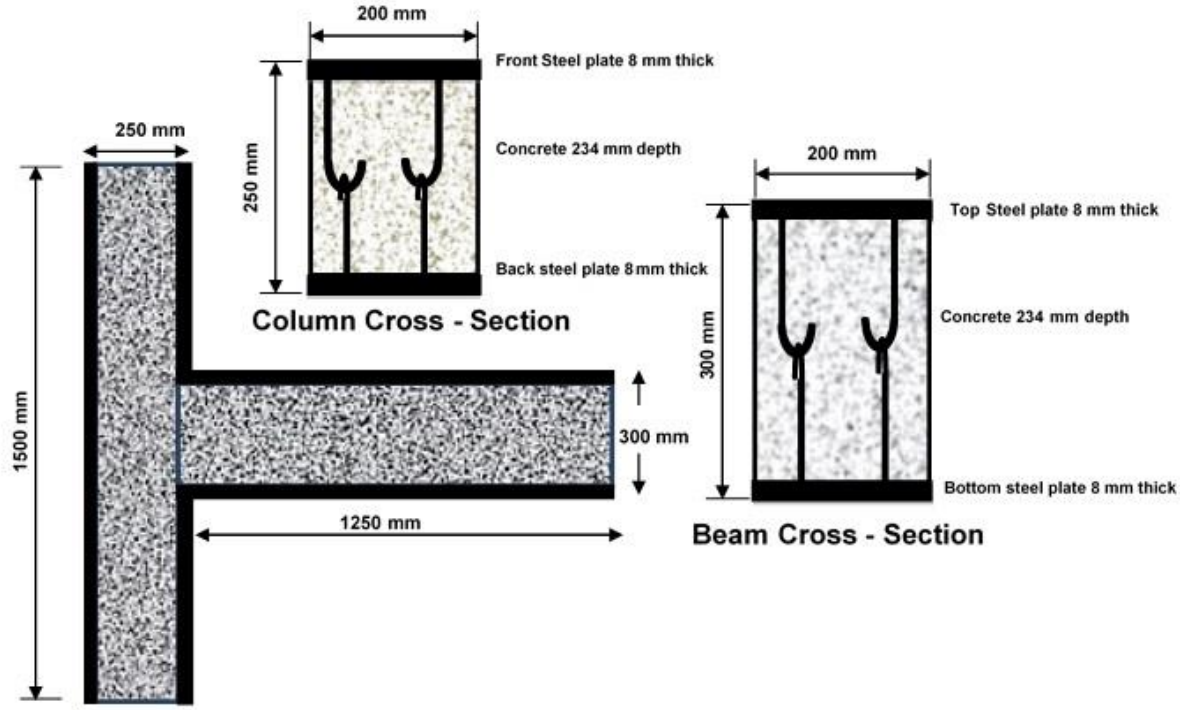

Figure 3-3: SCS beam-column joint – basic design

Photo 3-1: SCS Joint Studs and Plate

The skin plates of the beam and the column have been welded according to the American Welding Society structural welding code (AWS, 2006), and prequalified joints are shown in Figure 3-4 and Photo 3-2. Continuous

monitoring during tests indicated that the chosen welding arrangement performed well.

Photo 3-2: Welded joint of the steel plate

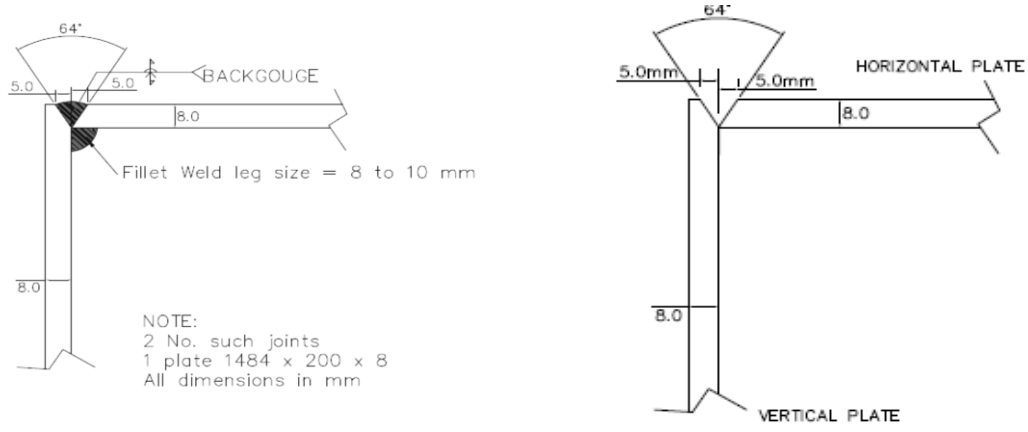

Figure 3-4: Welded joint of the steel plates

3.5 Welding of J-hooked Connectors

In composite constructions, there are many types of shear connectors, as discussed previously. In double skin composite constructions, there are three main types of shear connectors: the conventional shear connectors, friction-welded connectors (as in bi-steel) and the J-hooked connectors that are presented by Liew and Sohel (2009). The main advantages presented by the J-hooked connectors are:

1- There are no limitations on the thickness of the members and they can be as thin as 50 mm compared to 200 mm in bi-steel (Liew and Sohel, 2009; Liew et al., 2009).

2- As the J-hooked connectors are interconnected, no separation can occur until failure of the welding of the connectors or the connector itself takes place (Liew et al., 2009).

3- A modified welding machine is used to weld J-hooked connectors onto the steel plates. The stud chuck is adjustable in order to hold different stud lengths (Photo 3-3). The welding machine and the studs (straight studs) have been supplied by Advanced Stud Welding Systems Ltd. The J-hooked connectors have been cut and bent in the desired dimensions using the power-bending machine available in the concrete lab. These connectors were chosen for the current study due to their efficiency in maintaining the structural integrity under both static and dynamic loading conditions (Liew and Sohel, 2010).

Photo 3-3: J-hooked connector welding

3.6 Modified Double Skin Composite Joints

3.6.1 Double Skin Joint with Normal Steel Reinforcement

The first modification to treat anchorage leak in the double skin joint was made by adding a normal steel reinforcement to the core region, as shown in Figure 3-5. The reinforcement is located in a region at a distance of 300 mm from the face of the column and 300 mm above and down the faces of the beam. The beam was reinforced with 3B12 mm links, top and bottom, as well as B8 mm links spaced at 100 mm c/c. The column reinforcement was 4B16 mm for the main bars and B8 mm links spaced at 100 mm c/c.

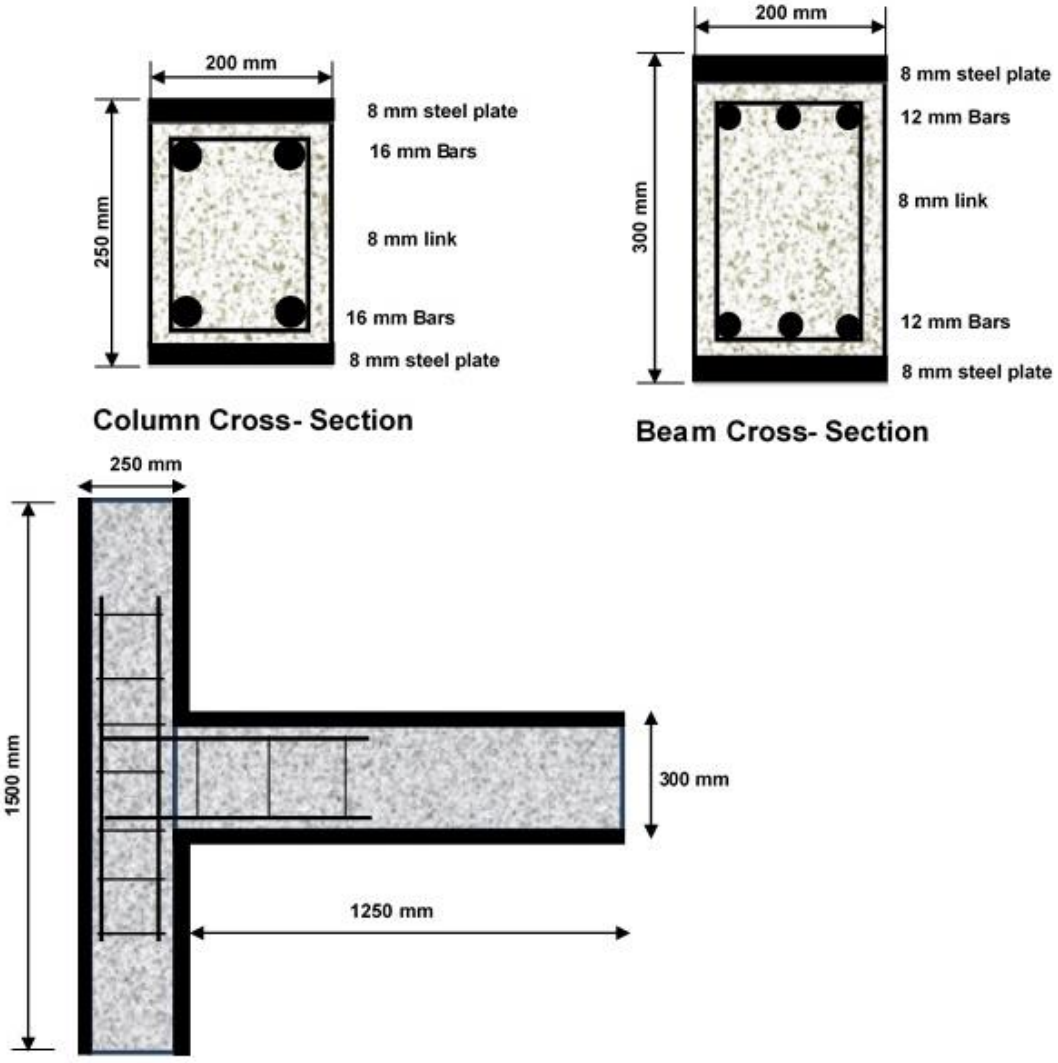

Figure 3-5: SCS joint with normal reinforcement

3.6.2 Double Skin Joint with Welded Steel Reinforcement

The second modification used the same steel reinforcement in the double skin joint with normal reinforcement, except that the steel bars of the beam were welded onto the top and bottom plates and no shear links were used in the beam, as shown in Figure 3-6.

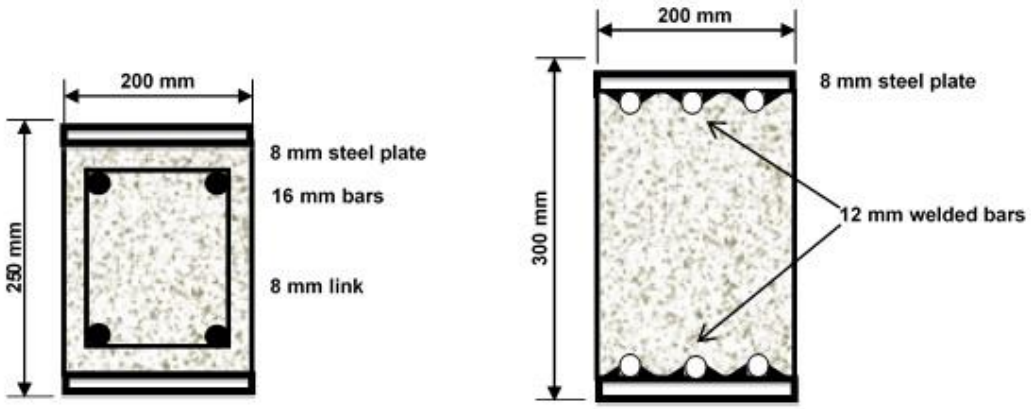

Figure 3-6: SCS joint with welded bars

3.6.3 Double Skin Joint with Extended Plates

A third method to provide anchorage for the tension plate was by extending the plate to meet the inner face of the back plate of the column, as shown in Figure 3-7. Angles of 75x75x5 mm and bolts of M16 were used to connect the plates. A standard universal column section (UKB254X146X43) was used to prevent/reduce rotation in the front plate.

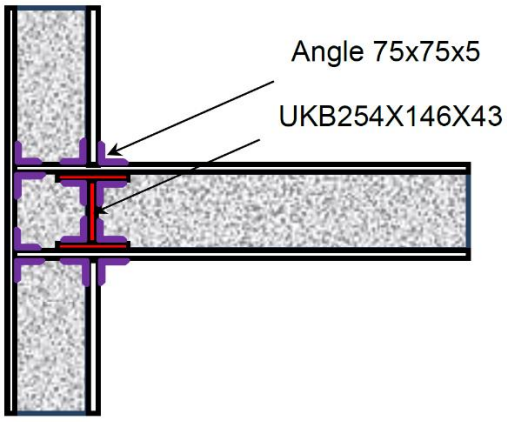

Figure 3-7: SCS joint with extended plate

3.7 Test Arrangement and Loading

In order to perform the experimental part of the current study, two reinforced concrete beam-column joints and 11 double skin composite joints were prepared, cast and tested at full-scale size. The test frame and supports are shown in Photo 3-4.

The test rig consists of two columns and a horizontal beam, all of which were made of composite sections (channels and plates). Bracing bars were used to keep horizontal movements to a minimum. Horizontal and vertical movements were monitored by using LVDTs (Linear Variable Differential Transformers) in different positions on the testing rig. 20M bolts and plates of 20 mm in thickness were used to support the beam-column joint on the column; four bolts were used in the tension region and two in the compression region.

A plate of 200x200x20 mm was used to transfer the load from the hydraulic jack to the end of the beam. The capacity of the hydraulic jack was 500 kN. The tests were performed using displacement control with a loading rate of 0.1 mm/min at the beginning of the test in order to capture the first crack formation. After the crack appearance, the loading rate increased to 0.5 mm/min until the maximum load capacity of the tested specimen was reached, then it increased to 1 mm/min and maintained this up to failure. The loading process continued until the complete collapse of the specimen.

Photo 3-4: Test frame and supports

3.8 Measurements and Data Processing

Deflections were measured using LVDTs at two positions on the beam: under the loading centre (100 mm from the free end of the beam) and at the mid-way point of the beam span (625 mm from the free end of the beam). The deformations of the column were measured at two positions; they were placed 100 mm above and below the beam face on the back of the column in order to monitor the rotation of the joint.

Strains of concrete were measured using DEMEC Points spaced at 150 mm on both sides of the beam and the column. Steel bar and steel plate strains were measured using 5 mm electrical strain gauges. In the reinforced concrete specimen, the strain gauges were placed on the steel reinforcement at 50 mm from the face of the column and the face of the beam. The strain gauges were fixed on the bars after fining and chemical treatment of the surface, and, after wiring, they were protected using special compressible foam to cover the entire length of the strain gauge.

A data logger was used to record output data of the test results to the computer every 5 seconds as a Microsoft Excel sheet.

3.9 Material Properties

3.9.1 Mixing and Curing Water

According to (EN, BS 1008 2002) *"water supplied as potable is deemed to conform [to] the requirements in this standard"*. Clean tap water, which was free from impurities such as oil and suspended matter, was used for mixing and curing.

3.9.2 Cement

Ordinary Portland Cement (OPC) strength class 52.5 N was used in the casting of all the tested specimens. The cement was supplied in waterproof bags of 25 kg and stored in good conditions so that it would not be affected by other atmospheric conditions and/or humidity. According to the supplier's certificate, the cement conformed to (EN, BS 196-2 2013).

3.9.3 Coarse and Fine Aggregate

Natural Coarse aggregates of sizes 20 mm and 10 mm were used in all tests, except in the specimens that were cast using high-strength concrete, which had a 20 mm aggregate size. The coarse aggregate was supplied to the casting shop's storage containers and dried locally.

River sand that had been washed, and which was clean and free from organic and clay matter was used to produce concrete mixes for all specimens.

3.9.4 Steel Fibres

Round hooked-ends Dramix steel fibres were used to improve concrete properties and to study the effect of this improvement on the structural behaviour of the double skin composite joint. Adding steel fibres highly affects both the fresh and hardened states of concrete; workability is affected inversely by the amount of fibres in the mix, and it is recommended not to exceed 2% by volume to maintain the workability. The main function of the fibres is to improve the concrete properties other than strength, such as ductility (energy dissipation ability), toughness, durability, fatigue, shrinkage resistance, and failure modes (Bentur and Mindess, 2006; Tadepalli et al., 2009).

The properties of steel fibres that were used in the experimental tests are presented in Table 3-2.

Table 3-2: Steel fibre properties

Fibre length	35 mm	Diameter	0.55 mm
Tensile strength	1345 N/mm2	Young's modulus	210000 N/mm2
Aspect ratio	63	Volume fraction	1% and 0.25%

3.9.5 Silica Fume

To study the effect of increasing the compressive strength of the double skin composite joint, a high-strength concrete was used to cast two specimens. In order to produce a concrete with a compressive strength of 100 MPa or more, most cement types need silica fume to be added to the mix (Aïtcin, 2011). Silica fume is a by-product of silicon and Ferro silicon. It is available in water

slurry, a very fine powder form (about 100 times smaller than cement grains), or blended with Portland cement in some countries. It is usually used in a dosage of 3 to 10% due to the high amount of superplasticiser needed, and if the dosage exceeded 10%, not all the silica fume would be located in the aggregate-cement paste interface (Neville, 2011; Aïtcin, 2011).

3.9.6 Superplasticiser

In the current study, two composite specimens were cast using concrete with steel fibres and two composite joints were cast using high-performance concrete (silica fume was used to achieve the desired compressive strength). Adding steel fibres and/or silica fume to the concrete mixes highly affects the fresh concrete properties, mainly the workability. Therefore, it is important to use mixtures to reduce or keep the water cement ratio within a specific range. The amount of superplasticiser to include was identified by using trial mixes.

3.9.7 Fly Ash (PFA)

Since fly ash is a by-product of coal burning in an electric power plant, it is highly affected by the chemical, physical, and mineralogical properties of the coal. Also, the burning conditions in the power plant affect the properties of the fly ash. It can be classified into low calcium content fly ash (less than 8% Cao), intermediate calcium content (Cao 8% to 20%) and high calcium fly ash (Cao more than 20%). Adding fly ash to concrete can reduce bleeding and drying shrinkage as it helps to make the surface finishing easier and presents about a 1 hour retarding effect (Neville, 2011; Thomas, 2013).

3.9.8 Mixing, Casting and Curing

Normal weight Concrete (NC) with f_{cu} of 40 N/mm^2, High-Strength Concrete (HSC) with f_{cu} of 90 N/mm^2 and Steel Fibre Concrete (SFC) with f_{cu} of 40 N/mm^2 were used to cast the specimens. The final mixture was based on trial mixes to reach the most suitable component proportions, as presented in

Table 3-3.

A horizontal rotary-type mixer with a capacity of 600 kg was used to mix the concrete for all specimens. Since each specimen needed more than 500 kg of concrete, the casting was carried out in two batches to avoid taking the

mixer to its maximum capacity. The workability was measured according to (BS EN 12350-2:2009).

One of the advantages of double skin composite members is the usage of the plates as a form or part of the form. In the current study, a T-shape of plywood was used as a base for the specimens and a set of steel brackets were welded to the outer faces of the plates and bolted to the wooden base.

A poker vibrator was used to vibrate the concrete in the specimen and a vibrating table was used for the samples (cubes, cylinders, and prisms). After casting, the specimen and the accompanying samples were covered with polyethylene to prevent drying and shrinkage, and curing started after 24 hours using two layers of damp hessian covered by polyethylene.

Table 3-3: Concrete mix proportions

Constituents	Plain Concrete	HSC	1% SFC	0.25% SFC
Water (kg/m^3)	193	145	184	184
Cement (kg/m^3)	250	468	238	238
PFA (kg/m^3)	107	-	102	102
Fine Aggregate (kg/m^3)	695	719	660	660
Coarse Aggregate (10 mm) (kg/m^3)	680	-	646	646
Coarse Aggregate (20 mm) (kg/m^3)	453	1070	431	431
Superplasticiser (kg/m^3)	-	7.8	1.104	1.104
Steel Fibre (V_f)	-	-	1%	0.25%
Silica Fume (kg/m^3)	-	52	-	-

3.9.9 Cubes, Cylinders and Prisms

Each test included at least three cubes, cylinders and prisms as control samples in order to determine concrete properties. The desired compressive cube strength was 40 N/mm^2 and, since the behaviour of the beam-column joint was mainly subjected to tensile stresses, no great attention was given to the slight variation in compressive strength (10 to 15% over 2 years). Cubes of 100 mm were used to find the cube compressive strength, a cylinder of 300 mm height and 150 mm diameter was used to find the compressive strength and split stress, and prisms with dimensions of 100x100x500 mm were used to find the flexural strength. The samples were tested according to EN (BS

12390-3 2011) and EN (BS 12390-5 2009) and the average test results are presented in

Table 3-4 below, which shows the average of three samples or more. The variation in the results of the compressive strength and in the modulus of rupture was expected because of the long period of the experimental programme, which was about three years. Many factors can affect the development of concrete strength, such as the water-cement ratio, aggregate's physical and chemical properties, age, vibration method and time as well as the test method, especially the compressive strength of the cylinders.

Table 3-4: Summary of average concrete properties

Specimen	Age at Test (days)	Cube Comp. N/mm^2	STD	Cylinder Comp. N/mm^2	STD	MoR N/mm^2	STD
RC Joint-1	28	41.44	0.27	33.77	0.48	4.42	0.64
RC Joint-2	29	42.73	0.33	30.74	0.94	4.34	0.24
DSC-No Modification	28	42.76	0.65	32.98	1.03	4.26	0.42
DSC-Normal Cage	28	38.52	0.24	30.73	0.79	4.10	0.36
DSC-Ext Pl	29	41.14	0.52	31.39	0.88	3.85	0.64
All the DSC beam-column joints below contain welded bars at the top and bottom plates, as detailed in section 3.6.2							
DSC- Weld-1	29	43.24	0.40	32.47	0.76	3.94	0.89
DSC- Weld-2	35	40.71	0.48	31.54	1.20	3.71	0.19
DSC- SF-1%	29	41.21	0.62	30.96	1.28	5.43	0.54
DSC- SF-0.25	28	41.75	0.52	-	-	5.00	0.28
DSC- HS-1	42	93.96	0.70	92.57	0.40	5.68	0.66
DSC- HS-2	42	95.09	0.17	-	-	6.37	0.49
DSC-Cyclic-1	38	44.76	0.35	31.86	0.64	4.29	0.60
DSC-Cyclic-2	39	43.44	0.86	32.76	0.93	-	-

Figure 3-8 shows the stress-strain curve of normal concrete, fibrous concrete with 1% and high-strength concrete under compression up to failure.

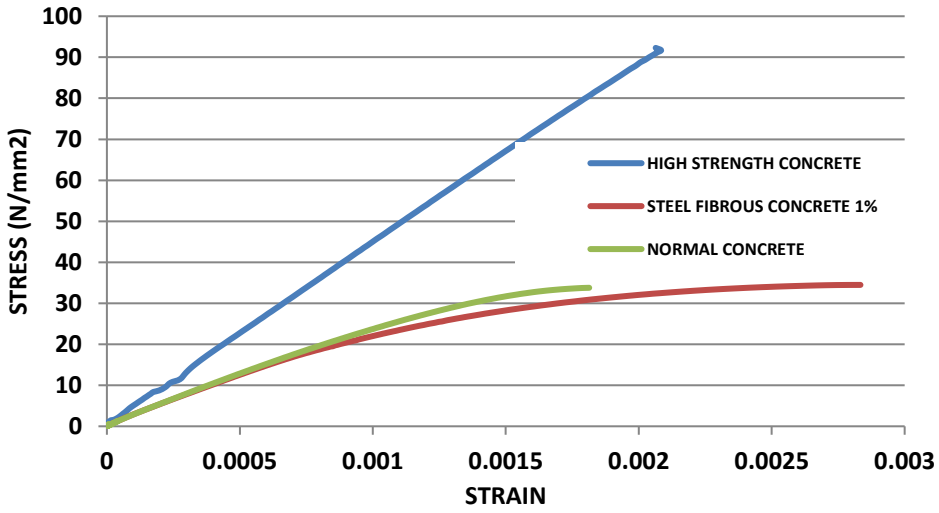

Figure 3-8: Stress-strain of NC, SFC and HSC under compression

3.9.10 Steel Tensile Tests

All the steel parts used in manufacturing the tested specimens, i.e. the steel reinforcement, steel plate, and stud connector, were tested under uniaxial tension according to ISO6892-1:2009 (2009). Photo 3-6 shows the prepared samples and the testing machine during the test.

Photo 3-5: (a) Prepared samples of plates and reinforcing bars and (b) tensile test machine

The averages of three samples or more were used to find the physical properties of the tested samples, as shown in Figure 3-9 and the summary in Table 3-4.

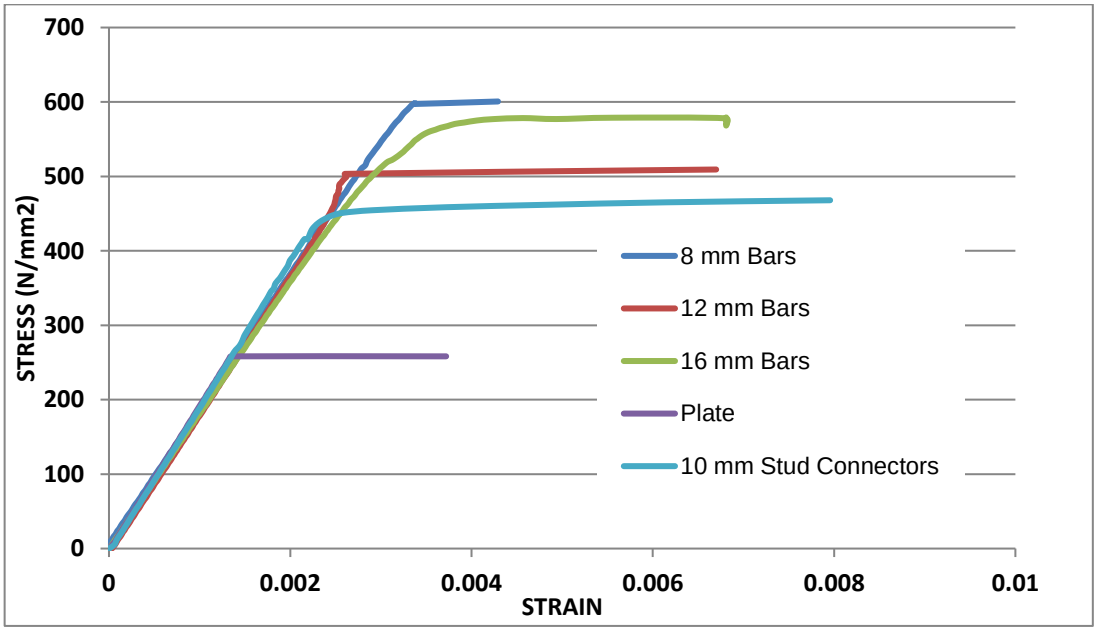

Figure 3-9: Stress-strain of steel

Table 3-5: Steel properties

Member	Yield Stress (N/mm^2)	Yield Strain	Ultimate Strain
8 mm Steel Bar	598	0.0034	0.173
12 mm Steel Bar	503	0.0026	0.205
16 mm Steel Bar	578.8	0.0036	0.230
8 mm Steel Plate*	258	0.0014	0.372
10 mm Stud*	450	0.0026	0.171

3.10 Summary

This chapter has presented all the details of the experimental programme for the tested specimens and the methodology used for the study. The procedure for setting up the experiment was described as well, as was the number of specimens to be tested under loading conditions. Also, the procedure for measuring and obtaining data from the investigation was set out. In addition, a summary of the material properties (steel, concrete, steel fibres, etc.) used for the study was presented. Geometric descriptions of the specimen components were presented for each specimen to be tested. Detailed material properties for each of the specimens were also presented and referenced.

The experiments included tests of reinforced concrete joints as well as double skin composite joints under monotonic and quasi-static.

The concrete core of the double skin composite joint was cast using three types of concrete, plain concrete, steel fibre concrete, and high-strength concrete, in order to study the effect of concrete properties on the behaviour of the composite joint.

Chapter 4 Results of Tests and Discussion

4.1 Introduction

In the present chapter, the experimental results will be presented and discussed in detail. First of all, the detailed behaviour of each specimen will be presented individually; this will be followed by a comparison between the responses of the tested specimens.

The experimental programme included three stages. The first stage involved testing: a reinforced concrete joint; a Double Skin Composite (DSC) joint in its basic design; a double skin composite joint with normal reinforcement; a double skin composite joint with welded bars; and a double skin composite joint with extended plates. In the second stage, a double skin composite joint with welded bars was used to study the effect of a steel fibre and high-strength concrete on the behaviour of the composite joint. The behaviour of the double skin composite joint cast with normal plain concrete under a cyclic load was tested in stage three.

4.2 Stage One

4.2.1 Reinforced Concrete Joint under Monotonic Loading

As stated in Chapter three, the load was applied at the end of the beam and controlled by displacement in order to capture the first crack formation. The first crack (Photo 4-1) was observed on the top of the beam at the beam-column junction, i.e. at the maximum bending moment region, at a load of 11.6 kN, which corresponded to a displacement of 1.06 mm below the load. A small change in the slope of the load-deflection curve can be seen in Figure 4-1, which reveals the reduction in the stiffness of the beam-column joint after cracking. The load-deflection relationship is linear up to 10 kN, with a change in slope beyond 10 kN up to 37 kN. It is obvious that there are some changes in the slope and these reflect the successive cracking of the concrete. After this load, the behaviour showed high nonlinearity because of the severe cracking of the concrete as well as the yielding of the tension steel and tension stiffening effects, as shown in Figure 4-2.

The current reinforced concrete joint had a tension reinforcement of ρ=0.6% and the observed behaviour was expected because of the low reinforcement ratio which resulted in the tension failure. The maximum load was 47 kN, which corresponds to the ultimate strain in the top steel of the beam. It is worth mentioning that the electrical strain gauges which were used to measure the steel strains in the beam reinforcement were located 50 mm away from the column face; i.e. they were not located exactly at the critical section but it can be said that they were close enough.

After a load of 46.7 kN and deflection of 45.7 mm, it can be seen that strains of the steel reinforcement decreased, which indicates the damage of the bond between the steel and the concrete.

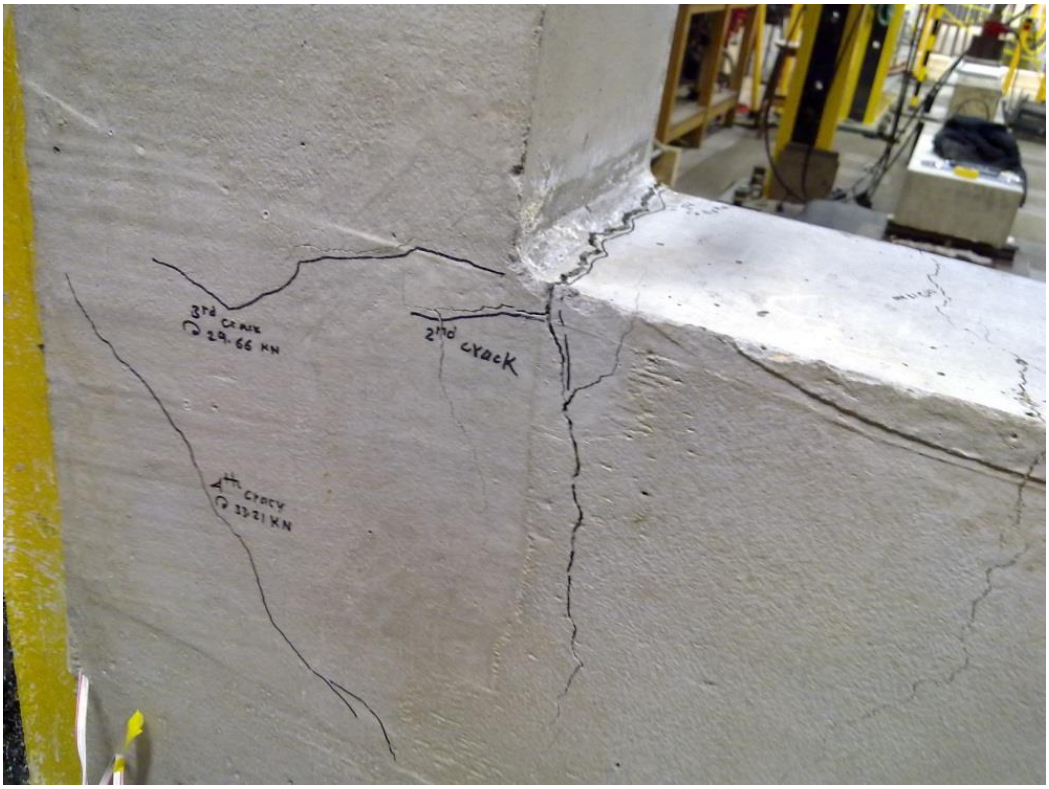

Photo 4-1: Cracking in the RC Joint

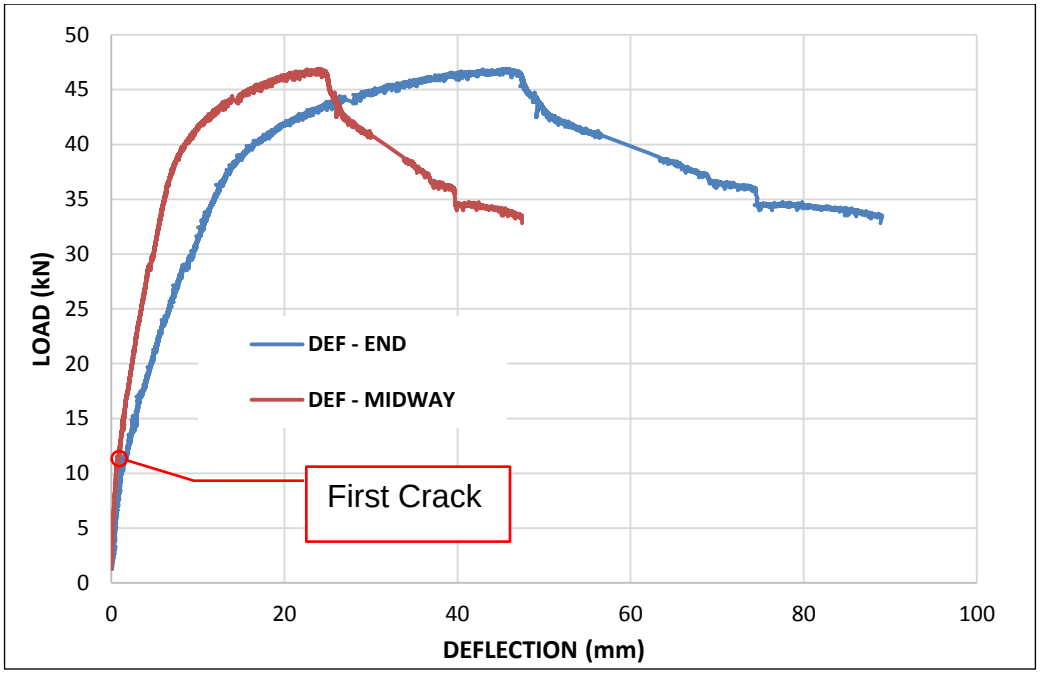

Figure 4-1: Load-deflection curve of the RC joint

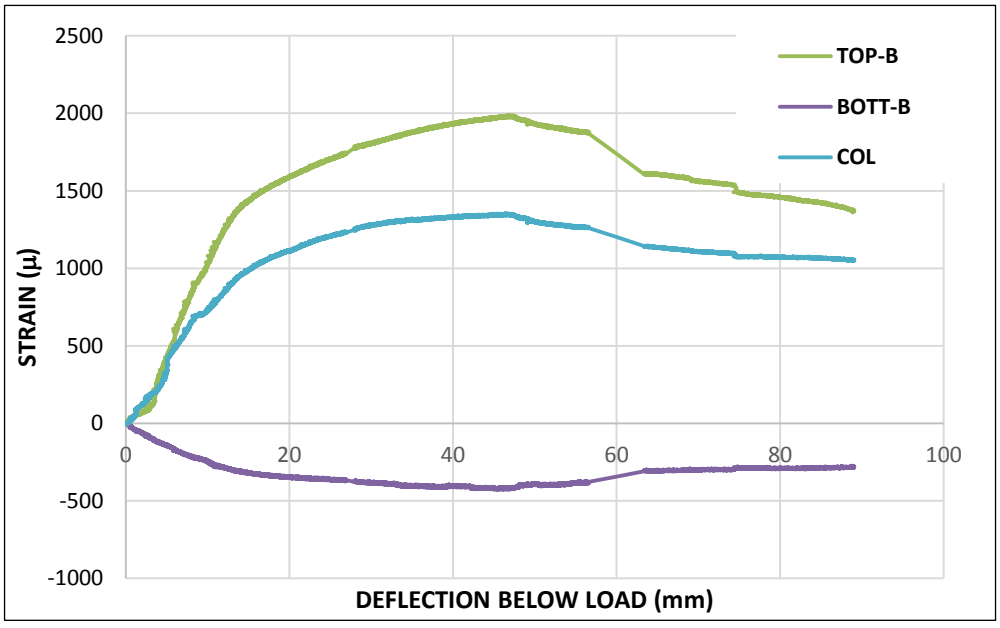

Figure 4-2: Stresses in the steel reinforcement of the RC Joint

4.2.2 Double Skin Composite Joint – Basic Design

The first test of double skin composite joints included a plated joint without any modifications, i.e. no welded or normal steel reinforcement has been added. From this test, the effect of the plates and the studs on the performance of the joint can be studied.

The test was performed by applying the load at the end of the beam at 1150 mm away from the column face; this load had been controlled by displacement at a loading rate of 0.1 mm/min. Before starting the test, it was decided to apply a seating load of 10 kN to eliminate any possible movement in the testing rig; however, unfortunately, the specimen cracked at the critical section of the beam in the mid-height of the column when the load reached 8.94 kN. It is obvious from the load-deflection curve shown in Figure 4-3 that the behaviour was linear up to the cracking load, and this was followed by a sudden drop in the load from 8.86 kN to 5.5 kN. The loading continued and when the load reached 10 kN, the specimen was removed and reloaded after checking the testing rig. After resuming loading, as shown in Figure 4-3 (red curve), the behaviour exhibited less stiffness, which can be attributed to the cracking in the previous stage. When the load reached 10 kN, a sudden drop in the load to 6.8 kN happened due to failure in one of the column studs of the first pair at the interface region with the plate, i.e. welding failure.

An increase in the load carrying up to 9.88 kN followed by a severe drop in the load due to failure of the second stud of the first pair of studs was accompanied by a widening in the flexural crack in the beam, while the crack in the column was not affected. After this stud's failure, the behaviour of the specimen showed very low stiffness compared to the first stage and its response was completely dependent on the connection (welding) between the top plate of the beam and the top plate of the column. No slip between the plates and the concrete was observed. In addition, no buckling in the compression plate was noted.

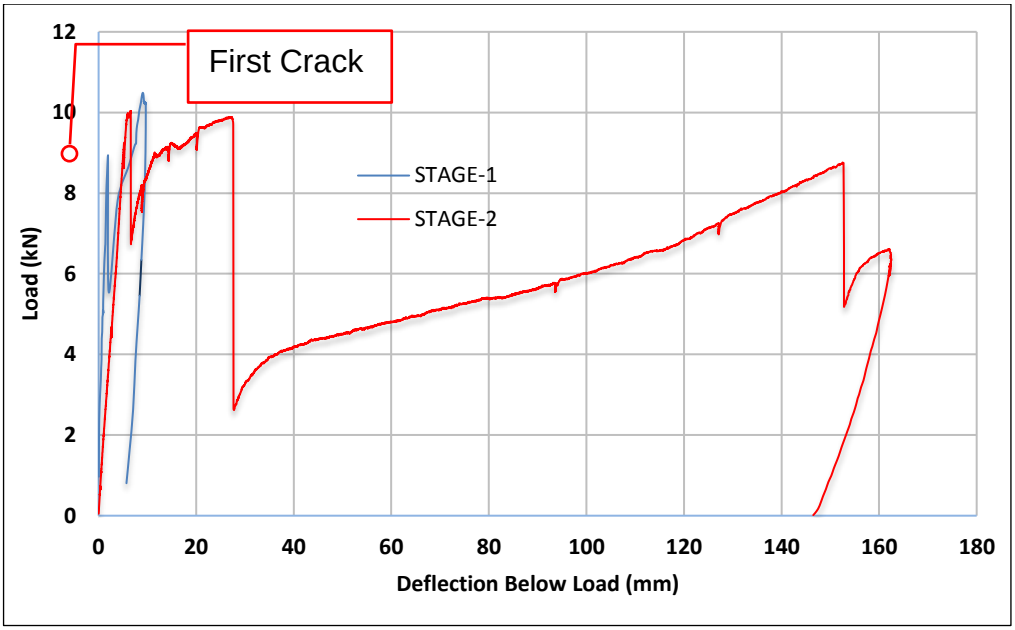

Figure 4-3: Load-Deflection of the SCS joint – basic design

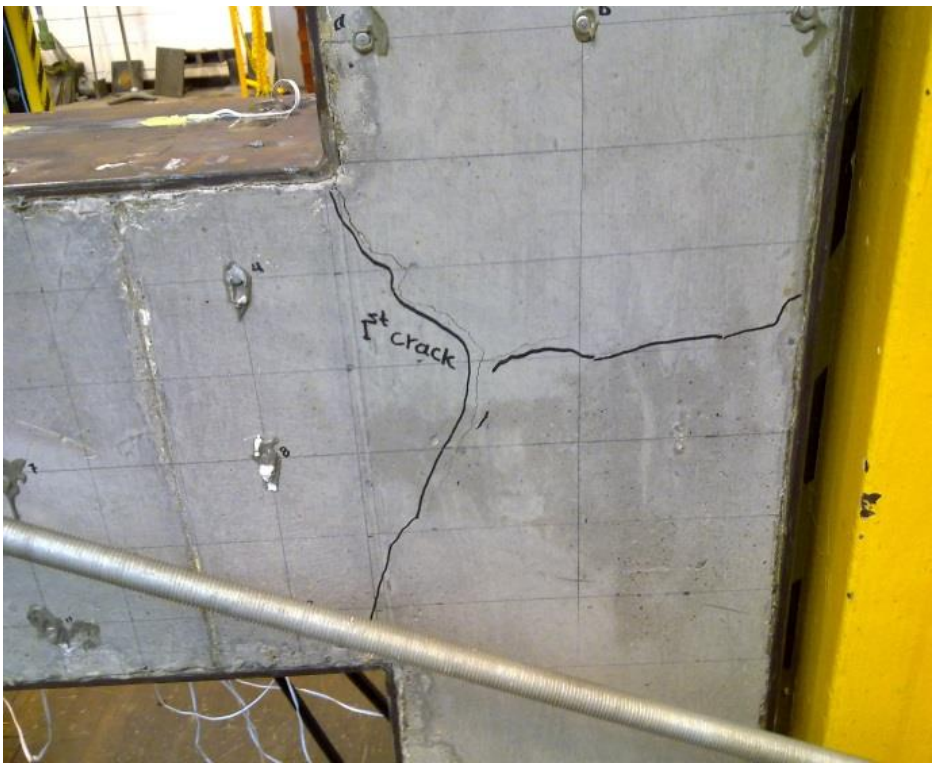

Photo 4-2: First crack in the SCS joint – basic design

Photo 4-3: Final failure in the SCS joint – basic design

4.2.3 Double Skinned Composite Joint – Normal Reinforcement

A normal reinforcement has been added to this specimen in the critical region of the joint, where the reinforcement consisted of 3B12 mm for the beam in the top and the bottom as well as B8 mm links spaced at 100 mm c/c. The column was reinforced with 4B16 longitudinal bars and links of B8 mm spaced at 100 mm. The reinforcement was placed in the junction of the beam column and extended in the column 300 mm from the face of the beam in both directions. The reinforcement of the beam started from the junction and extended in the beam to 300 mm from the face of the column. This reinforcement was identical to that used in the reinforced concrete specimens and would reflect the effect of the skin plates and the shear studs on the performance of the beam-column joint.

The load was applied under displacement control with a loading rate of 0.1 mm/min and increased as the test progressed after most of the cracks had developed, i.e. when the specimen approached the stabilised cracking phase. The first crack appeared at the critical section for bending and at the junction

region between the beam and the column when the load was 10.5 kN and the displacement below the load was 1.7 mm (Photo 4-4).

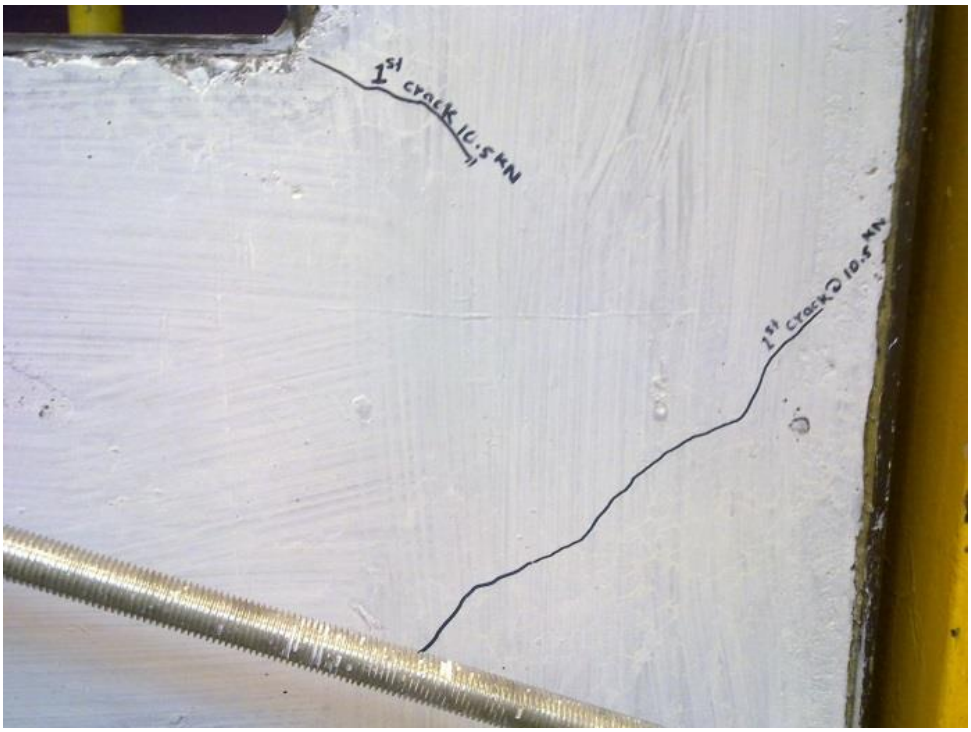

Photo 4-4: First crack in the SCS joint with normal reinforcement

From the load-deflection curve shown in Figure 4-4, it is obvious that the behaviour was linear between two regions, from the starting point to the first crack's appearance and between the first crack to the load of 44.31 kN, which corresponded to the displacement of 14.1 mm. The effect of the successive cracking can be seen on the load-deflection curve where the small variations in the curve represent the crack formation.

When the load reached the maximum load of 53.9 kN, it decreased gradually, which revealed the elongation in the stud welding region before the failure which happened when the load was 53 kN (Photo 4-5) and which was followed by a drop in the load to 48 kN. Without a large increase in the load, the second welded stud of the first row in the column failed, which resulted in another fall in the load, from 48 kN to 42 kN.

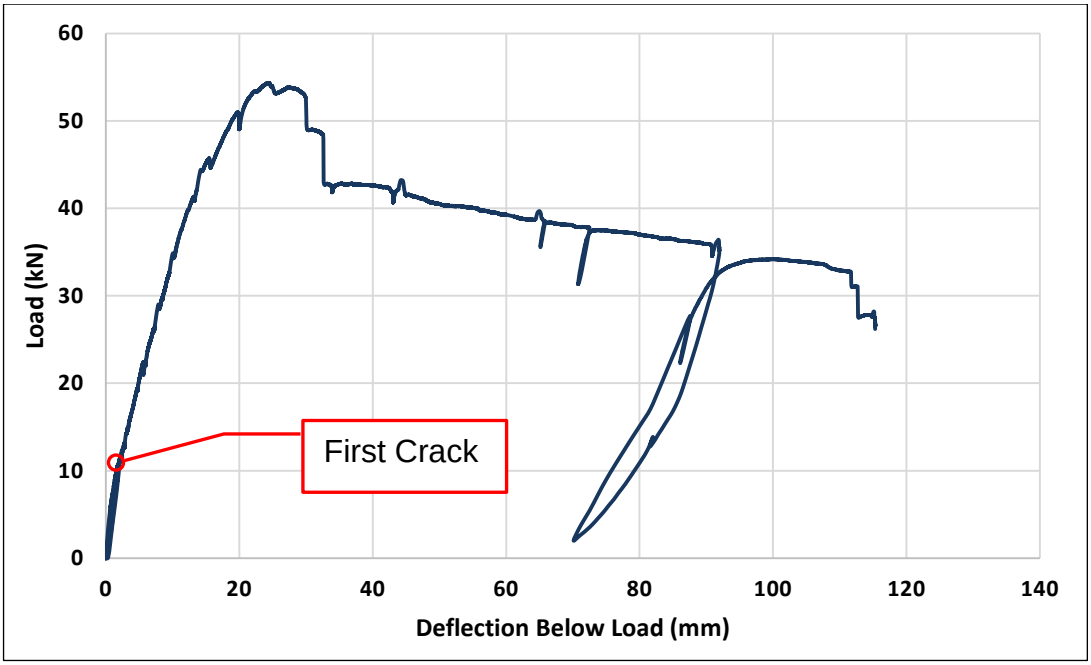

Figure 4-4: Load deflection of SCS joint with normal reinforcement

Failure of the first row of studs increased the width of the flexural crack (Photo 4-6) and continuous degradation in the carried load. The separation of the tension plate started when the load was 14.3 kN and increased after the studs' failure. There was no crushing in the concrete, i.e. the failure was completely controlled by cracking and steel yielding (tensile) failure. The test stopped after the failure of the studs in the second row.

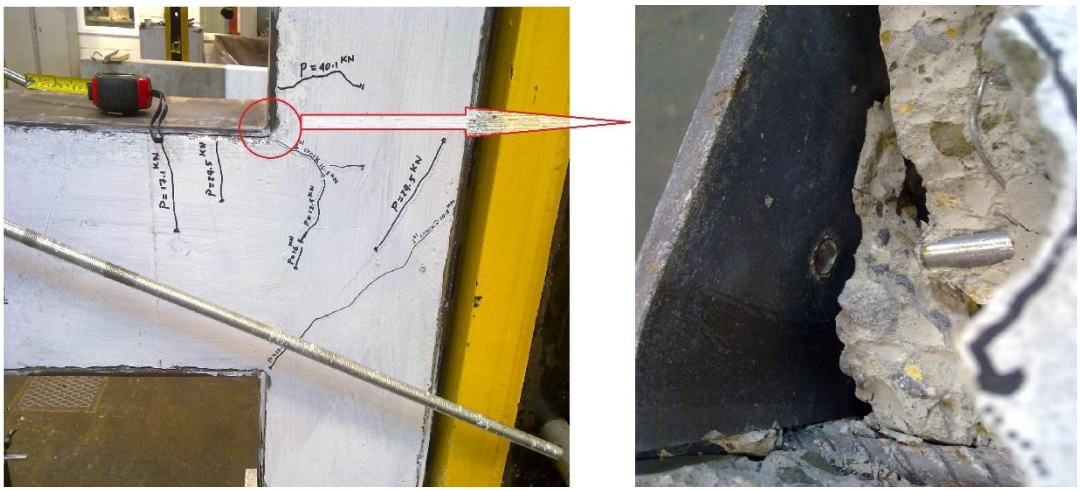

Photo 4-5: Welded stud failure in the SCS joint with normal steel

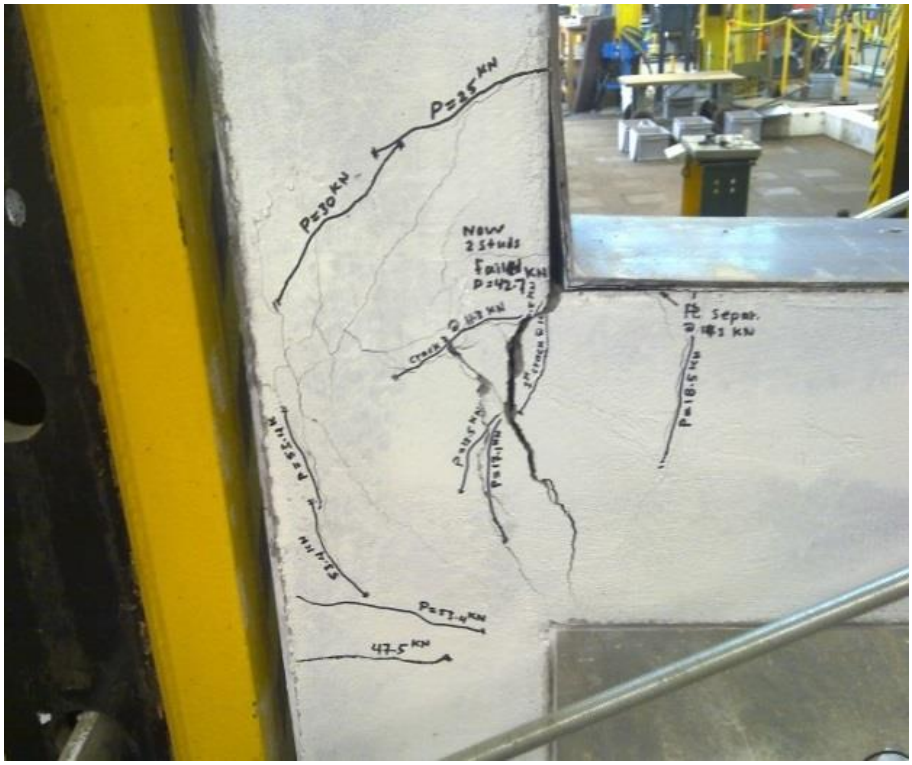

Photo 4-6: SCS joint with normal steel cracking after studs' failure

4.2.4 Double Skin Composite Joint with Welded Bars – First Test

In an attempt to provide anchorage for the tensile steel plate, 3B12 mm steel reinforcement bars were welded onto the top and the bottom plate without shear reinforcement in the beam. In the column, the same reinforcement (4B16 mm and links spaced at 100 mm) was used in the region of 300 mm from the face of the beam in both directions.

The first crack was observed when the load was 13 kN, which is obvious on the load-deflection curve shown in Figure 4-5. The behaviour is linear and has high stiffness from the beginning up to the point of the first crack, and the slope of the load-deflection curve decreased, which reflects the decrease in the stiffness of the specimen due to cracking. The first stud in the first row in the column failed when the load reached 62.71 kN, causing a drop in the load to 58.57 kN; the load increased up to 62.02 kN and the second stud of the first row failed and the load fell to 59.45 kN and at this point the deflection of the beam below the load position was 30 mm. There was another increase in the load to 62 kN, which remained constant until a deflection of 67 mm and was followed by a sudden decrease in the load to 55 kN due to failure of one of

the welded reinforcing bars in the beam at the critical bending moment section (column face). There was a continuous increase in the deflection after the bar failure and decrease in the load, and when the deflection and the load reached 92.9 mm and 48.14 kN respectively, the specimen was unloaded, i.e. the test was stopped and resumed the next working day. From the load-deflection curve shown in Figure 4-5 (red part), the loading path did not follow the same unloading path due to the concrete cracking and steel bar failure. When the load reached 43 kN, another one of the welded reinforcing bars failed, causing a drop in the load to 41 kN followed by a continuous decrease in the carried load.

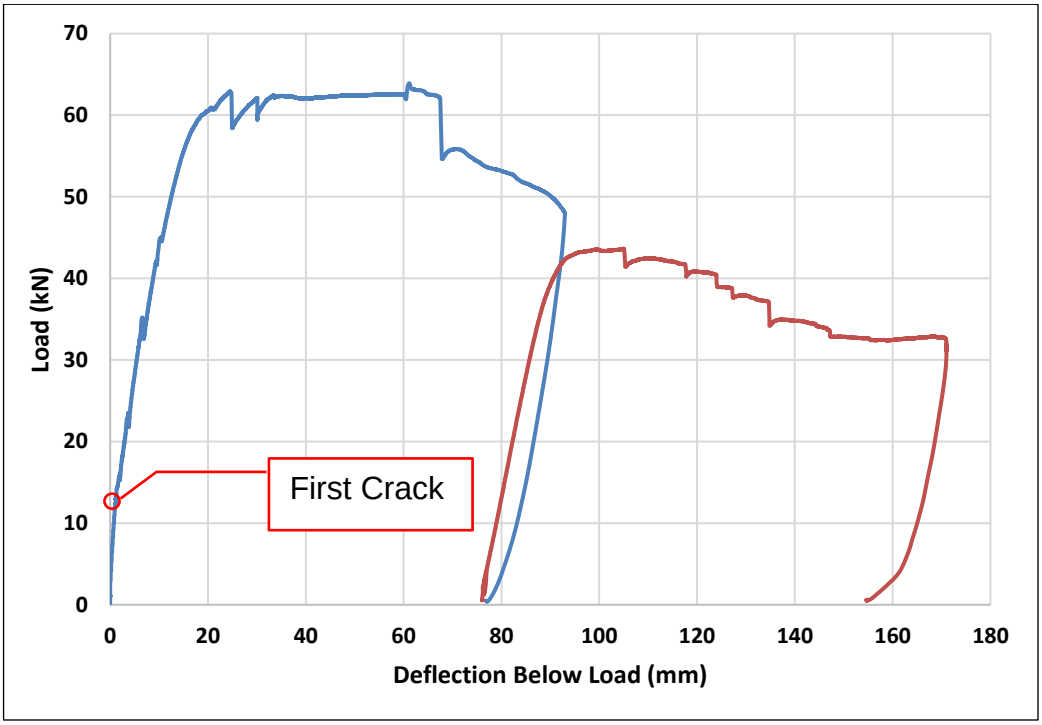

Figure 4-5: Load-deflection curve of SCS joint with welded bars

At a load of 37.27 kN, the third bar failed and the load decreased to 34 kN, and severe deformation and cracking can be seen in Photo 4-7. At this stage, the test was stopped when the deflection below the load reached 170 mm.

Photo 4-7: Failure of SCS joint with welded bars

4.2.5 DSC Joint with Welded Bars – Second Test

Despite the repetition of this test in stage two of the experimental programme, it is more convenient to present the test results here in order to understand the behaviour of the double skin composite beam-column joint with welded bars, as the result was not identical in both tests. It is obvious from the load-deflection curve shown in Figure 4-6 that the second specimen was stiffer than the first specimen, which can be attributed to the high strength of the welding of the first row of studs in the column. The first stud of the first row of studs in the column failed when the load reached 67.9 kN and the deflection below the load was 14.4 mm, while the second stud failed when the load and the deflection reached 72.5 kN and 29.6 mm, respectively.

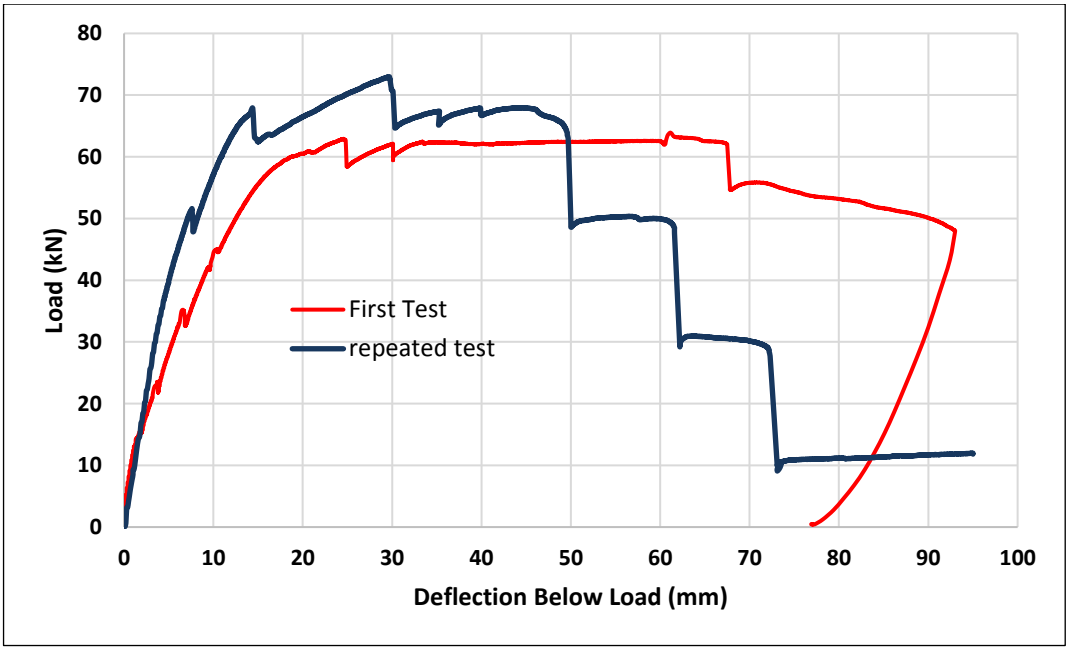

Figure 4-6: Load–Deflection curve of SCS joint with welded bars (both tests)

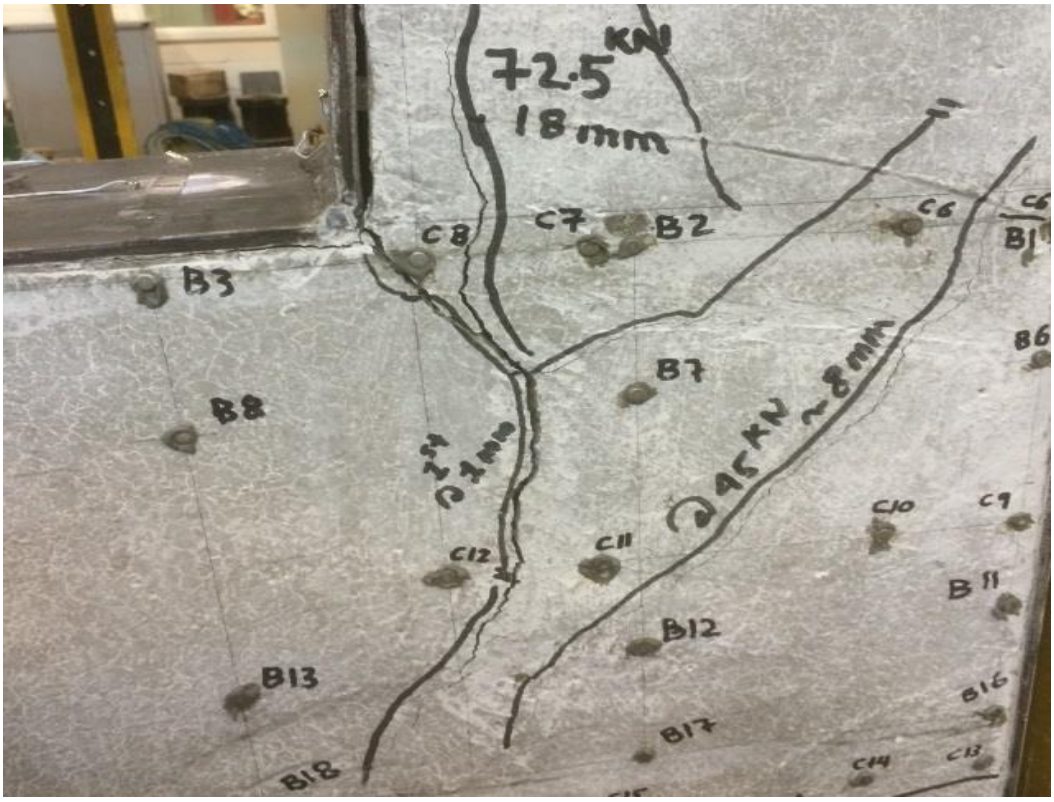

Photo 4-8: Second SCS joint with welded bars before stud failure

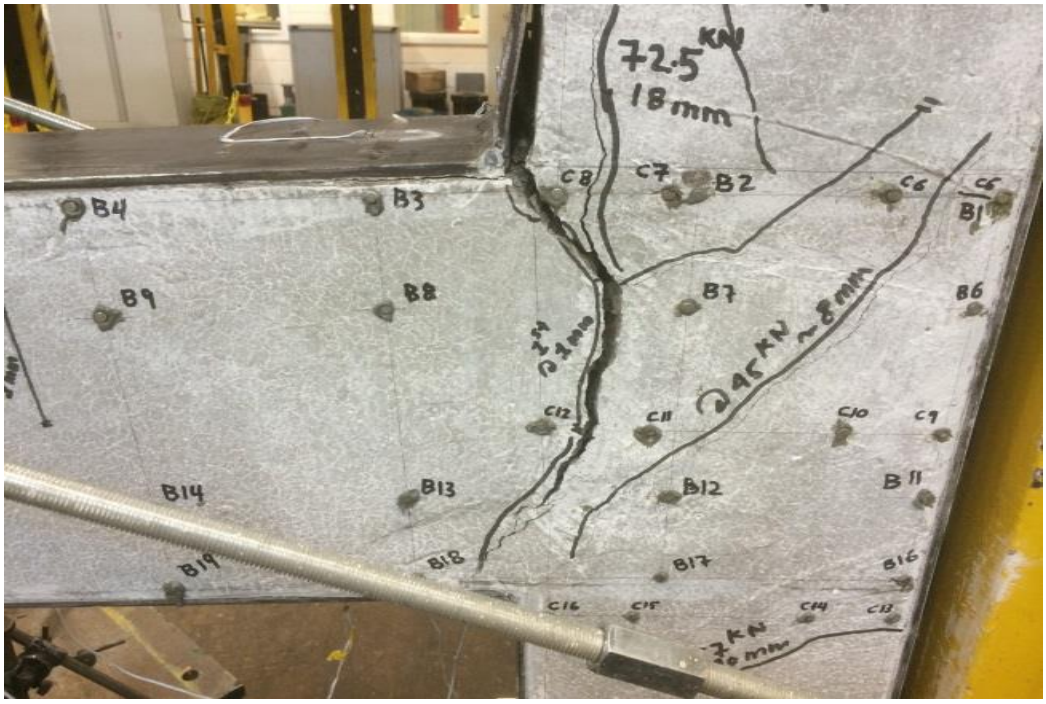

Photo 4-9: Stud failure in SCS joint – second test

After the failure of the first row of studs, the flexural cracks increased dramatically in width and in length where all the sections cracked through their entire depth, as shown in Photo 4-9. Some hardening in the load-deflection curve appeared after the failure, which could be a result of the strain-hardening stage in the steel reinforcement because no other resources for this hardening were available. The hardening was followed by a decrease in the carried load and a failure (rupture) of one of the reinforcing bars welded to the top plate, where the load decreased to 48.6 kN. A second reinforcing bar failed (ruptured) after some increase in the load and the load dropped to 29 kN, which caused the failure of a third tension bar, and the total deflection at the failure of the last bar was 73.1 mm.

4.2.6 Double Skin Composite Joint with Extended Plates

The third option used to provide anchorage for the tension plate was to extend the beam plates in tension and in compression to the interior face of the column back plate where they were joined together using angles and bolts, as explained in Chapter three.

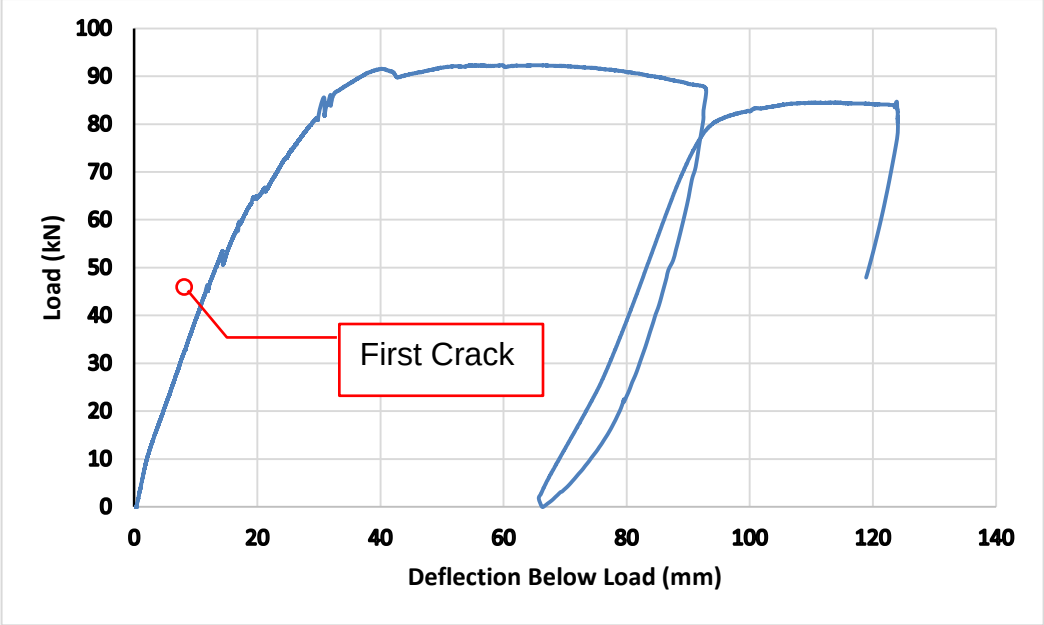

Figure 4-7: Load deflection of SCS joint with extended plates

Figure 4-7 shows the load-deflection curve of the test, with the specimen loaded monotonically under displacement control with a loading rate of 0.1 mm/min, the first crack appeared under a load of 39.2 kN in the lower back corner of the joint concrete core. The second crack appeared under 45.1 kN in the beam at 300 mm from the column face. When the load reached 53.5 kN and the deflection below the load was 14.3 mm, a third crack appeared diagonally in the junction region. The increase in the carried load continued up to 91.5 kN and, with a deflection below the load of 40.3 mm, a large number of cracks formed diagonally in the junction region followed by column cracking where a crack formed diagonally along the lower part of the column. The load decreased to 87.6 kN and continued semi-constant up to a deflection of 92.8 mm, where the test was stopped and the specimen unloaded. On the next working day, the specimen was reloaded but it did not reach the same load (87.6 kN) before the test was stopped due to the effect of the cracks; the maximum deformation was 122 mm below the load and the load was 84.1 kN. There was severe cracking in the junction region and concrete fell off due to the shear cracks formed in it, as well as a high deformation in the back plate of the column in the region where it connected with the tensile plate. Photos 4-10 and 4-11 show the formation of cracks and the failure of the joint.

Photo 4-10: First crack in the SCS joint with extended plates

Photo 4-11: Failure of the SCS joint with extended plates

4.3 Stage Two

4.3.1 Double Skin Composite Joint with High-Strength Concrete

In the current double skin composite joint, high-strength concrete was used in the core in order to study the effect of increasing the concrete's compressive strength. Figure 4-8 shows the load-deflection curve of the tested specimen;

here the loading rate was 0.1 mm/min. The first crack appeared at 300 mm away from the column face, i.e. at the interaction surface between the normal concrete and the high-performance concrete, when the load was 23 kN and the displacement below the load was 1.7 mm.

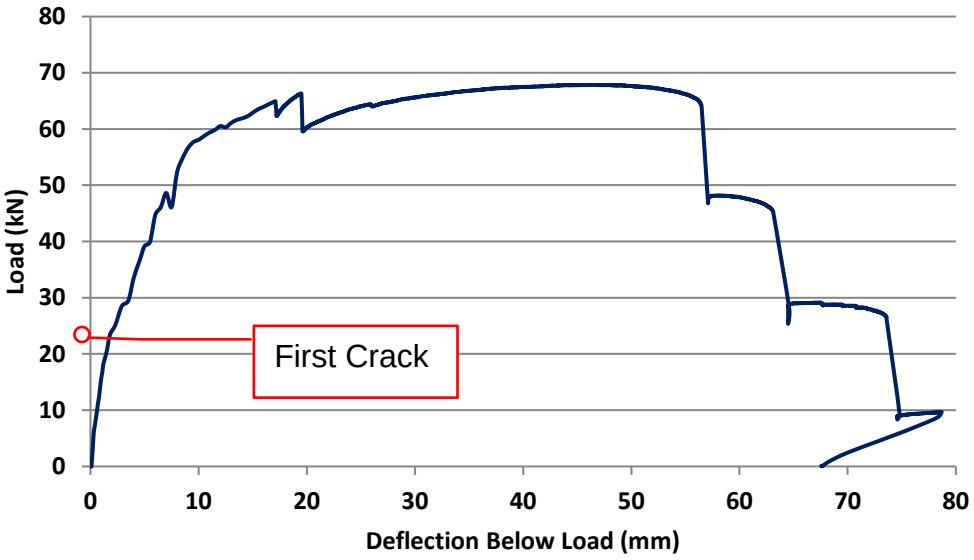

Figure 4-8: Load deflection of SCS joint with HSC

The changes in the slope of the load-deflection curve reflect the growth and development of the cracks in the specimen. A second crack formed at the critical section for bending, i.e. the face of the column, when the load was 26 kN which affected the response, as can be seen in the load-deflection curve. A crack appeared in the top part of the column at the interaction face with the beam under a load of about 50 kN when the displacement below the load was 7 mm.

The first stud of the first row of the column studs failed when the load was 64.9 kN, causing a drop in the load to 62 kN followed by an increase in the load to 66 kN, where the second stud failed and the load decreased to 59.8 kN. The load increased again up to 67.8 kN and then decreased to a load of 64.7 kN and a displacement of 56.4 mm, where the first tension bar in the beam failed. The second and third reinforcing bars of the beam failed when the load was 45 kN and 26 kN respectively and the maximum displacement corresponding to the failure of the third bar was 73.5 mm, and here the load dropped to 9 KN.

Photo 4-12: Cracking in the SCS joint with HSC

Photo 4-13: Failure of the SCS joint with HSC

4.3.2 Double Skin Composite Joint with Steel Fibre V_f=0.25%

A double skin composite joint was cast with steel fibrous concrete and a volume fraction of 0.25%; it had the same properties as the joint with a volume fraction of 1% in order to study the role of steel fibres when used in a low dose.

The test started by applying the load under displacement control with a loading rate of 0.1 mm/min, and, when the load reached 16.63 kN and the deflection below the load was 4.4 mm, no cracks appeared and the section can be said to be unaffected. However, an unforeseen technical issue occurred, and therefore the test was stopped and the specimen completely unloaded. When the specimen was reloaded, the first crack appeared in the beam at the face of the column under a load of 11.5 kN. This early cracking can be attributed to the loading and unloading cycle in the previous step, which might have caused internal cracks and some weak points. Figure 4-9 shows the load-deflection curve of the tested reloaded specimen and Photo 4-14 shows the location of the first crack observed when the specimen was reloaded.

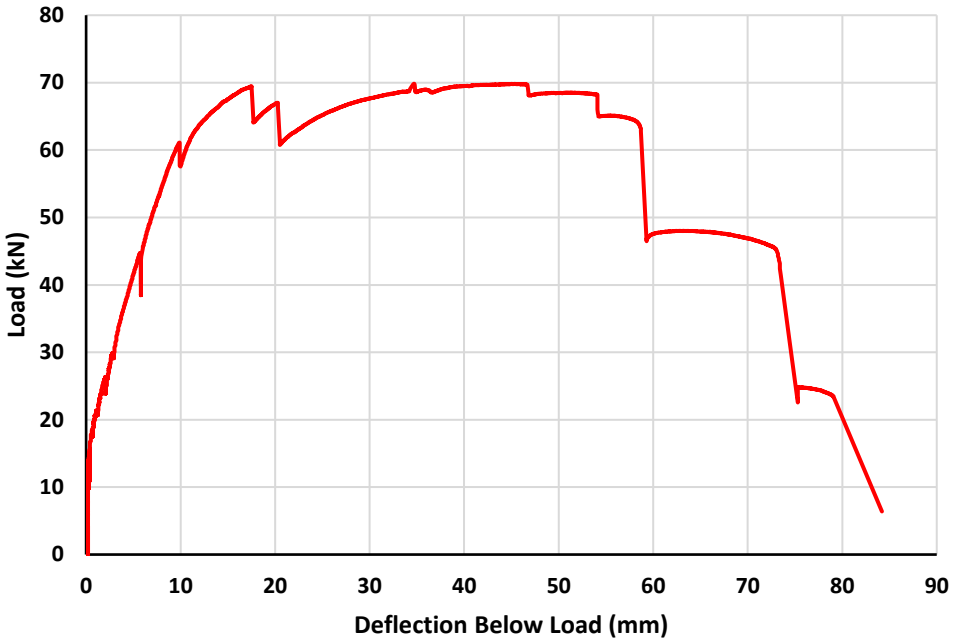

Figure 4-9: Load Deflection of SCS with SF of V_f=0.25%

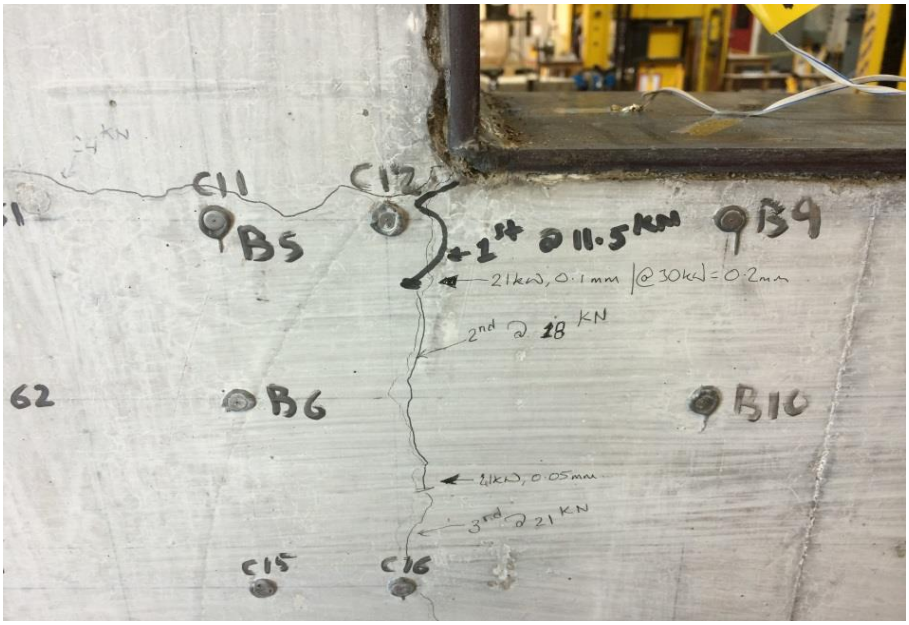

Photo 4-14: Cracking in the SCS joint with SF 0.25%

At the interface region between the fibrous concrete and the non-fibrous concrete, i.e. 300 mm away from the column face, a crack appeared when the load was 24 kN and under the same load a crack formed in the column at the top face of the beam. When the load was 58 kN and the deflection below the load was 8 mm, two diagonal cracks appeared in the joint region (the junction region of the beam and the column).

The first stud failed when the load was 69.4 kN, causing a drop in the load to 64 kN which was followed by an increase in the carried load to 67 kN, which dropped to 60.9 kN due to failure of the second stud in the first row in the column. The load increased up to 69.7 kN and this was followed by a sudden drop to 68 kN due to the failure of one of the studs in the second row of the column. After that, the load remained constant with a deflection of 54 mm where the second stud in the second row of the column failed, causing a drop in the load to 65 kN. The first reinforcing tension bar failed (ruptured) when the load reached 63 kN and the deflection was 59 mm. The load dropped to 46 kN and the second reinforcing bar failed when the deflection reached 73 mm, resulting in a drop in the load to 22 kN, and the test was stopped.

Photo 4-15: Failure of the SCS joint with SF 0.25%

4.3.3 DSC Joint – Steel Fibre V_f=1%

A double skin composite joint was concreted with a fibrous concrete containing steel fibres of volume fraction (V_f=1%) and the fibres have an aspect ratio (l_f/d_f) of 60. Figure 4-10 shows the load-deflection curve of the tested specimen and the load distribution is due to the formation of cracks. The first crack appeared at the critical bending section when the load was 19.5 kN and the deflection below the load was 1.8 mm, as shown in Photo 4-16.

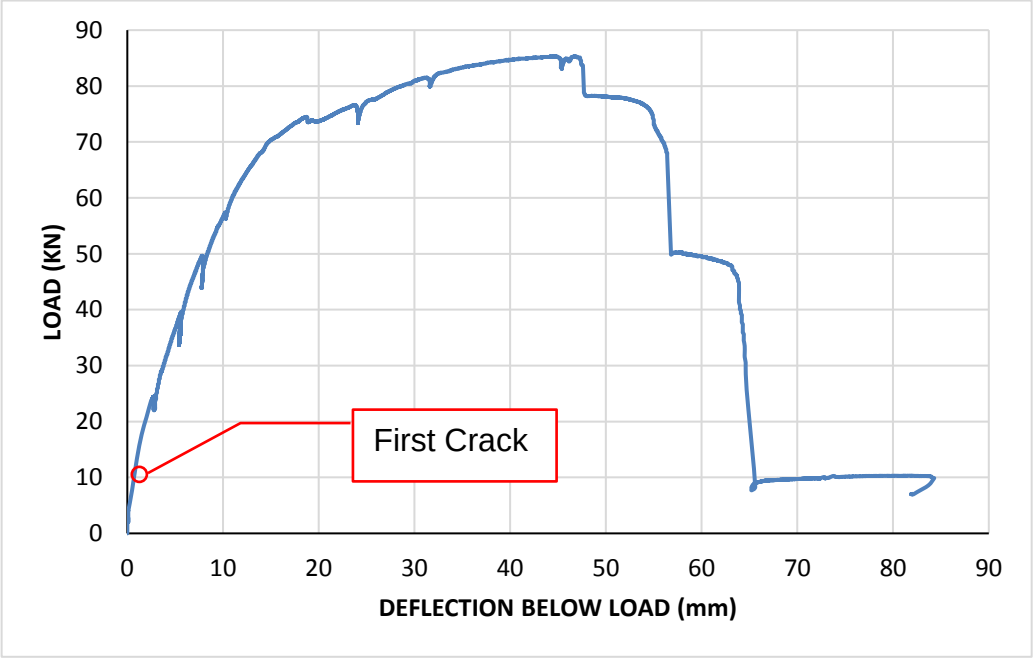

Figure 4-10: Load–deflection curve of SCS with 1% SF

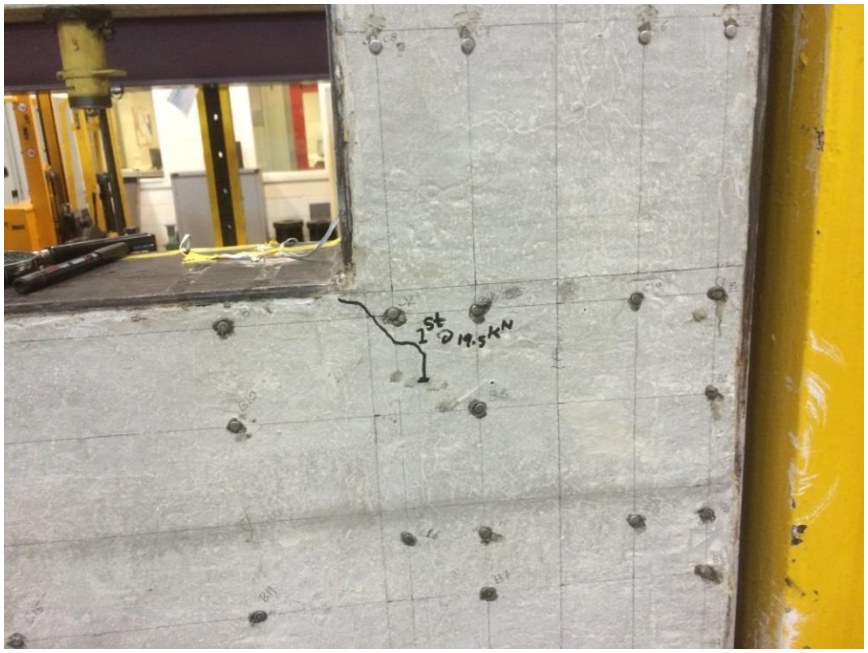

Photo 4-16: First crack formation in the SCS joint with SF

The second crack appeared in the beam at 300 mm from the column face when the load was 23 kN and the deflection was 2.4 mm. A flexural crack appeared in the top part of the column at the intersection face of the beam under a load of 37 kN. A diagonal crack in the junction region started when the load was 49 kN.

Nonlinear response in the load deflection increased due to the increase in the number and width of the cracks up to a load of 85.1 kN, which corresponded to a deflection below the load of 47 mm, and there was a sudden decrease in the load due to failure of the first row of the column studs. After the studs' failure, the load dropped to 78 kN and continued to be semi-constant until a deflection of 48 mm where one of the reinforcing bars failed (rupture). This was followed by a decrease in the load and, when the deflection reached 63 mm, the remaining two reinforcing bars failed at the same time, causing a severe drop in the load from 45 kN to 10 kN. The locations and distribution of the cracks are affected by the studs' locations, which can be considered as crack inducers.

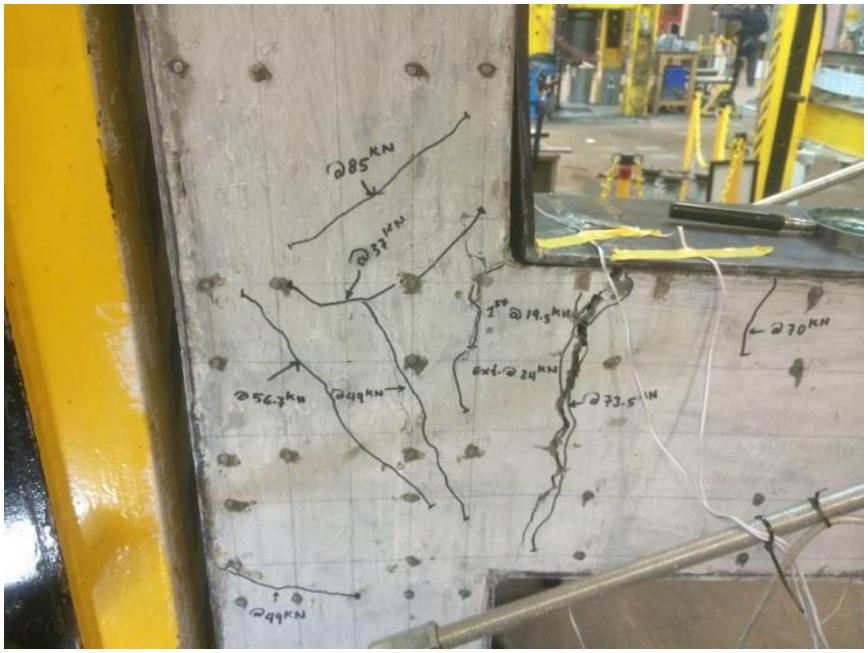

Photo 4-17: Stud failure effect on SCS with SF

4.4 Performance Discussion

In the next sections, the responses of the tested specimens will be compared and an attempt to interpret the variations in their responses will be made. Table 4-1 displays a comparison between six aspects, which are cracking load, displacement at cracking, maximum load during loading period, maximum displacement before severe degradation, load at which stud failure started and failure mode. Figure 4-11 displays a comparison between the load-deflection curves of all tested specimens. It is worth mentioning that the current study represents the first attempt to study experimentally and numerically the response of the SCS beam-column joint, as stated in Chapter one of this thesis. Therefore, it is not possible to compare the behaviour of the current SCS beam-column joint with previous studies, except in some places from beam studies. However, a comparison with conventional reinforced beam-column joint behaviour can be made to assess the structural response of the present joint in line with similar elements.

4.4.1 General Behaviour

Due to the absence of anchorage in the tension plate of the first DSC joint, it failed early, which is obvious from Figure 4-11 and by comparing the data in

Table 4-1. In all tested specimens, no slip was observed between the steel plates and the concrete, neither in the beam nor in the column, which reflects the efficiency of the shear stud connectors in providing the composite action. Also, no buckling in the compression plate happened, indicating the efficiency of the J-hooked connectors in preventing buckling, as indicated by Liew and Sohel (2009), Liew and Sohel (2010) and Sohel and Liew (2011). In addition, the chosen spacing between studs welded to the compression plate was sufficient to prevent buckling of the plate in compression.

An analysis based on Euler's buckling load formulae can be presented by calculating the critical strain, i.e. buckling strain, for the plate between two rows of studs (100 mm apart). By assuming simple support conditions for the plate between the stud rows (Liang et al., 2004), the strain at buckling is 5.234×10^{-3}. Comparing the calculated strain with yield strain (3.6×10^{-3}) of the steel rebar welded onto the steel plate to provide anchorage, it can be concluded that the tension reinforcing bars will reach the yield before the buckling of the plate in compression. Because of the cracking of the concrete in the tension zone, the neutral axis will move towards the compression face and that leads to reducing the strains in the compression compared to the strain in the tension zone, and hence the proposed stud spacing will not allow for buckling of the plate.

4.4.2 Maximum Load

Based on the strength requirements, the maximum load that can be carried by the joint is controlled by: 1- maximum flexural capacity of the beam, 2- maximum shear capacity of the beam, 3- column flexural capacity, 4- column shear capacity, and 5- shear capacity of the joint. These factors are dependent on many variables: 1- composite action between the steel plates and the concrete, which depends on the efficiency of shear connectors in transferring forces between the concrete core and the steel plates, 2- strength of steel skin plates, 3- core strength, and 4- anchorage (bond) mechanism of the tension plate to the joint region.

By providing anchorage in three different ways, the enhancement ratio for the maximum load can be varied from 517% to 871% of the original double skinned specimen (Table 4-1). Adding normal steel reinforcing bars

(longitudinal bars and links) to both the beam and the column raised the maximum carried load from 10.5 kN to 54.3 kN. Adding the welded reinforcing bars to the beam plates and normal steel reinforcement in the column (longitudinal bars and links) enhanced the load to 62.7 in the first test and to 72.5 in the repeated test (about 15% difference). In the joint with extended beam plates the load increased to 91.5 kN.

It was expected that the welded bars would give higher resistance because the location of the added bars is larger than the normal reinforcement, which increased the lever arm of the tensile force.

The double skin beam-column joint with bars welded to the beam plates and normal steel reinforcement in the column was selected for the parametric study, i.e. to study the effect of the concrete's compressive strength and the effect of steel fibres as well as to study its behaviour under a cyclic load. It can be said (Table 4-1) that increasing the concrete compressive strength (by using HSC) has no great effect on the maximum load, which can be attributed to the nature of the failure mechanism in the current SCS beam-column joint. The failure was mainly dependent on the initiation of stud failure, which highly affected the joint's response. By comparing shear cracking in the joint region it can be concluded that improving the concrete compressive strength by using HSC reduced the number and width of cracks, especially shear cracks. This enhancement in the joint shear resistance coincides with the finding of Kim and LaFave (2007), Kularni and Patil (2103) and Roehm et al. (2015). The fibres maintain the integrity of the concrete by bridging the cracks. This observation can be confirmed by findings from Liew and Sohel (2010): *"The presence of fibres in the concrete increases the ultimate load carrying capacity of the beam"*.

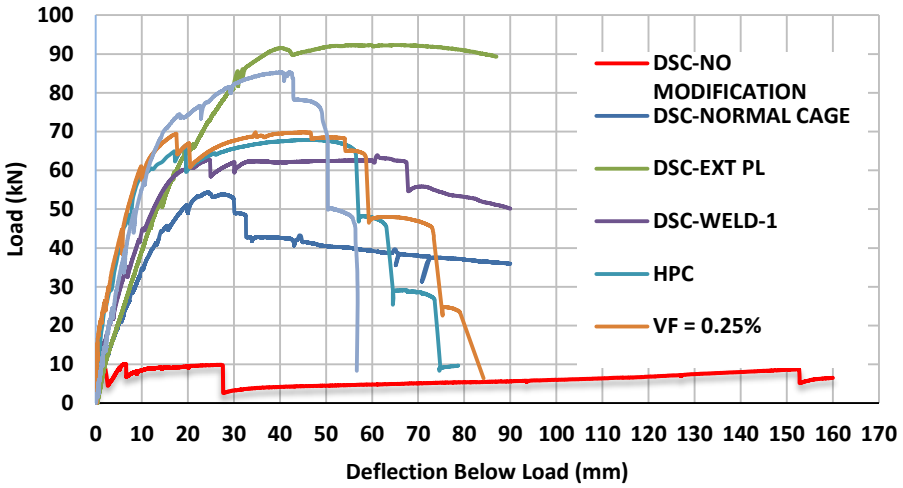

Figure 4-11: Load deflection for all tested SCS joints

Moreover, Figure 4-12 shows the increase in the load corresponding to the indicated percentage of maximum deflection of the joint cast with NC core. During initial load stages, it can be seen that the improvement in the load was pronounced (up to 82% improvement); on the other hand, the enhancement in the maximum load was very low in correspondence to the final stages in the NC joint, although other joints (SFC and HSC) reached greater load. This comparison reflects the effect of steel fibres on the ductility, as discussed in the previous paragraph.

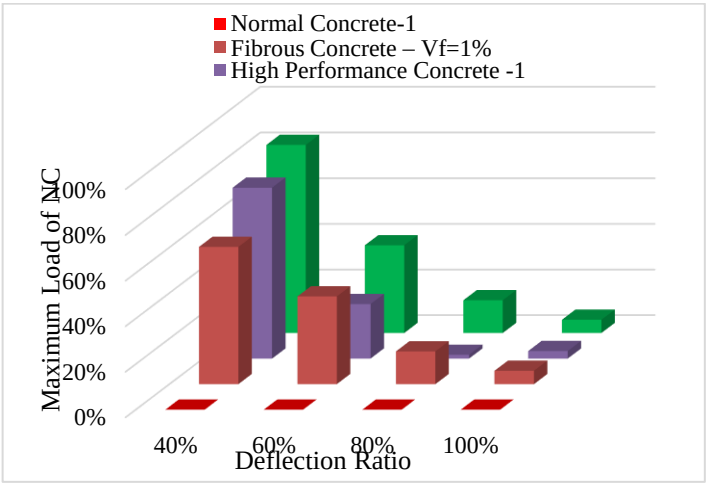

Figure 4-12: Variation in Maximum Load with Concrete Type

The previous discussion has taken into account the flexural capacity of the beam; no shear failure has been identified in any of the tested joints, which reflects the efficiency of the presented design to resist shear stresses. The beam resists shear through two components, concrete and shear studs, as

well as a low amount of resistance being produced by the dowel action of the steel plates.

The core of the joint has been reinforced by shear links spaced at 100 mm, as detailed in Chapter three of this thesis; these shear links increased the joint shear resistance, as indicated by Hamil (2000). Shear links enhance the joint region's ability to resist shear by arresting the cracks by dowel action.

As reported by Pauletta et al. (2015), the maximum capacity of a reinforced beam-column joint is achieved after extensive cracking in flexural regions; moreover, Hamil (2000) showed that the joint can resist a further significant load after shear cracking has appeared. In the present study, all the tested specimens showed the same behaviour, i.e. increase in load capacity after severe cracking in the critical flexural regions and after initial shear cracking in the core region.

This behaviour can be attributed to the similarity in the resistance mechanisms of SCS beam-column joint and RC beam-column joints in the connection zone. The SCS joint exhibited very low strength without any strengthening, as presented in section 4.2 of this thesis; therefore, the structural behaviour of the SCS joint in flexural mainly depends on the welded bars that are used to provide anchorage and flexural resistance. Shear strength in the SCS joint is enhanced by using shear reinforcement in the core of the joint. In RC joints, flexural strength and shear resistance, in the same manner, depend on the flexural capacity of the beam as well as bond (anchorage) capacity in the joint, and the shear strength showed dependency on the concrete and presence of links in the core (Sharma et al., 2011).

Using steel fibre concrete improves the overall structural response and increases the load-carrying capacity of the RC beam-column joint (Campione, 2015; Liang et al., 2016; Abbas et al., 2014). The effect of steel fibres on the behaviour of the beam-column joints can be attributed to the role of steel fibres in improving: 1- flexural strength, 2- shear strength,3- ductility, 4- energy dissipation, and 5- fracture toughness (Shakya et al., 2012; Bischoff, 2003; Jo et al., 2001). In the present study, the SCS beam-column joint with SFC core showed better load-carrying capacity and increase in ductility, which coincides with the advantages of using SFC in RC beam-column joints.

Table 4-1: Comparison between the SCS Joints

Joint	Max. Load (kN)	Cracking Load P_{crack} (kN)	Percentage of P_{max} after providing anchorage	Maximum Displ. Δ_{max}(mm) Based on Load Decreasing	Maximum Displ. δ_{max}(mm) Based on Max. Strain	Stud failure Load (kN)	Failure Mode
No modification	**10.5**	**8.9**	**100**	**27.7**	**-**	**9.9**	**-**
With Normal Bars	**54.3**	**10.5**	**517**	**91.8**	**-**	**53**	**-**
With Extended Plates	**91.5**	**39.1 - 45.5***	**871**	**92.8**	**-**	**Non**	**-**
All the DSC joints listed below have welded bars							
Normal Concrete-1	**62.7**	**13**	**595**	**67**	**-**	**62.7**	**PL- Ten.**
Normal Concrete-2	**72.5**	**13**	**690**	**50**	**28.7**	**67.9**	**PL- Ten.**
Fibrous Concrete – V_f=1%	**85.3**	**19.5**	**812**	**50**	**47**	**85.1**	**PL- Ten.**
Fibrous Concrete – V_f=0.25%	**69.7**	**11.5 - 16.63****	**664**	**54**	**24**	**69.4**	**PL- Ten.**
High Performance Concrete -1	**67.8**	**23**	**646**	**56**	**30**	**64.9**	**PL- Ten.**
High Performance Concrete -2	**66.8**	**23.3**	**636**	**59.3**	**-**	**66.8**	**PL- Ten.**

*: first crack appeared at the corner of the lower corner of the beam column intersection region under a load of 39.1 kN but the author believes it was because of the presence of the bolts. The second flexural crack appeared in the beam at a distance of 300 mm away from the column face under 45.5 kN.

**: due to a technical issue, the test stopped when the load reached 16.63 kN and the specimen was not cracked and, when the specimen was reloaded, the crack appeared under a load of 11.5 kN.

4.4.3 Cracking Load

Cracking of concrete members highly affects the overall structural behaviour of the members, which means it reduces strength and stiffness. A crack forms when the principal tensile stress in the concrete reaches its tensile strength; therefore, the crack will form vertically due to bending or diagonally due to shear stress. Many parameters control the initiation, propagation, number, spacing, penetration depth and crack width, such as the concrete tensile strength, reinforcement ratio (flexural reinforcement and shear reinforcement), and presence of fibres.

Comparing values of the cracking load presented in Table 4-1, it can be concluded that the cracking load was mainly controlled by the allowed movement in the plate. In other words, in the case of the extended plate double skin composite joint, the cracking load raised from 8.9 kN (in the case where no anchorage was case) to 45.1 kN due to the restraint provided for the plates. Another clue that confirms the above conclusion is that the cracking load in the double skin joint with normal reinforcing bars was 10.5 kN compared to 13 kN in the joint with welded bars. This is because the welded bars provided anchorage to the plate, which is not the case with normal reinforcement.

Steel fibres improve the concrete tensile strength as well as its role in maintaining the integrity of the concrete, as reported by Liew and Sohel (2010) and Yan et al. (2014), which resulted in an increase in the cracking load to 16.63 kN and 19.5 kN with a volume fraction of 0.25% and 1% respectively.

It is normal that HSC has greater tensile strength compared to normal concrete. Therefore, the double skin composite joint cast with HSC has a greater cracking load than the joint containing a normal concrete core. The cracking load was 23 kN, which can be attributed to two reasons: firstly, the HSC has larger tensile strength and, secondly, the HSC is denser than the normal concrete, and this led to more anchorage being provided for the tension plate through adhesion between the HSC and the steel plate.

The location of the first crack in all tested double skin composite joints was at the critical beam-bending section and, except in the joint with extended beam

plates, the first crack appeared in the beam at 300 mm away from the column face. The difference in the cracking behaviour of the extended beam plate can be attributed to the rigidity provided by the steel plate and the added UB section as well as the confinement provided at the critical section region.

Stiffness of RC joints depends on the cracking level and it started to degrade when the cracking started. Moreover, the presence of steel fibres enhances the stiffness because of its role in ,improving concrete properties, as presented previously (Kim and LaFave, 2007; Ricci et al., 2016; Kadarningsih et al., 2014; Shakya et al., 2012; Bousselham, 2009).

The same observations were identified during when testing the fibrous SCS joint, which indicates a direct relationship between the stress drop after cracking and the stiffness degradation.

4.4.4 Steel Strains and Maximum Deflection

In order to decide the failure type occurring in each tested specimen, steel stresses will be used. This is because no crushing in the concrete happened in any of the tested specimens and neither rupture nor buckling happened in the steel plate. The type of failure noticed during the tests was the rupture of the steel reinforcement in advanced stages, i.e. after severe cracking in the concrete. Figure 4-13 (a-d) below shows the longitudinal strains in the outer face of steel plates in different locations, as follows:

CT: strain in the top plate of the column at 50 mm from the beam plate face

BT50: strain in the top beam plate at 50 mm from the column face

BT400: strain in the top beam plate at 400 mm from the column face

CB: strain in the bottom plate of the column at 50 mm from the beam face

BB50: strain in the bottom beam plate at 50 mm from the column face

BB400: strain in the bottom beam plate at 400 mm from the column face

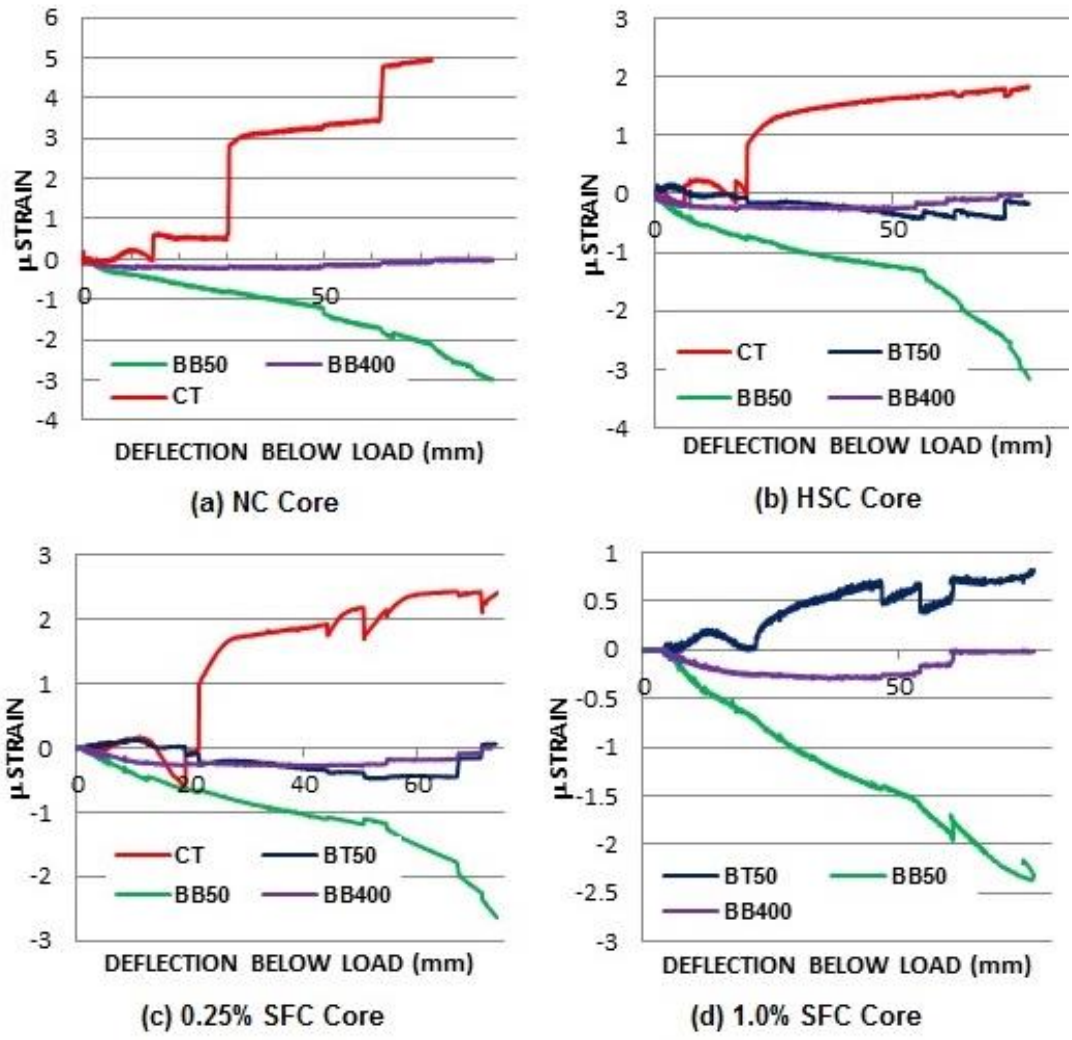

Figure 4-13: Plates' strains in SCS beam-column joints

It is obvious that strains in all locations remained semi-constant and within the elastic range, with the exception that the strains in the top and bottom plates of the column suffered from a rapid increase (jump) in the strain when the column J-hook connector stud failed. These strain gauges experienced compression and tension stresses during the loading progress and this was because of the welded studs that were on the opposite side of the plates to the strain gauges' locations.

By comparing steel plate strain values between the double skin composite joint containing a core cast using normal concrete, steel fibres of 0.25% volume fraction and high-performance concrete, it can be said that the failure occurred in the top plate of the column face.

A comparison between the maximum displacements based on the steel plate yielding is presented in Table 4-1 (the strains have not been measured in all tests; therefore, the comparison is based on the available data). The lowest displacement (24 mm) corresponding to steel plate yielding was in the joint containing steel fibres of 0.25% and the highest displacement (47 mm) corresponding to the plate yielding was in the joint containing steel fibres of 1%. This difference in behaviour can be attributed to the early failure of welded studs in the column, which caused a rapid increase in the plate stresses.

It is important to report that the top steel plate of the column suffered from severe stress concentration at the stud connector locations before the studs' failure, as shown in Photo 4-18.

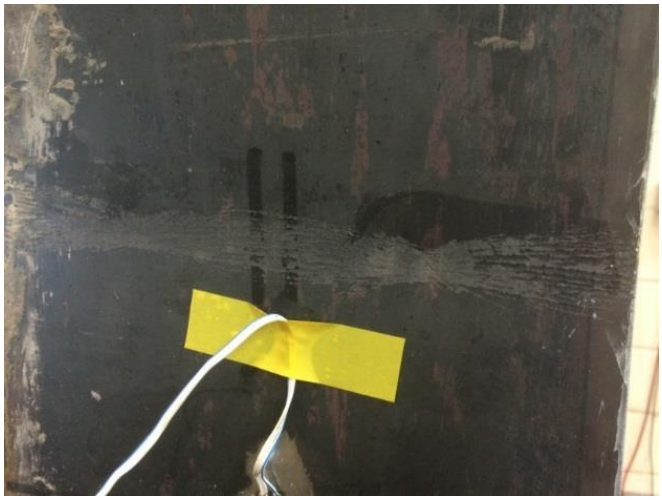

Photo 4-18: Stress concentration at the location of welded studs

4.4.5 Cracking Progress and Specimen Integrity

The mechanism of cracking is affected by concrete strength, fibres' presence and confinement degree. It is vital to control cracking in beam-column joints because it affects their strength and ductility. Both are reduced with progressive cracking due to degradation of stiffness.

A general description for the cracking initiation and development of the composite joint cast using normal concrete, the steel fibrous joint at 0.25%

volume fraction, the 1% volume fraction and HSC will be presented in this section.

First crack: the double skin composite joint cast with normal concrete cracked under a load of 18% of the maximum load and at two locations, at the critical bending section of the beam and at the critical section of the column. On the other hand, the joints cast with steel fibre of a volume fraction of 1%, 0.25% and HSC cracked under a load of 23%, 23% and 34% of the maximum load respectively at the critical section of the beam. This behaviour could be attributed to the improvement in the tensile properties due to the presence of steel fibres (despite the steel fibre improving the behaviour of the cracked section more than the tensile strength) and HSC.

At 50% - 60% of maximum load: at this stage, the composite joint cast with normal concrete suffered from multiple cracks in the junction region and at the critical sections, whereas this was not the case for the joints with steel fibres and HSC. The main reason for this was the ability of the steel fibres to dissipate the energy through the fibres' elongation and/or pull out rather than developing new cracks and the high tensile strength of the HSC compared to the NC.

At 70% - 100% of the maximum load: as in the previous two stages, the fibrous concrete joint and the HSC joint showed better integrity compared to the NC joint. This was because of the steel fibres' role in bridging the cracks.

Photo 4-19 (a-d) shows the cracking state at the final stages of loading; the effect of HSC and SFC on the number and location of cracks as discussed before is obvious.

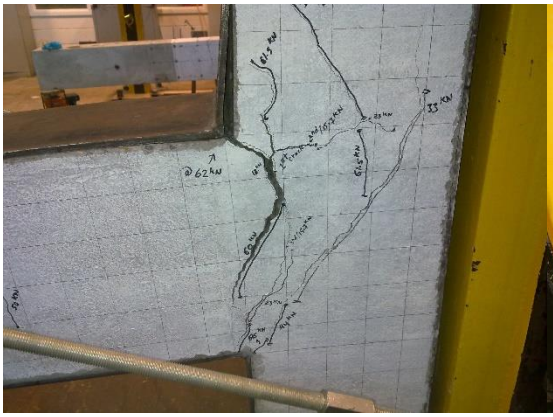

(a) NC

(b) HSC

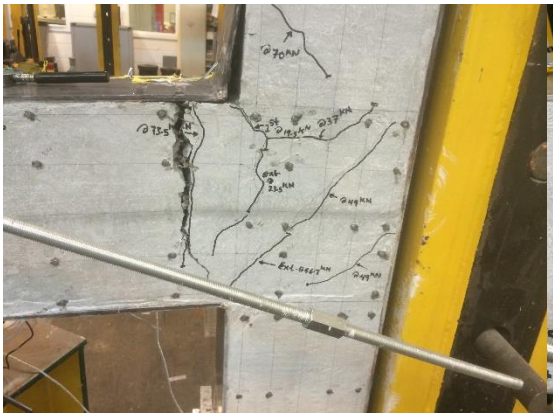

(c) SFC 1%

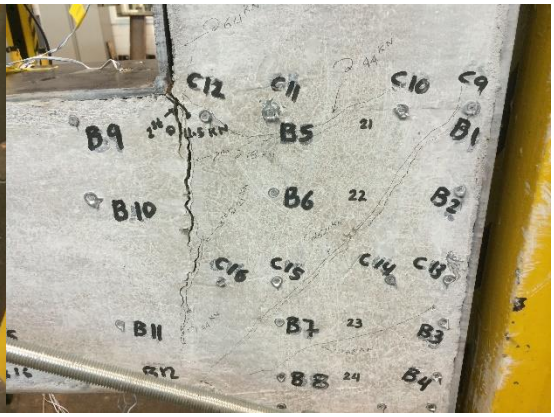

(d) SFC 0.25%

Photo 4-19: Cracking at Final Load Stage

4.5 Stage Three

4.5.1 Double Skinned Composite Joint Subjected to Cyclic Load

4.5.1.1 Test Arrangement

A double skin composite joint cast with normal concrete and the same previous dimensions and test arrangement (8 mm steel plates, J-hook connectors of 10 mm in diameter welded to the compression and tension plates of the beam. The column's plates were spaced at 100 mm longitudinally, 300mm x 200 mm beam cross-section, 250 mm x 200 mm column cross-section, 1500 mm column height, 1250 mm beam span, three steel bars were welded to the tension and compression plates and normal steel reinforcement added to the column within 300 mm of the beam's face in

both directions) was tested under cyclic load according to ACI 352R-02. The aim of this test was to gain some initial ideas about the behaviour of a double skin composite joint under a cyclic load, i.e. no parametric studies have been conducted to study the main variables that control the response of such a joint.

As shown in Photo 4-20, two hydraulic jacks were used to apply the load at 100 mm from the free end of the beam in both directions (up and down). Six strain gauges were used to monitor the strain in the steel plates, two on the column front plates at 50 mm above and below the beam plate face, and four SG on the beam top plate and bottom plate at 50 mm and 400 mm from the column face.

Photo 4-20: Cyclic test arrangement

The load was applied using position control with a loading rate of 0.2 mm/min and increased after cracks appeared at 0.5 mm/min then 1 mm/min after 4 cycles. Each cycle consisted of 3n mm upward displacement and 3n mm downward displacement where n represents the number of the cycle.

4.5.1.2 General Response, Maximum Load, Cracking and Failure

As described in the previous section, the load was applied using displacement control before starting the test; 5 kN was applied as a seating load and the specimen was unloaded to take the initial reading of the strain gauges and strain DEMEC point as well as the LVDTs.

Every cycle started by applying a downward load until the displacement of the beam end reached 3n mm and then the specimen was unloaded gradually

and reloaded upward up to 3n mm. The specimen showed an increase in the carried load in subsequent cycles until the tenth cycle, where the load decreased. Table 4-2 shows the load of each cycle and the corresponding displacement. It is obvious that the upward load was less than the downward load regardless of the symmetry of the section, which can be attributed to the degradation caused by the previous half cycle.

Table 4-2: Cyclic test results

Cycle No.	1	2	3	4	5	6	7	8	9	10	11	12	13
Displacement (mm)	3	6	9	12	15	18	21	24	27	30	33	36	39
Down Load (KN)	26	39	47	53	56	57	54	59	60	59	57	55	53
Up Load (KN)	23	39	45	50	51	55	54	55	55	53	50	47	47

The first crack was observed at the critical bending section when the load was 13 kN during the first half of the first cycle and, by the end of the first cycle, the depth of the crack had reached 230 mm of the concrete depth.

During the second cycle (6 mm downward), a flexural crack formed in the beam at 350 mm away from the column face when the load was 13 kN. When the load reached 38.5 KN, the crack was observed at the critical section of the column, i.e. at the interface between the beam and the column.

The first diagonal shear crack in the junction region appeared during the third cycle (9 mm), as shown in Photo 4-21.

Figure 4-14 and Figure 4-15 show the load-deflection curves of the tested specimen. Figure 4-14 represents cycles 3-9-12 mm that have been separated from the remaining cycles in order to show the degradation that happened as the test progressed. It is obvious that the stiffness (in terms of the slope of the load-deflection curve) decreased in successive cycles due to the cracking. Also, it can be noticed that the width (or area under the consecutive cycles' curve) increased, which indicates that the increase in the energy dissipated due to the crack development and growth.

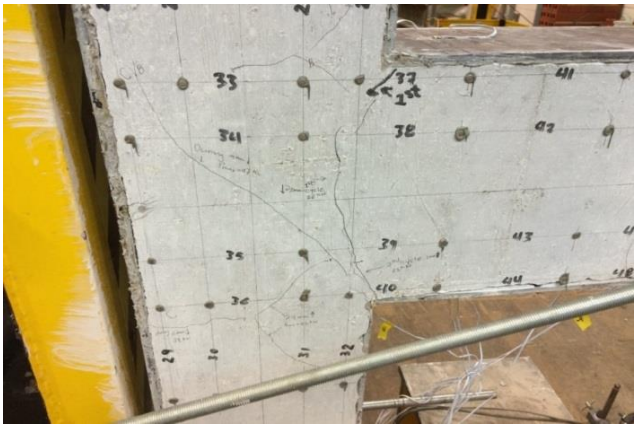

Photo 4-21: Crack formation in the SCS under cyclic load

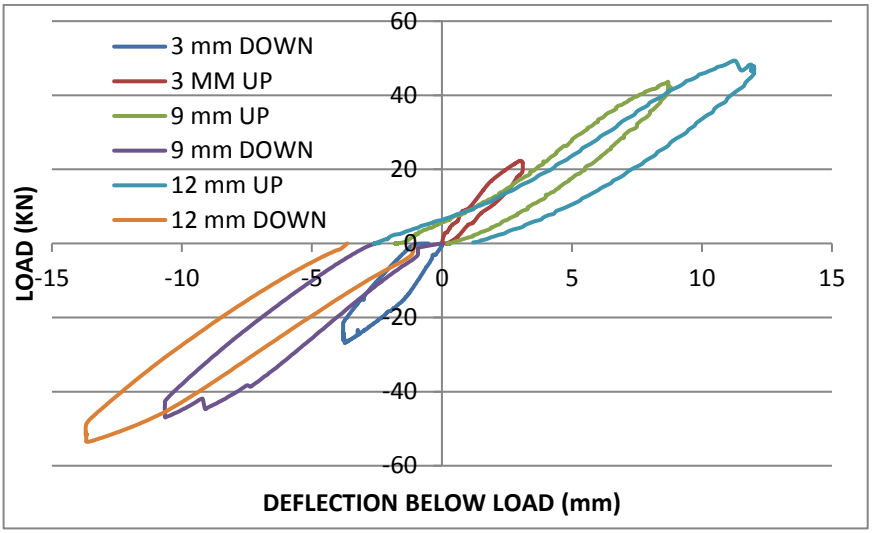

Figure 4-14: Load deflection of the first three cycles

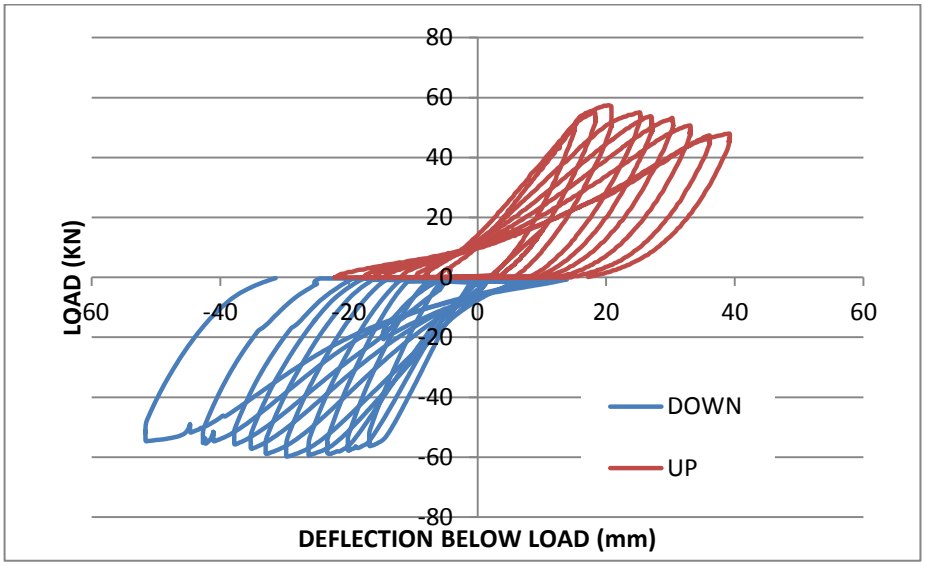

Figure 4-15: Load –deflection of SCS under cyclic load (all cycles**)**

As the test progressed, more diagonal cracks developed in the junction region and the flexural cracks widened, especially at the critical section, until the tenth cycle (30 mm), when the specimen reached the stable crack stage (no new crack development). Neither stud failure nor bar abrupt happened, which can be attributed to the loss of the bond between the steel (stud and reinforcement) because of the load reversal, which damaged the bond gradually.

Maximum load (60 KN) was reached at the ninth cycle (27 mm) and started to decrease during the following cycles until 53 KN in the thirteenth cycle, where the concrete started falling off from the junction region and the section cracked severely.

4.6 Summary

This chapter has presented all the test results in detail and discussed them in order to determine the main factors that affect the response of a double skin composite joint under both monotonic and cyclic load.

From the presented experimental tests, the following observations can be reported:

- The Double Skin Composite beam-column joint can be strengthened to be used as an alternative to the conventional beam-column joint. As can be seen in the test results for the joint with steel fibres and the joint with HSC, the failure occurred (plastic hinge formed) in the beam away from the column face.
- Based on the structural performance and the secondary consideration of the cost of the strengthening method, the DSC joint containing welded bars on the steel plates of the beam can be considered the most efficient solution.
- The recommended stud spacing to steel plate thickness ratio (s/t) and stud diameter to steel plate thickness ratio (d/t) were used as a guide to produce the initial design of the DSC joint. The s/t of 12.5 and d/t of 1.25 used in the present study showed efficient behaviour against the buckling of the steel plate under compression and against the slip.

- Using HSC significantly improves joint shear resistance.
- The DSC joint containing steel fibre showed the best performance regarding the integrity of the concrete during loading up to failure (this behaviour was reported in the previous studies of beams and slabs). The crucial improvements were the improvements in the maximum load capacity and the location of the plastic hinge.
- In the DSC joint tested under a quasi-static load, the width (area under the consecutive cycles' curve) increased, which indicates the increase in the energy dissipated due to the crack development and growth.

Chapter 5 Finite Element Modelling

5.1 Introduction

Both reinforced concrete structures and composite structures consist of multiphase materials and elements which make the formulation of the governing differential equation(s) or the closed form solution of these equations impossible. On the other hand, the experiments present an excellent way to understand the behaviour of such members (structures), but the following complications are generally common:

- Cost of the experimental programme
- Time required for preparation and testing
- Accuracy and reliability
- Possible hazard and safety requirements
- Limits on the parameters that can be read during a test

An approximate solution can be presented using numerical methods that are considered efficient in predicting the response of complicated structures and materials. One of the most common and powerful methods is the finite element method and, due to its extensive usage and the huge number of publications on it, it can be said that everyone who is interested in simulation and numerical methods has a background in it. Therefore, the only details presented in this thesis will be those relating to the finite element package used in a simulation.

The general finite element package ABAQUS 6.10 licensed for the University of Leeds has been used to analyse the beam-column joints that were presented in previous chapters. This chapter consists of three main sections; the first section presents a general background and abilities of ABAQUS. The second section presents the models of materials of steel reinforcement, steel plate, stud connectors and the concrete in compression and tension in addition to the interaction between beam-column joint elements. The third section presents the details of modelling and verification of the following joints using ABAQUS:

- The reinforced concrete joint under a monotonic load

- A Double Skin Composite joint with welded bars and NC under a monotonic load
- A Double Skin Composite joint with welded bars and SFC under a monotonic load
- A Double Skin Composite joint with welded bars and HPC under a monotonic load
- A Double Skin Composite joint with welded bars and NC under a cyclic load

5.2 ABAQUS General Background

A large number of finite element codes are presented using different programming languages such as FORTRAN, BASIC, C, C++, etc. In these codes, the modeller used an input file to feed all the data regarding nodes, elements, materials, constants and used loops to generate nodes and elements. The manual method used to feed in the data was time-consuming, boring and needed revision and correction; therefore, interactive methods, especially the Graphic User Interface (GUI), have become the most desired methods in all finite element packages. In processing input files, the GUI method helps to identify any error in the geometry as well as saving time. ABAQUS 6.10 documentation (Simulia, 2010) is the main source for the following information.

ABAQUS/CAE 6.10 is used in the current project to perform the analysis of the reinforced concrete joint and the double skin composite joint. Modelling using ABAQUS consists of the following steps:

5.2.1 Pre-processing, which Includes

a. Geometry
b. Assembly
c. Material definition
d. Meshing
e. Step and solution technique
f. Loading and boundary conditions
g. Interactions
h. Submission

i. Post-processing, which includes:

a- Drawings

b- Tables

This step comprises all the input data required to perform the required analysis. ABAQUS accepts both the written input file (called “name.inp”) and/or the graphical input method which can be modified by editing the generated input file; it is worth mentioning that using writing to produce the input file is limited to the simple geometry as complex geometries are time-consuming and vulnerable to editing mistakes. ABAQUS/CAE 6.10 has a wide range of commands that enable any complicated structures to be built easily and precisely. In the finite element analyses, the choice of the best simulation of a specific physical problem depends on the understanding and modelling of its behaviour rather than the precision of drawings. For example, it is possible to disregard part or more of the real physical problem. The Main ABAQUS types can be divided into:

1- ABAQUS/Standard for static analysis
2- ABAQUS/Explicit for dynamic analysis
3- ABAQUS/CFD for computational fluid dynamics

ABAQUS has the ability cover a wide range of fields, e.g. static/dynamic stress analysis, fluid dynamic, electrical analysis, coupled pore fluid flow and stress analysis, etc.

Any structure can be (it is preferred and sometimes must be) divided into sub-parts that are assembled together to form the final geometry using merge and/or interaction facilities. All the parts that are used to form the entire structure should have a specific material definition. ABAQUS enables the modeller to define any material properties, either through its huge library or by using a special subroutine which can be written to assign the required material model.

An extensive library of elements can be found in ABAQUS and element choice is affected by many parameters such as the geometry of the problem, supports and loading. The elements in ABAQUS are divided based on five criteria:

1- Family: includes solid (continuum) elements, shell elements, beam elements, etc. http://abaqusdoc.ucalgary.ca/books/usb/default.htm
2- Degrees of freedom http://abaqusdoc.ucalgary.ca/books/usb/default.htm?startat=pt01ch01s02aus02.html
3- Number of nodes and order of interpolation
4- Formulation
5- Integration

Any model can be meshed using one element type or any number of element types depending on the modeller's decision and the nature of the problem under consideration. Structural elements such as solid, beam, truss, shell and special purpose like spring elements and connectors are available that provide a flexible tool to simulate different components of structures.

To control the type of solution (static, dynamic, etc.), to specify solution parameters (increments, period, etc.) and to specify the desired output variables, ABAQUS provides a module called STEP.

Different loading types are available in ABAQUS as well as the ability to use special subroutines to incorporate the user loading which is not included in the library. Boundary conditions are provided using the boundary condition module using pinned support and/or fixed support as well as the symmetry, if any.

It is important to understand that ABAQUS does not consider the parts connected or embedded although they appear connected in the ASSEMBLY module until the modeller specifies the interaction or contact between these parts.

After completing all the previous modules, the model is ready to be solved; a module called JOB controls the submission task.

Post-processing includes all the methods to display the analysis results, which can be tabulated or different graphic types such as curves, contours and animation.

5.3 Materials' Modelling

In the following sections, the materials' models used in the present study to model the behaviour of the reinforced concrete joint and the double skin composite joint will be presented in detail. It is worth mentioning that there are some parameters that are not measured during the study because of the limited time or due to certain difficulties; therefore, the author used the recommended values used in codes or in previous studies.

5.3.1 Steel Reinforcing Bars

The reinforcing steel bars used in the reinforced concrete joint (longitudinal and transverse reinforcement) and the bars used in the composite joint, the steel plate and the steel J-hook stud connectors were modelled using an elastic-perfectly plastic isotropic model with a von Mises yield surface. As detailed in Chapter two, all the steel parts (bars, plates, studs) were tested under uniaxial tensile in order to find their properties, such as the modulus of elasticity, stress–strain diagram and ultimate strain. Stress–strain diagrams for steel reinforcement of diameters 8mm, 12mm, 16mm, the steel plate and stud connector are presented in Figure 3-9, and Table 3-5 presents a summary of their properties.

In ABAQUS the elastic-plastic model is defined by defining the elastic properties, which are the modulus of elasticity and Poisson's ratio, and the plastic part is defined using the stress-strain values. In the plastic region, the stresses and strains should be converted to the true values rather than nominal (measured) values and the equations used in the conversion are as follows:

$$\sigma_{true} = \sigma_{nom}(1 + \varepsilon_{nom}) \tag{5-1}$$

$$\varepsilon_{true}^{pl} = \ln(1 + \varepsilon_{nom}) - \frac{\sigma_{true}}{E} \tag{5-2}$$

Where:

σ_{true}: is the true stress,

σ_{nom}: is the nominal (measured) stress,

ε_{true}: is the true strain,

ε_{true}: is the nominal strain, and

E: is the modulus of elasticity.

5.3.2 Concrete

ABAQUS presents three models to model the concrete behaviour:

1- Smeared Crack model,
2- Brittle Cracking model, and
3- Concrete Damage Plasticity (CDP) model.

In the present study, the concrete damage plasticity model is adopted to model the concrete in all the modelled beam-column joints. CDP was introduced by Lubliner et al. (1989) to model concrete and the model developed by Lee and Fenves (1998) is used to model concrete under cyclic loading and monotonic loading. To model the inelastic behaviour of concrete, the CDP model uses a combination of isotropic damage elasticity and isotropic tensile and compressive plasticity. The CDP model assumes that the failure mechanisms are mainly due to cracking of concrete under tensile stresses and crushing under compression. The response of concrete under uniaxial tension and uniaxial compression defined by damage plasticity used in ABAQUS is represented in Figure 5-1 (a) and (b) (Simulia, 2010).

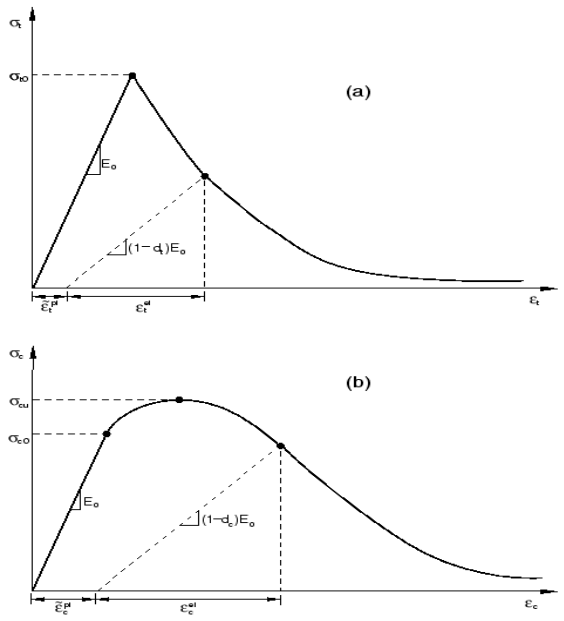

Figure 5-1: Concrete modelling in concrete damage plasticity (a) Tension (b) Compression

In the above figures, the stress is defined as a function of the equivalent plastic strain, equivalent plastic strain rate, temperature and predefined field variables, as is shown in the following equations (Simulia, 2010):

$$\sigma_t = \sigma_t\left(\tilde{\varepsilon}_t^{pl}, \dot{\tilde{\varepsilon}}_t^{pl}, \theta, f_i\right) \tag{5-3}$$

$$\sigma_c = \sigma_c\left(\tilde{\varepsilon}_c^{pl}, \dot{\tilde{\varepsilon}}_c^{pl}, \theta, f_i\right) \tag{5-4}$$

Where:

σ_t: is the uniaxial tensile stress,

σ_c: is the uniaxial compressive stress,

$\tilde{\varepsilon}_{c,t}^{pl}, \dot{\tilde{\varepsilon}}_{c,t}^{pl}$: are the equivalent plastic strain and equivalent plastic strain rate respectively,

θ: is the temperature,

f_i: is the predefined field variable.

In terms of the initial stiffness elastic matrix (E_0) and damage variables, the stress–strain relationships for tension and compression are defined as follows:

$$\sigma_t = (1 - d_t)E_0\left(\varepsilon_t - \tilde{\varepsilon}_t^{pl}\right) \tag{5-5}$$

$$\sigma_c = (1 - d_c)E_0\left(\varepsilon_c - \tilde{\varepsilon}_c^{pl}\right) \tag{5-6}$$

Where:

d_t and d_c: are the damage in tension and in compression respectively.

The damage variables d_t and d_c are defined as a function of the plastic strains, temperature and field variables, as follows:

$$d_t = d_t\left(\tilde{\varepsilon}_t^{pl}, \theta, f_i\right) \qquad 0 \le d_t < 1 \tag{5-7}$$

$$d_c = d_c\left(\tilde{\varepsilon}_c^{pl}, \theta, f_i\right) \qquad 0 \le d_c < 1 \tag{5-8}$$

The reason for choosing this model is its applicability to monotonic and cyclic loading and, since the present study includes both monotonic and cyclic tests,

therefore the model will be used in both cases without changing any of the assumptions that might be needed. Also, this model depends mainly on the uniaxial tensile and compressive tests to specify most of its parameters in most cases. In addition, it has been used in many studies and provided good results (Qian and Li, 2011; Nguyen and Kim, 2009; Li et al., 2012; Qureshi et al., 2011; Coronado and Lopez, 2006; Chen et al., 2010; Yan, 2014; Barth and Wu, 2006).

The next sections present the concrete models in tension and compression for Normal Concrete (NC), Steel Fibrous Concrete (SFC) and High-Strength Concrete (HSC). These details are explained separately because of the differences in the behaviour of different types of concrete which affect their response in tension and compression.

The steel parts (plates, studs and reinforcing bars) are modelled using the elastic-perfectly plastic isotropic model as seen in section 5.3.1. Since there are no essential changes in the properties of steel between the modelled specimens for concrete, only concrete models (Normal concrete, Steel Fibre Concrete and High-Strength Concrete) are presented in the following sections and no further models for steel are used.

5.3.3 Normal Concrete in Compression

The concrete damage plasticity model uses the uniaxial compression stress-strain behaviour. Since the complete stress-strain curve needs special testing apparatus, it can be said that all the previous studies adopted the available stress-strain relationships, such as the model of Eurocode2 (2004) which was used by a number of authors (Qureshi et al., 2011; Coronado and Lopez, 2006; Chen et al., 2010; Yan, 2014; Barth and Wu, 2006; Nguyen and Kim, 2009), the model presented by Saenz (1964) which was used by Chen et al. (2010) and Qian and Li (2011), and the model presented by Carreira and Chu (1985) which was used by Yan (2014).

In the present study, since the beam-column joint behaviour is dominated by the tensile cracking, which was established by the experimental tests and as reported by Abbas et al. (2014), the stress-strain relationship which was obtained experimentally is used up to the maximum compressive stress, as shown in Figure 5-2.

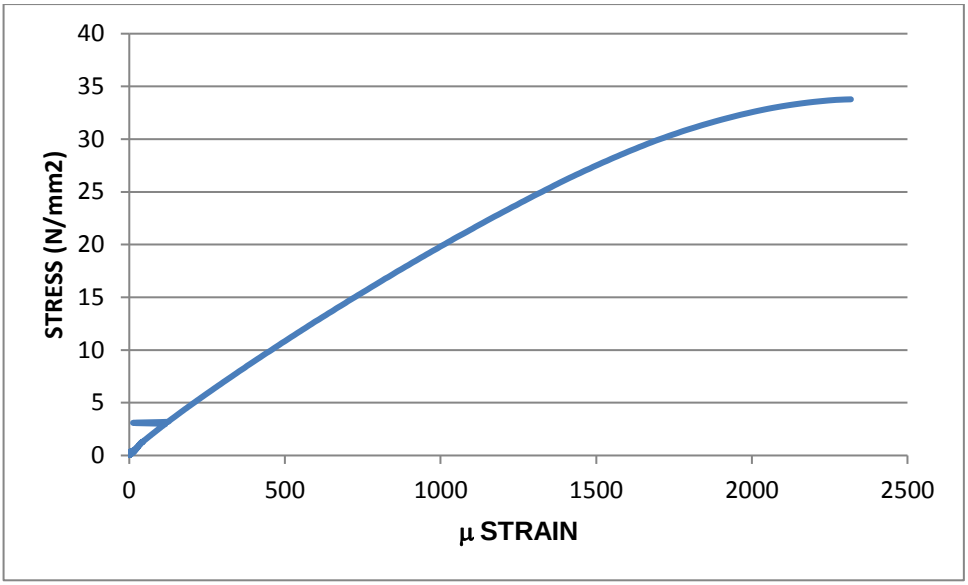

Figure 5-2: Stress-strain of NC under compression

The descending part of the compression stress-strain curve has not been found; therefore, it has not been simulated because it has no effect on the results as the concrete stresses did not exceed the maximum compressive strength (no crushing in the concrete was observed). The maximum compressive strength was 33.77 N/mm^2 and the maximum strain corresponding to the maximum compressive strength was 0.0023.

According to Eurocode2 (2004), the elastic secant modulus can be approximated to be the slope of the stress-strain curve part between 0 and $0.4f_{cm}$ and it has been found to be 23872 N/mm^2.

5.3.4 Normal Concrete in Tension

The concrete is defined as linear elastic up to the maximum tensile strength (cracking stress),f_t, after which it shows strain softening, which represents the tension-stiffening effect. Tension stiffening provides the behaviour of concrete beyond cracking because it is basically defined as the ability of cracked concrete to resist or carry tensile stresses between cracks. ABAQUS allows for the stress-strain relationship of the concrete in tension to be defined using three techniques, which are:

1- Stress-strain tabular values
2- Tensile strength versus fracture energy tabular values
3- Fracture energy versus crack width tabular values

The concrete has a low tensile strength and this can be determined experimentally with three common methods: the direct tensile test, split cylinder test and modulus of rupture test. In the present study, the model presented by Hordijk (1991) was used to define the relationship between the crack width and the tensile strength after cracking. According to Hordijk's model, the tensile strength is a function of the maximum tensile stress f_t, maximum crack displacement w_{cr}, and two constants, c1 and c2, as follows:

$$\frac{\sigma_t}{f_t} = \left[1 + \left(c_1 \frac{w_t}{w_{cr}}\right)^3\right] e^{-c_2 \frac{w_t}{w_{cr}}} - \frac{w_t}{w_{cr}}(1 + c_1^3) e^{-c_2} \qquad (5\text{-}9)$$

Where:

σ_t: is the concrete tensile strength,

f_t: is the maximum tensile strength,

C_1: is a constant = 3.0,

C_2: is a constant = 6.93,

W_t: is the crack opening displacement,

W_{cr}: is the maximum crack opening displacement, which can be calculated using the formula used in Chen et al. (2010), as follows:

$$w_{cr} = \frac{5.14 G_F}{f_t} \qquad (5\text{-}10)$$

Where G_f is the fracture energy which can be estimated using the following formula from the CEB-FIP Model Code (Committee Euro-International du Beton-Fedration International de la Precontrainte) (CEB, CEP-FIP Model Code 1993):

$$G_f = (0.0469 d_a^2 - 0.5 d_a + 26)\left(\frac{f_{ck}}{10}\right)^{0.7} \qquad (5\text{-}11)$$

Where (d_a) is the maximum aggregate size.

Figure 5-3 shows the tensile stress vs. crack opening displacement relationship.

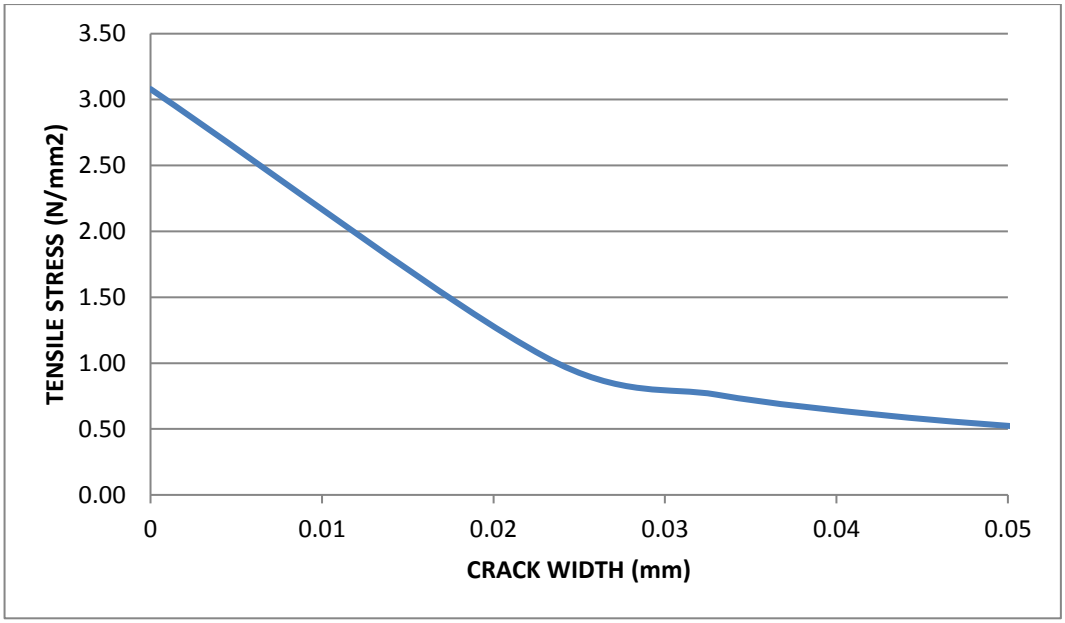

Figure 5-3: Tensile stress – crack width curve for the NC

Finally, it is important to report that the material properties presented in the previous sections have been used to model the reinforced concrete joint and the double skin composite joint with normal concrete.

5.3.5 Fibrous Concrete in Compression

The stress-strain of the fibrous concrete in compression tested experimentally is shown in Figure 5-4. As discussed previously, the complete stress-strain curve of the concrete needs special testing apparatus; therefore, the descending part is computed using the model presented by Ezeldin and Balaguru (1992). This model was chosen from among other available models (Soroushian and Lee, 1989; Nataraja et al., 1999; Barros and Figueiras, 1999) because of its applicability to steel fibres with hooked ends and due to its simplicity, as it does not need a large number of empirical parameters. This model is summarised as follows:

$$\sigma = f'_{cf} \frac{\beta\left(\frac{\varepsilon}{\varepsilon_{pf}}\right)}{\beta - 1 + \left(\frac{\varepsilon}{\varepsilon_{pf}}\right)^{\beta}} \tag{5-12}$$

For hooked-end fibres:

$$\beta = 1.093 + 0.7132RI - 0.926 \tag{5-13}$$

$$RI = W_f \frac{D_f}{L_f} \quad (5\text{-}14)$$

Where:

σ: is the compressive stress in the fibrous concrete,

$f_{cf}^{'}$: is the compressive strength,

ε: is the fibrous concrete strain corresponding to σ,

σ_{pf}: is the compressive strength of the fibrous concrete,

W_f: is the weight percentage of steel fibres,

D_f: is the diameter of the steel fibres, and

L_f: is the length of the steel fibres.

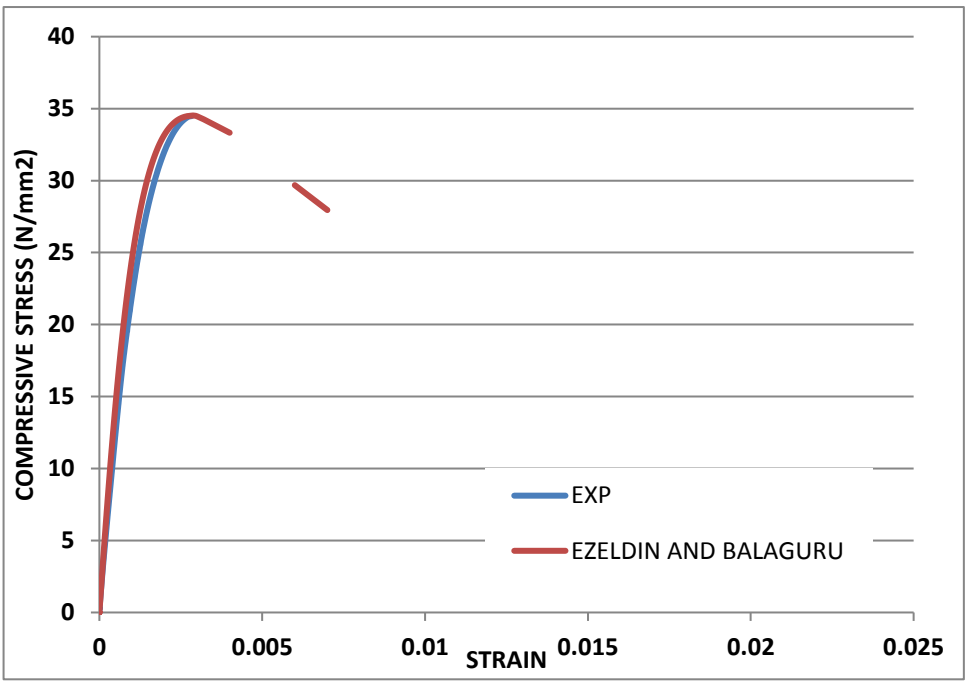

Figure 5-4: Stress-strain curve of 1% SF concrete under compression

5.3.6 Fibrous Concrete in Tension

The presence of steel fibres in the concrete gives a more ductile tensile response compared to the concrete without fibres. This behaviour is attributed to the role of the steel fibres in bridging the cracked region.

The model presented by Lok and Xiao (1999) was adopted in the present study as it had been used recently by Abbas et al. (2014), which confirmed its suitability. The model can be described as follows:

$$\sigma = f_t \left[2\left(\frac{\varepsilon}{\varepsilon_{to}}\right) - \left(\frac{\varepsilon}{\varepsilon_{to}}\right)^2\right], \qquad 0 \le \varepsilon \le \varepsilon_{to} \tag{5-15}$$

$$\sigma = f_t \left[1 - \left(1 - \frac{f_{tu}}{f_t}\right)\left(\frac{\varepsilon - \varepsilon_{to}}{\varepsilon_{t1} - \varepsilon_{to}}\right)\right], \qquad \varepsilon_{to} \le \varepsilon \le \varepsilon_{t1} \tag{5-16}$$

$$\sigma = f_{tu}, \qquad \varepsilon_{t1} \le \varepsilon \le \varepsilon_{tu} \tag{5-17}$$

Where:

σ: is the tensile stress,

f_t: is the fibrous concrete's ultimate tensile stress,

ε: is tensile strain,

ε_{to}: is the ultimate tensile strain, and

f_{tu} and ε_{t1} are the residual tensile strength and the corresponding strain that can be calculated according to Lok and Pei (1998), as follows:

$$f_{tu} = \eta V_f \tau_d L/d \tag{5-18}$$

$$\varepsilon_{t1} = \tau_d \frac{L_f}{D_f} \frac{1}{E_s} \tag{5-19}$$

Where:

η: is the orientation factor to take into account the three dimensions' random distribution of fibres,

V_f: is the fibre volume fraction,

L_f/ D_f: is the fibre aspect ratio,

E_s: is the fibre modulus of elasticity, and

τ_d: is the bond stress.

In the concrete damage plasticity model, the stress-strain behaviour is taken as linear elastic up to the ultimate tensile strength; therefore, equation 15

above will not be used. Figure 5-5 shows the post-cracking tensile stress-strain relationship used in the current study.

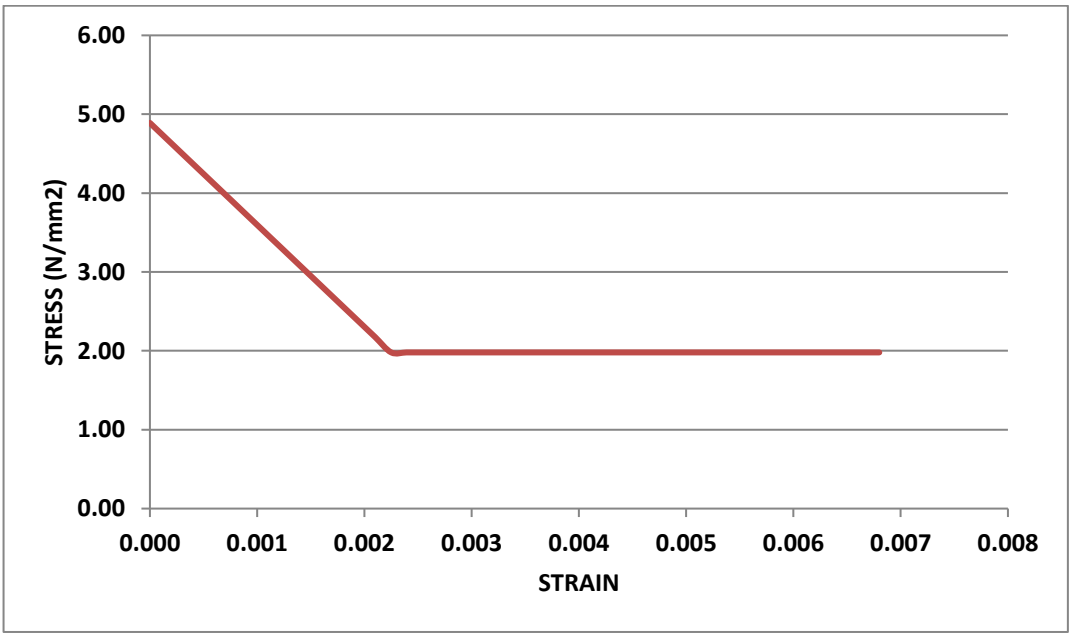

Figure 5-5: Tensile plastic stress-strain of SF concrete

5.3.7 High-Strength Concrete in Compression

The double skin composite joint cast with high-strength concrete was modelled using the concrete damage plasticity model. The properties of high-strength concrete in compression and in tension were provided to ABAQUS based on the available (measured) data as well as using the validated models to simulate the region and parameters that have not been measured. The compressive stress-strain relationship was measured experimentally using a 75x150 mm cylinder, as shown in Figure 5-6 and as explained in previous sections; the measured part represented the response up to the maximum strength. The descending part of the stress-strain curve can be found using one of the available models, such as those by van Gysel and Taerwe (1996), Hsu and Hsu (1994), and Güler et al. (2012).

In the present study, the model presented in Wee et al. (1996) was used to find the descending part of the compressive stress-strain because it does not need a large amount of empirical data and it is presented in an official code,

which means it is based on a large number of tests and analyses. The model can be described as follows:

$$\sigma_c = f_{cm}\left[\frac{k_1\beta\left(\frac{\varepsilon}{\varepsilon_0}\right)}{k_1\beta - 1 + \left(\frac{\varepsilon}{\varepsilon_0}\right)^{k_2\beta}}\right] \quad (5\text{-}20)$$

$$k_1 = \left(\frac{50}{f_{cm}}\right)^{3.0} \quad (5\text{-}21)$$

$$k_2 = \left(\frac{50}{f_{cm}}\right)^{1.3} \quad (5\text{-}22)$$

$$\beta = \frac{1}{(1 - f_{cm}/\varepsilon_0 E_{it})} \quad (5\text{-}23)$$

Where:

σ_c and ε are the compressive stress and corresponding compressive strain,

ε_0: is the strain at peak stress,

f_{cm}: is the cylinder's compressive strength, and

E_{it}: is the initial tangent modulus of elasticity.

Figure 5-6 shows the complete stress-strain curve of high-strength concrete.

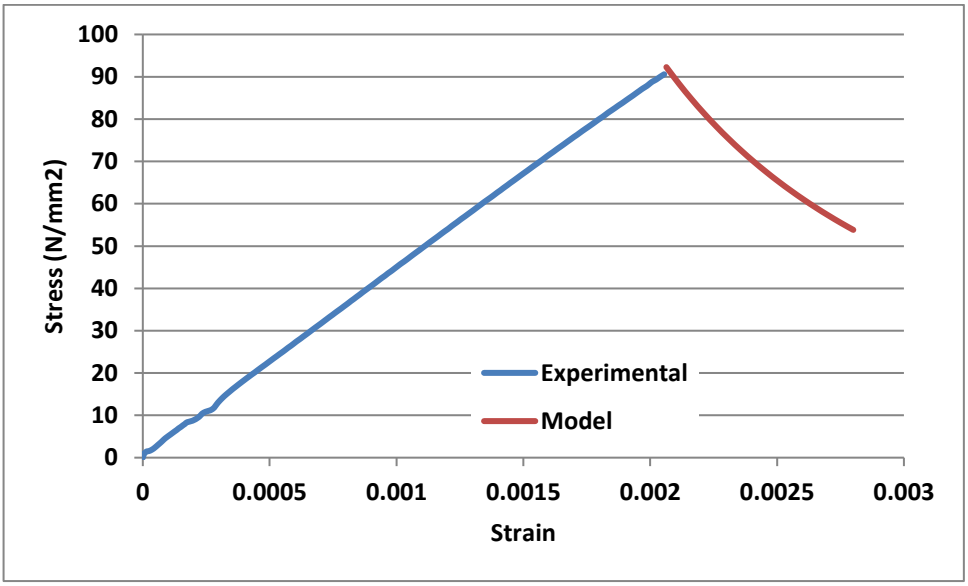

Figure 5-6: Stress-strain of HSC under compression

5.3.8 High-Strength Concrete in Tension

The behaviour of the high-strength concrete in tension was modelled based on the model presented by Li and Ansari (2000), which was used by Begum et al. (2013) to model concrete behaviour in tension for the ABAQUS package, and has confirmed its suitability for this purpose. The proposed model gives the relationship between the tensile stress and the crack width, as follows:

$$\sigma = f_t' \left\{ 1 - exp\left[-\left(\frac{\frac{k}{w}}{w_f} \right)^n \right] \right\} \quad (5\text{-}24)$$

Where:

k=0.03 and n=0.9,

σ: is the tensile stress in the concrete,

f_t' : is the tensile strength of the concrete,

w: is the crack width, and

w_f: is the maximum crack width.

The fracture energy is defined as follows (Li and Ansari, 2000):

$$G_f = (0.31 f_t' + 1.81) \times 10^{-3} \quad (5\text{-}25)$$

The above equation is based on lb-in units. Figure 5-7 shows the tensile stress crack width curve used in ABAQUS.

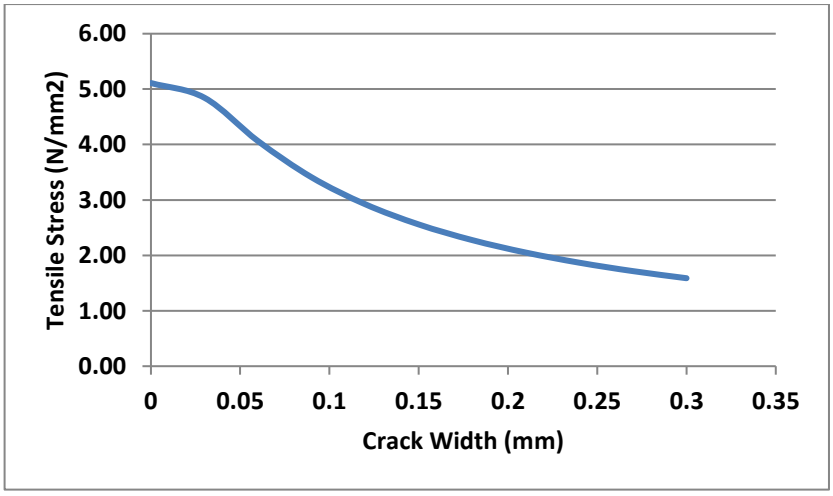

Figure 5-7: Tensile stress–crack width of HSC

5.4 Modelling of the Reinforced Concrete Joint Subjected to Monotonic Loading

The reinforced concrete joint was modelled according to the following steps:

5.4.1 Element Type

A three-dimensional solid element with eight nodes and a reduced integration C3D8R were used to discretise the concrete part. This element has been used by Yan (2014), Qureshi et al. (2011), Abbas et al. (2014), Li et al. (2012), Nguyen and Kim (2009), and Qian and Li (2011). This first-order element provides less accurate results compared to the second-order element and this is because of the shear-locking phenomenon, which results in an inaccurate displacement calculation because the curvature is ignored. The accuracy can be increased by increasing the number of elements, or, in other words, decreasing element size decreases the shear-locking effect. The use of a reduced integration technique reduces the computation time required, but it can cause an hourglassing problem in the element, with one Gaussian (integration) point, which is not the case in the current element type.

For the steel reinforcement, a three-dimensional truss element with two nodes (T3D2) was used to represent the longitudinal reinforcing bars as well as the transverse reinforcement. This element type can transfer one direction (longitudinal) stresses, which is the case in steel reinforcement. Also, this element was used by Nguyen and Kim (2009), Qureshi et al. (2011), Qian and Li (2011), and Abbas et al. (2014).

5.4.2 Mesh

In general, the finer the mesh size the more accurate the solution. This is because it increases the accuracy of the strain and stress distribution in the structure. A balance between the desired accuracy and the computation time should be studied because, as the number of elements increases (finer mesh), the time increases as well. It is well known in finite element solutions that mesh sensitivity analysis should be performed by starting from coarse mesh and monitoring the convergence of one of the variables as the mesh is refined until a suitable mesh size is reached. In the present model, the concrete is the material that is most sensitive to the mesh size due to high nonlinearity in its

behaviour because of the cracking and stiffness degradation. Figure 5-8 shows a comparison between the experimental test result and different mesh sizes using a reduced integration element with eight nodes (C3D8R). Figure 5-9 shows a comparison between the experimental tests result and different mesh size using a fully integrated element with eight nodes (C3D8).

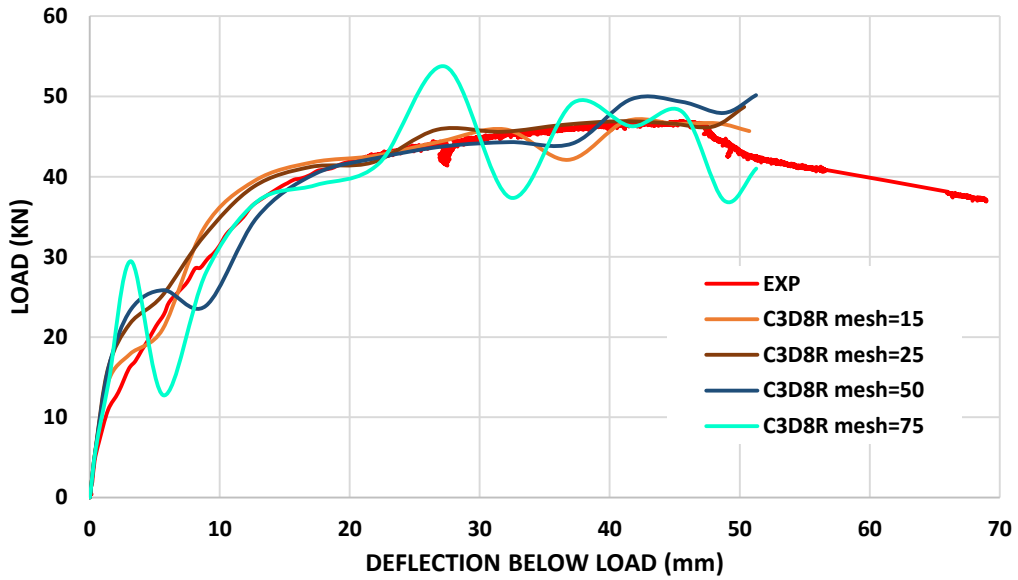

Figure 5-8: Effect of element size on the solution accuracy – C3D8R

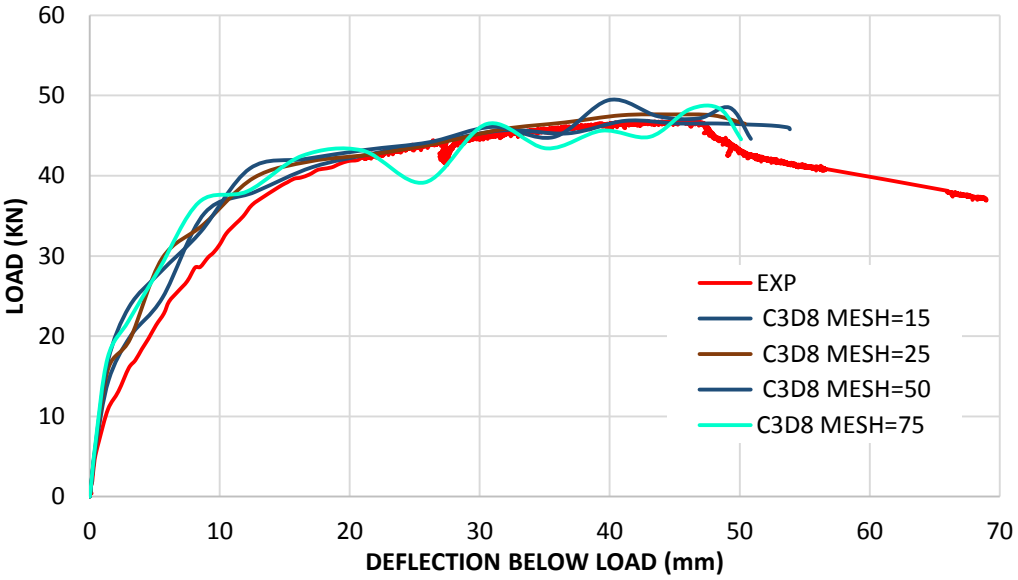

Figure 5-9: Effect of element size on the solution accuracy – C3D8

5.4.3 Reinforcement and Concrete Interaction

The steel reinforcement interacts with the surrounding concrete by a bond effect which transfers the stresses and deformation between the concrete and the steel. Simulation of the bond has been ignored in many studies, such as those by Qureshi et al. (2011), Qian and Li (2011), Li et al. (2012) and Abbas et al. (2014), where the reinforcing steel is considered fully embedded in the concrete, i.e. a perfect bond is assumed between the steel and the surrounding concrete. In the present study, the reinforcement is considered perfectly bonded with concrete by using the EMBEDDED region technique available in ABAQUS (Figure 5-10).

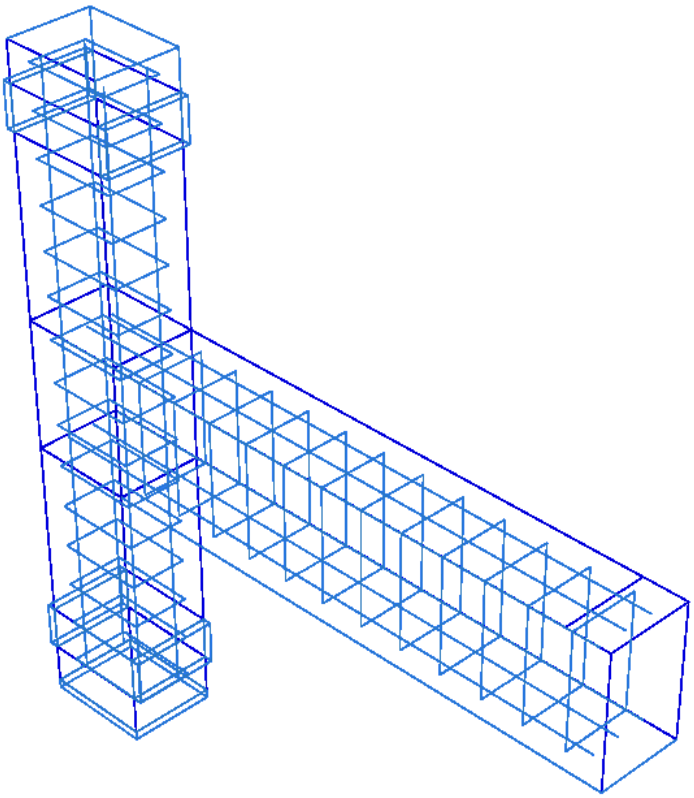

Figure 5-10: Reinforcement embedded in the concrete

5.4.4 Loading and Boundary Conditions

ABAQUS enables simulation of different types of loading such as concentrated force, distributed forces, pressure, etc. All tested specimens were supported using plates and bolts to tie them to the testing rig column, and a steel block was used between the ground and the lower face of the column. The real supports were located on the models using PARTITION and

were considered to be fixed faces since there were no deformations observed during experimental tests.

As detailed in Chapter 4, all the tests were conducted using displacement control and the same technique can be used in ABAQUS. In the experimental tests, the load was applied at 100 mm from the free end of the beam. The nodes on the line at the same location (100 mm from the free end) were displaced using the boundary conditions Displacement/ Rotation.

5.4.5 Solution Technique

In the current study, two solution strategies were used to solve the nonlinear equations that resulted because the material nonlinear response was considered. ABAQUS/Standard performs an implicit solution which needs a huge number of iterations and/or increments to avoid divergence problems and a premature solution abortion. Due to the time required to perform the implicit solution, a quasi-static solution can be introduced using ABAQUS/ Explicit solver, which is used for dynamic problems. It is possible to consider the static loading case as a dynamic loading with a long duration. In other words, if the inertia forces' effects caused by the mass can be eliminated, the solution will be a quasi–static solution. This can be achieved in ABAQUS/ Explicit by monitoring the Kinetic Energy (E_{KE} = ALLKE), which should be negligible and should not exceed 1 – 5 % of the Internal Energy (E_I = ALLIE). ABAQUS/Explicit solves problems without iterations by using the kinematic state, depending on the previous increment, and in this way the computations will be reduced significantly.

Figure 5-11 and Figure 5-12 show the EXPLICIT solution using two types of elements with different mesh sizes, and Figure 5-13 shows a comparison between the internal energy and the kinetic energy.

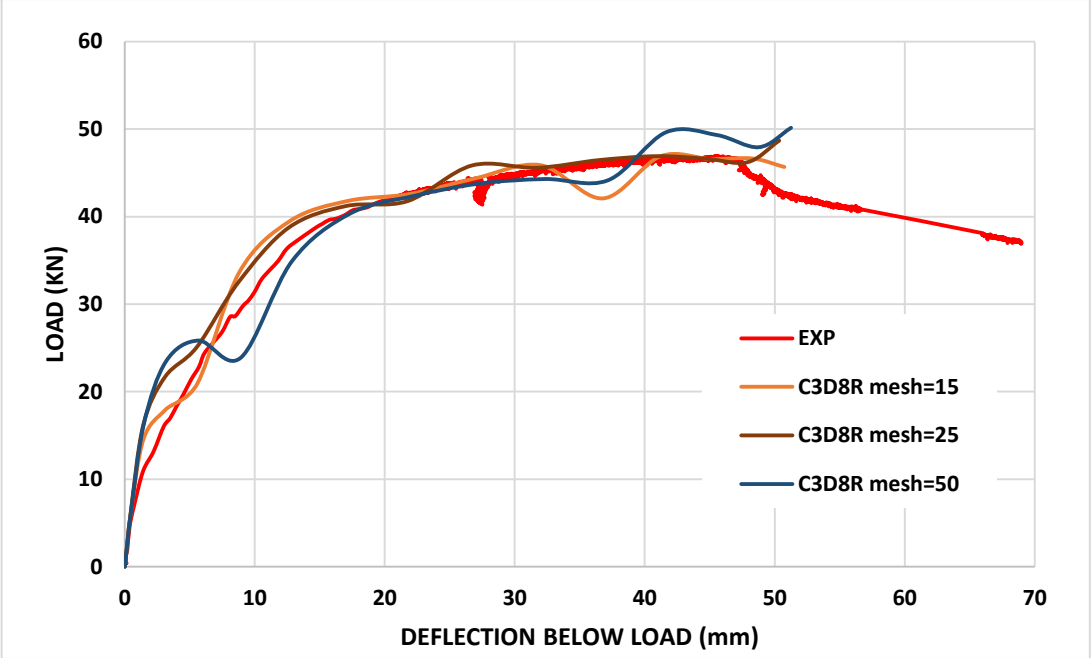

Figure 5-11: Explicit solution with different mesh sizes – C3D8R

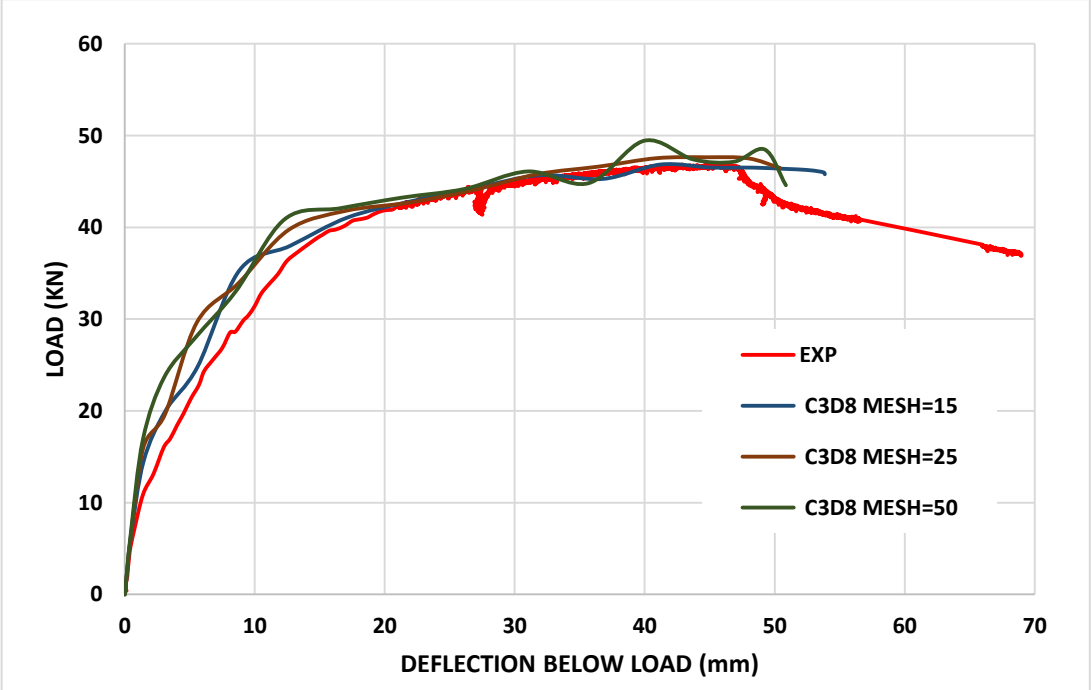

Figure 5-12: Explicit solution with different mesh sizes – C3D8

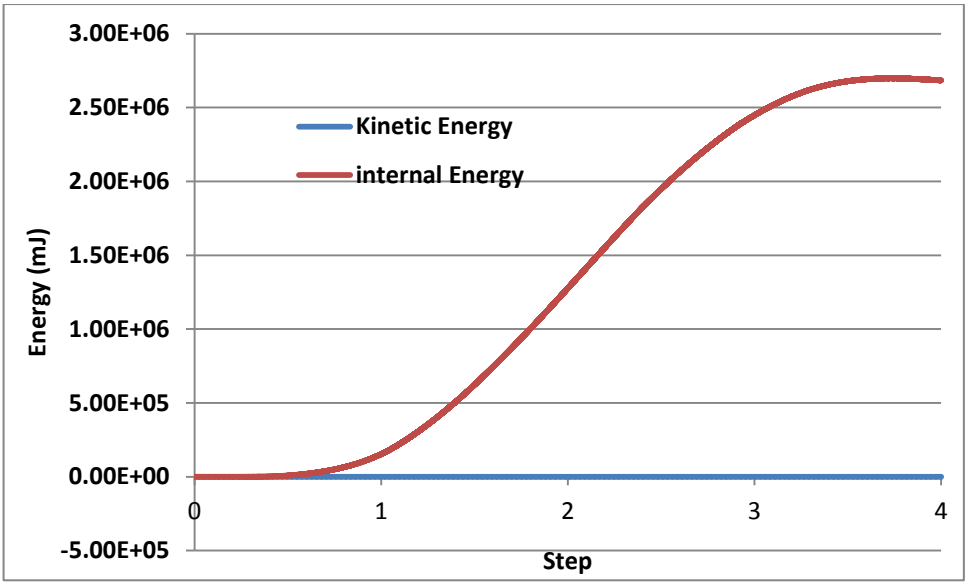

Figure 5-13: Kinetic energy and internal energy variation

In the present simulation ABAQUS/Standard and ABAQUS/Explicit are used with different mesh sizes and different element types in order to decide the best model to be used for the remaining part of the finite element modelling based on the accuracy and the time consumed. Figure 5-14 and Table 5-1 show comparisons between the accomplished analyses.

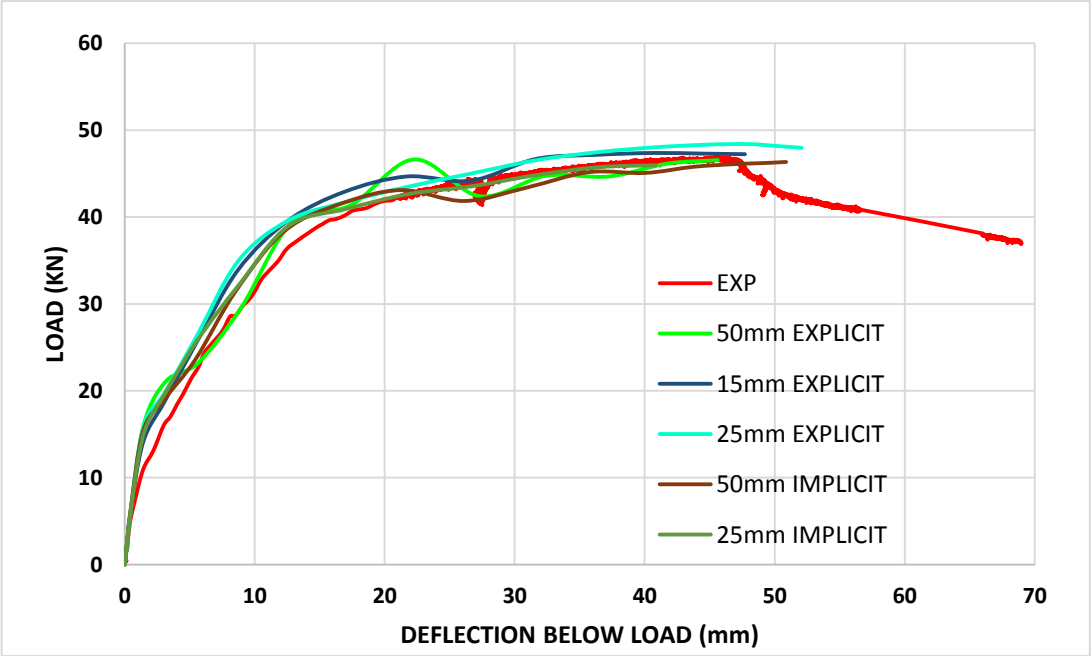

Figure 5-14: Comparison between explicit and implicit solution

Table 5-1: Solution types, element types, and mesh size (RC Joint)

Solution	Element Type (Concrete)	Mesh Size (Concrete)	Time (sec.)
IMPLICIT	C3D8R	75	295
		50	832
		25	10340
		15	151826
	C3D8	75	493
		50	978
		25	7599
EXPLICIT	C3D8R	75	75
		50	187
		25	1265
		15	2655
	C3D8	75	307
		50	700
		25	6630

In addition, Figure 5-14 shows a comparison between two mesh sizes (25 mm and 50 mm) using the EXPLICIT and IMPLICIT SOLUTION C3D8R element. The EXPLICIT solution using the 25 mm element size gives a 3% difference in the maximum load, which is higher than the experimental result.

Based on the comparison of the accuracy and the time required, the best element is C3D8R of size 25 mm using the EXPLICIT solution, which gives a difference of about 1.04% in the maximum load, which is higher than the maximum experimentally measured load. Therefore, this element (type and size) will be used in the remaining joints for concrete discretisation.

5.4.6 Validation of Reinforced Concrete Joint Model

The previous sections have presented the model of the reinforced concrete beam-column joint which was validated by using the recommendations in ABAQUS documentation and the large number of previous studies. In this section, the analysis of the reinforced concrete joint based on the final chosen model will be compared with the available experimental results.

Figure 5-15 shows a comparison between the experimental results and ABAQUS result of the load – which is a deflection curve. The ratio between the maximum load and the experimentally measured load, which is 92.4%, was calculated using ABAQUS. The finite element model response is stiffer than the real response, which can be attributed to the approximation introduced during modelling, such as the perfect bond between the steel and the concrete.

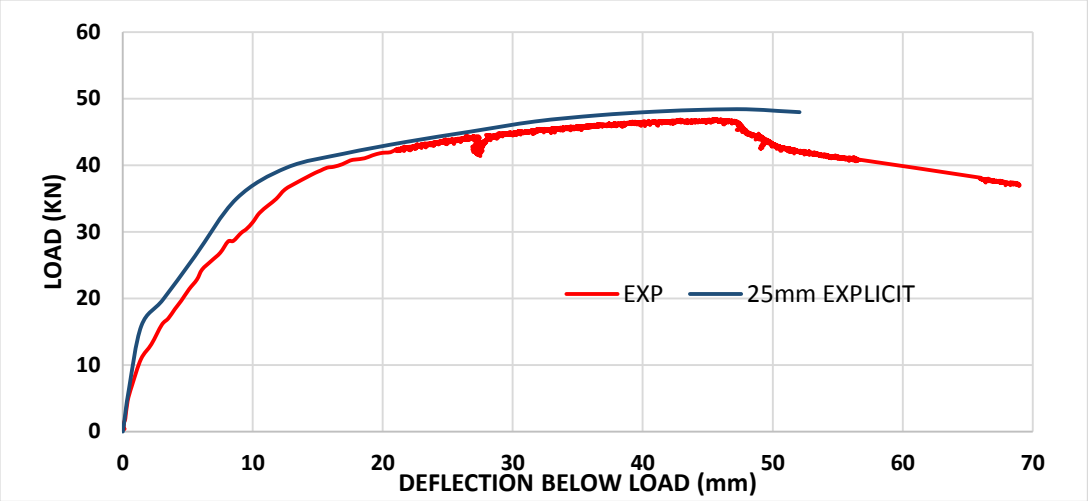

Figure 5-15: Comparison between experimental and ABAQUS results

After cracking, the finite element model stiffness decreased and, when the steel reinforcement reached the yielding stress, the carried load continued to be semi-constant up to the ultimate strain of the steel.

Photo 5-1: First crack location in the RC joint - experimental

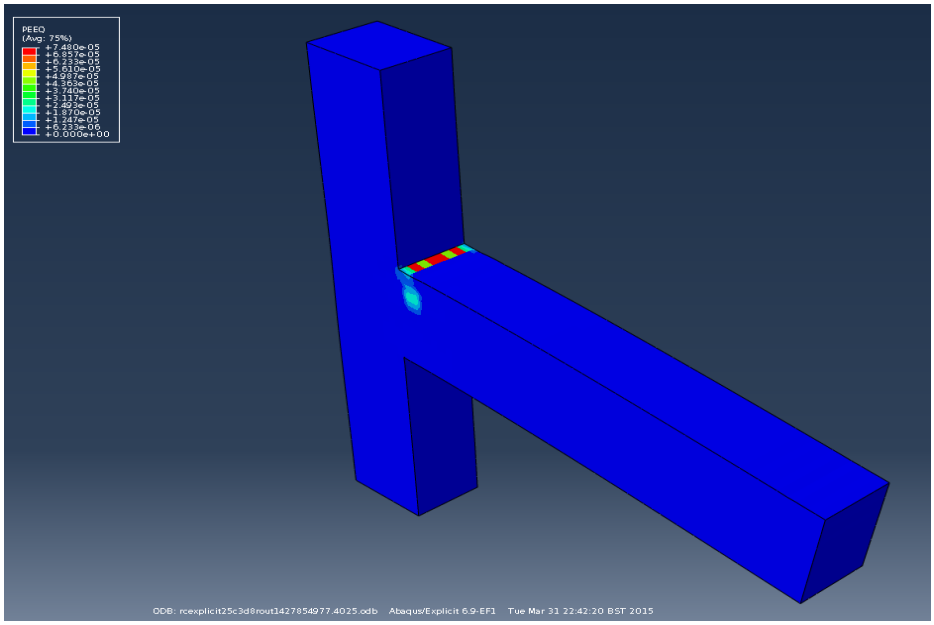

Photo 5-2: Location of first crack in the RC joint – ABAQUS

Photos 5-1 and 5-2 above show the first crack location observed during the experimental test and from the finite element analysis, respectively.

5.5 Double Skin Composite Joint with Normal Concrete

All SCS joints consist of five main different parts, which are:

1. Concrete
2. Steel plate
3. J-hooked steel connectors
4. Steel bars welded onto the inner face of the beam's steel plate
5. Conventional steel reinforcement (longitudinal bars and links) in the column

The same material properties used in the reinforced concrete joint will be used to define the material properties of the double skin composite joint which are cast using normal concrete. The concrete damage plasticity model was used for concrete.

The concrete part, the steel plates, and the stud connector were modelled using the C3D8R element. The longitudinal steel and links reinforcement used in the column were modelled using the truss element (T3D2). The steel bars welded to the beam's plates were modelled using C3D8R solid elements

because using solid elements allows for contact simulation in contrast to the truss element. The welded stud and reinforcing bars were combined together with steel plates using the MERGE technique available in ABAQUS, which means that the welding regions were not modelled. In the author's opinion this assumption is sufficient in the present study because no separation was noticed in the welded bars.

The J-hook connectors were modelled using a cylindrical shape in order to avoid the problems of interaction between the hooked parts of the connectors. The interconnected part was replaced by a spring connecting the inner ends of the connectors through small gaps (4 mm) between each pair of connectors. The steel reinforcement, the links, and the stud connectors were embedded in the concrete.

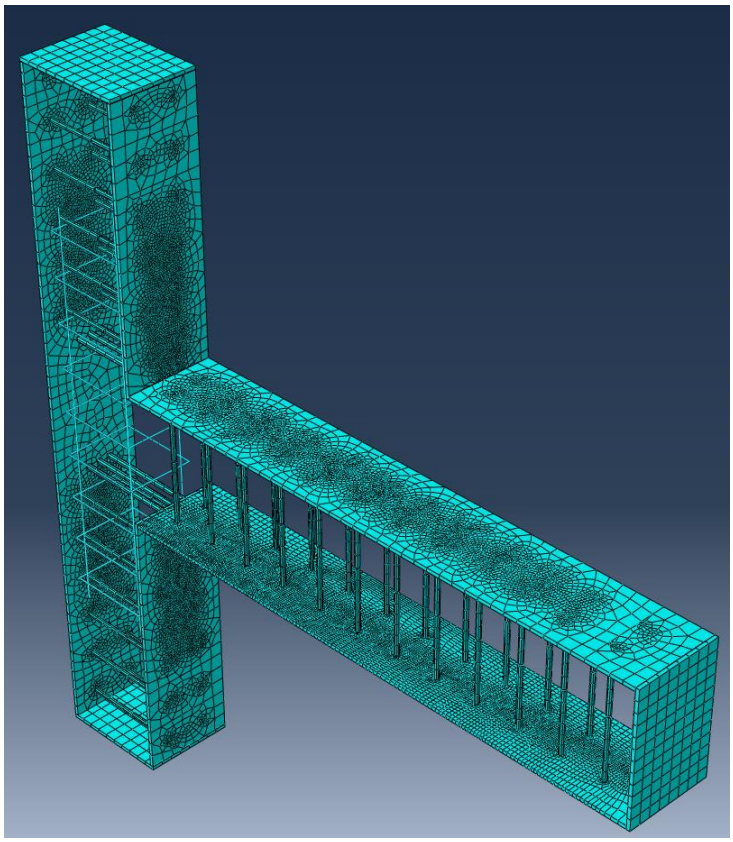

Photo 5-3: SCS joint modelling

5.5.1 Validation of Double Skin Composite Joint with the NC Model

Figure 5-16 shows a comparison between the experimental and finite element analysis load-deflection curve of the double skin composite joint cast using normal concrete. The maximum experimentally measured load is 5% higher than the load predicted using finite element analysis. The finite element model coincides with the experimental results during the elastic range (up to 14 kN) and it has a stiffer response beyond an elastic range up to 46 kN, where a large number of cracks developed and the welded steel bars started to yield. This behaviour can be attributed to the loss of integrity of the beam-column joint parts due to cracking in the concrete and to the deformation in the top steel plate of the beam.

Figure 5-17 shows a comparison between the steel plate strains measured experimentally using electrical strain gauges and the strains predicted using ABAQUS. BB50 on the graph refers to the strain gauge located on the bottom face of the beam plate at 50 mm from the column face and BT 400 refers to the strain gauge located on the top face of the beam plate at 400 mm from the column face.

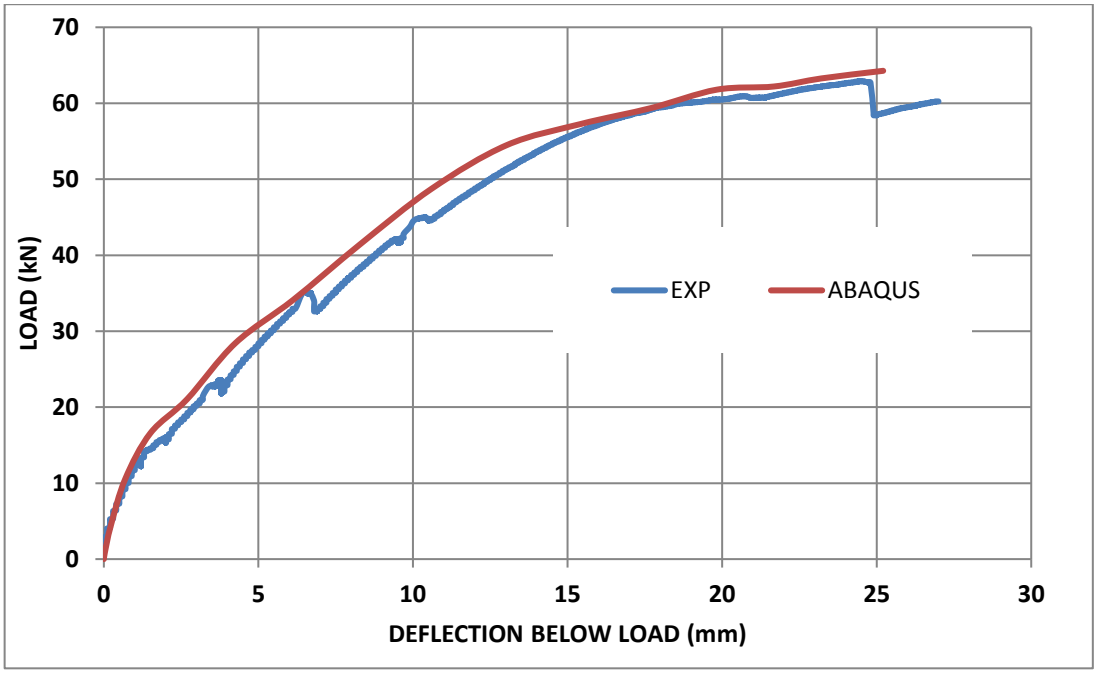

Figure 5-16: FEA and experimental results of the DSC joint with NC

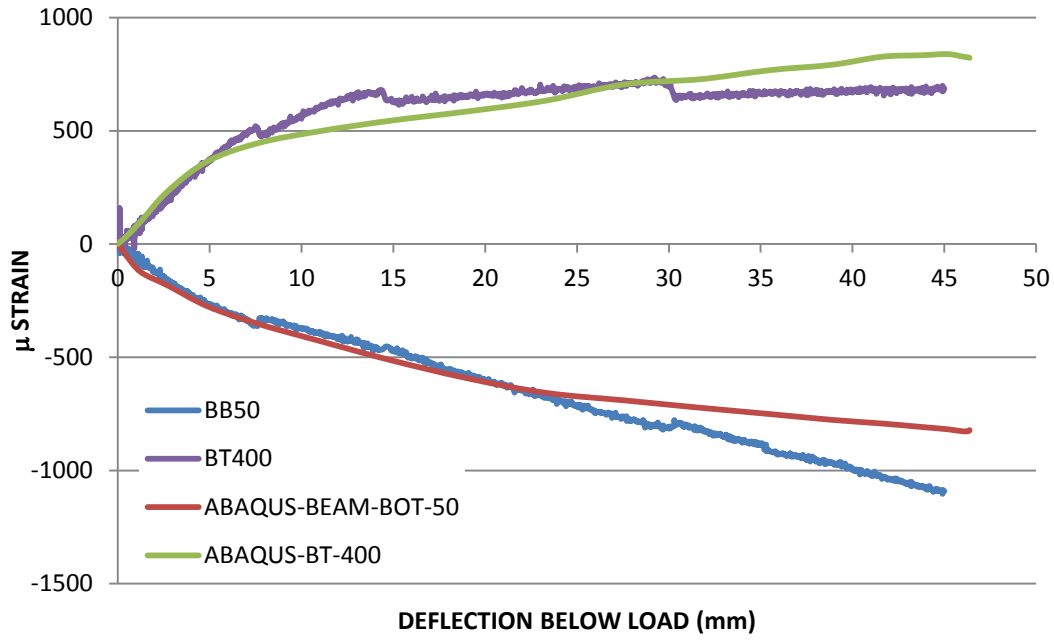

Figure 5-17: Steel stresses comparison DSC joint with NC

The region at 50 mm from the column face has a complicated stress distribution because it is very close to the critical section region, and also because of the welded steel bars on the inner face of the plate. This complication in stress distribution leads to insufficient accuracy in the measured strains, especially after crack development and growth. Photo 5-4 shows Von Mises stress distribution, which reflects the failure of the steel plate.

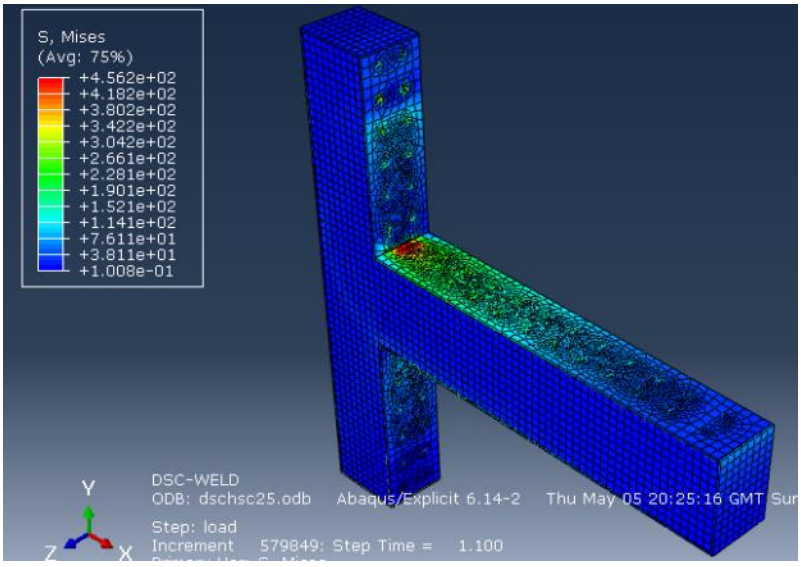

Photo 5-4: Von Mises stress distribution SCS- NC

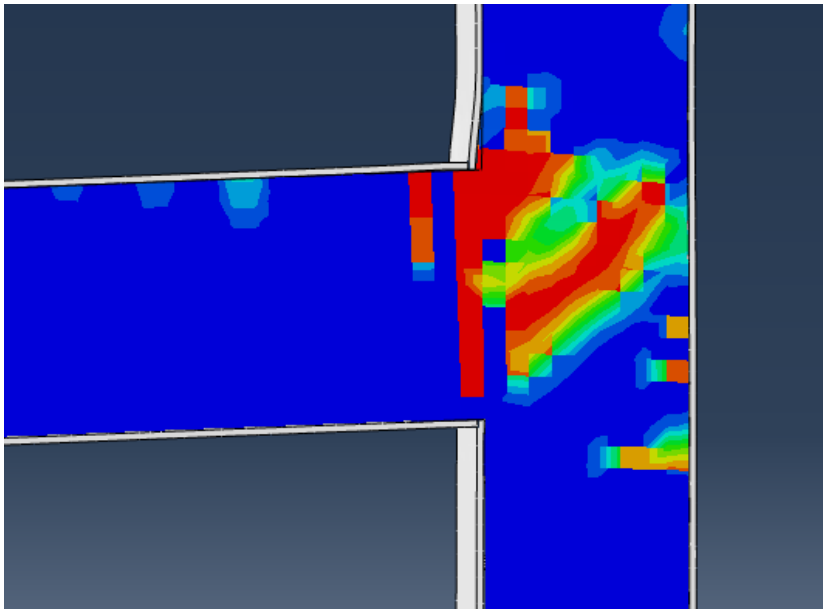

Photo 5-5: Damage distribution - ABAQUS

Photo 5-6: SCS with NC cracking

Photo 5-5 shows the crack distribution from ABAQUS and Photo 5-6 shows the crack distribution during the test; it is obvious that ABAQUS is an efficient tool by which to study initiation and crack development.

5.6 Double Skin Composite Joint with Steel Fibres Model

In order to study the effect of the steel fibres on the behaviour of the double skin composite joint, two joints were cast using steel fibrous concrete in the

most critical region (300 mm from the face of the column up and down and 300 from the column face for the beam). One of the joints was cast using concrete containing (1%) steel fibres by volume and the second joint was cast using concrete with a very low percentage of steel fibres (0.25%) by volume in order to identify if a low percentage of steel fibres enhances the response of the joint.

In the present section, the modelling of the double skin composite joint for the joint with 1% volume fraction of steel fibres will be presented. The Concrete Damage Plasticity (CPD) model is used to model the behaviour of the concrete. The CDP model requires the definition of the concrete behaviour in compression and in tension.

5.6.1 Validation of the DSC Joint with Steel Fibres Model

Steel fibre concrete was used to cast a double skin composite in order to study the effect of steel fibres on the behaviour of the composite joint. The steel fibre concrete was used in the junction region and was extended to 300 mm in the column and in the beam and the remaining parts was cast using plain concrete, as shown in Photo 5-7, which shows the material distribution of the simulated joint in ABAQUS.

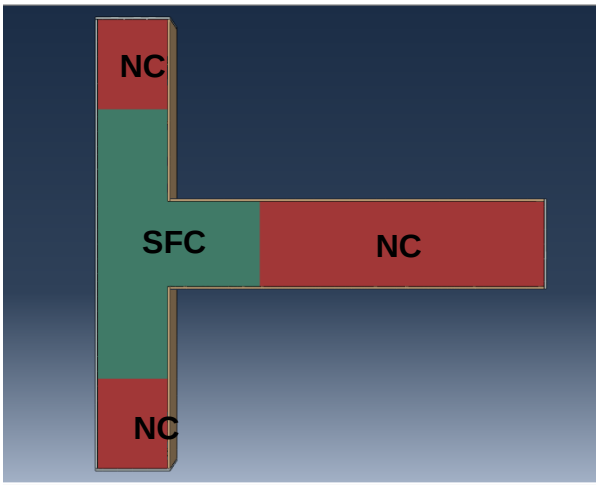

Photo 5-7: SCS joint with SFC – concrete casting

A comparison between the load-deflection curves of the double skin joint was tested experimentally and the finite element analysis is presented in Figure 5-18 below. As in the previously modelled joints, the response is identical in

the elastic range up to the crack initiation, followed by stiffer behaviour until the steel begins to yield and a large number of cracks begin to form.

The maximum predicted load is accurate up to 99% of the experimentally measured load, while the model overestimates the load in the region between the cracking initiation point up to the steel yielding point, which reflects the dependency of the composite joint on the steel components rather than on the concrete part.

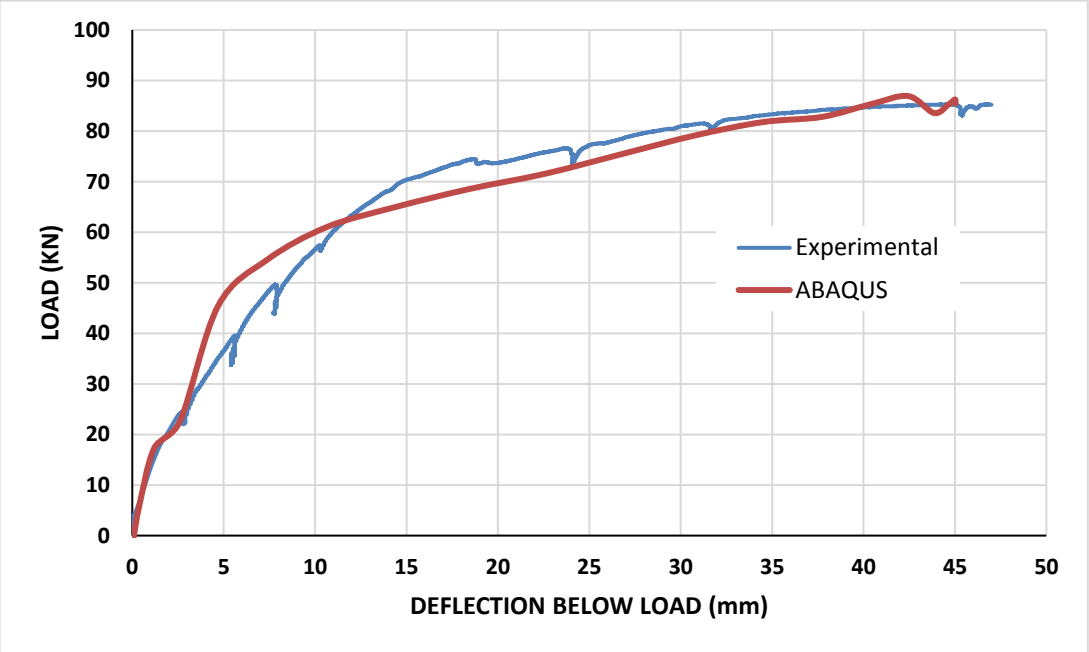

Figure 5-18: DSC with SFC Load – Deflection curve comparison

Figure 5-19 shows a comparison between the experimentally measured steel plate strains and ABAQUS values, and it is obvious that the strains at the region close to the critical section have deviated because of the complicated stresses and deformations at that location which affected the measured values.

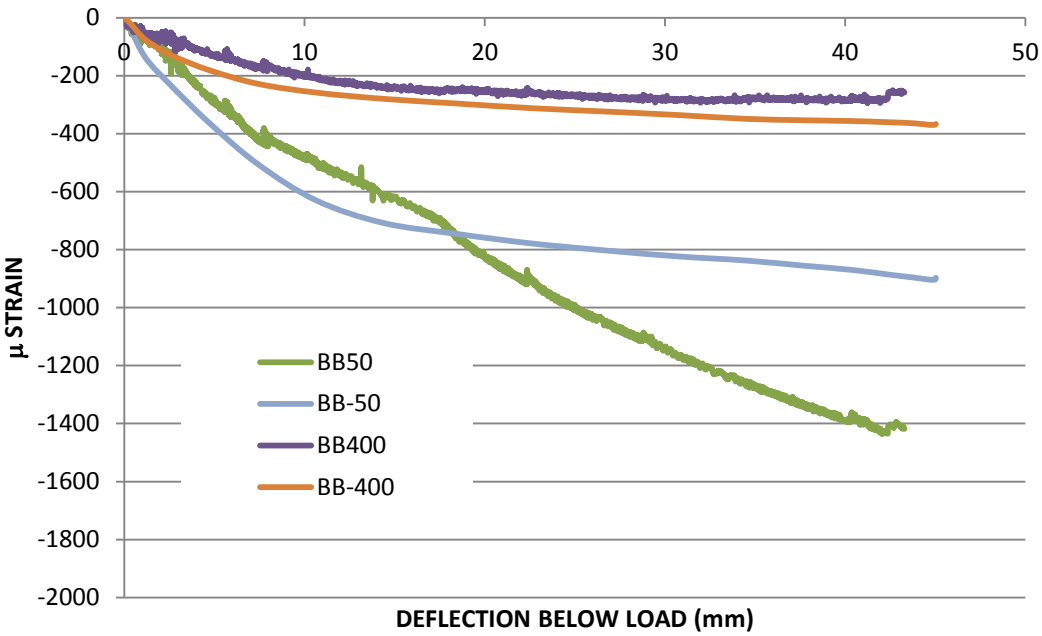

Figure 5-19: Steel plate strains comparison

Photo 5-8 and Photo 5-9 show the crack distribution according to ABAQUS and from experimental tests respectively, and it can be seen that the predicted cracking distribution agrees well with the cracking in the tested composite joint in both number and location. Photo 5-10 shows Von Mises stress distribution.

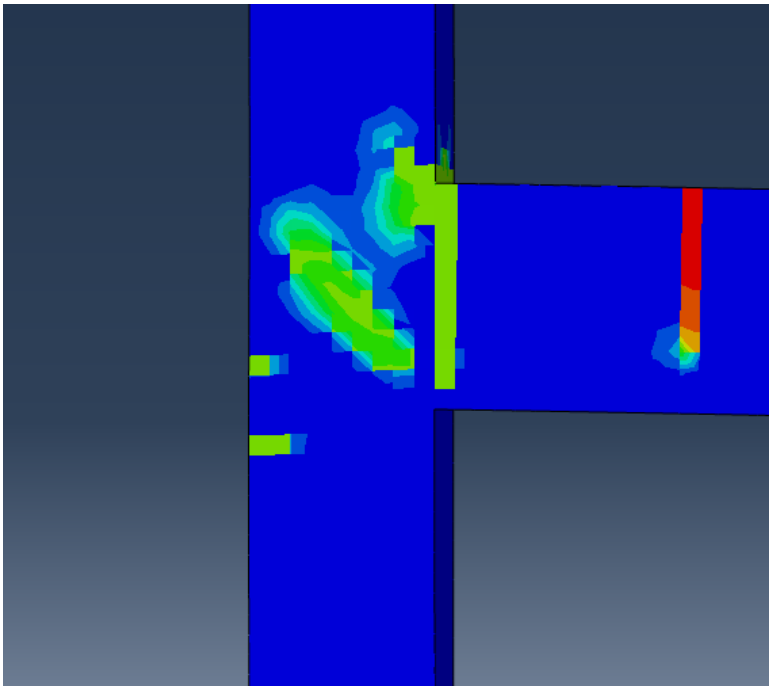

Photo 5-8: Cracking of SCS joint with SFC - ABAQUS

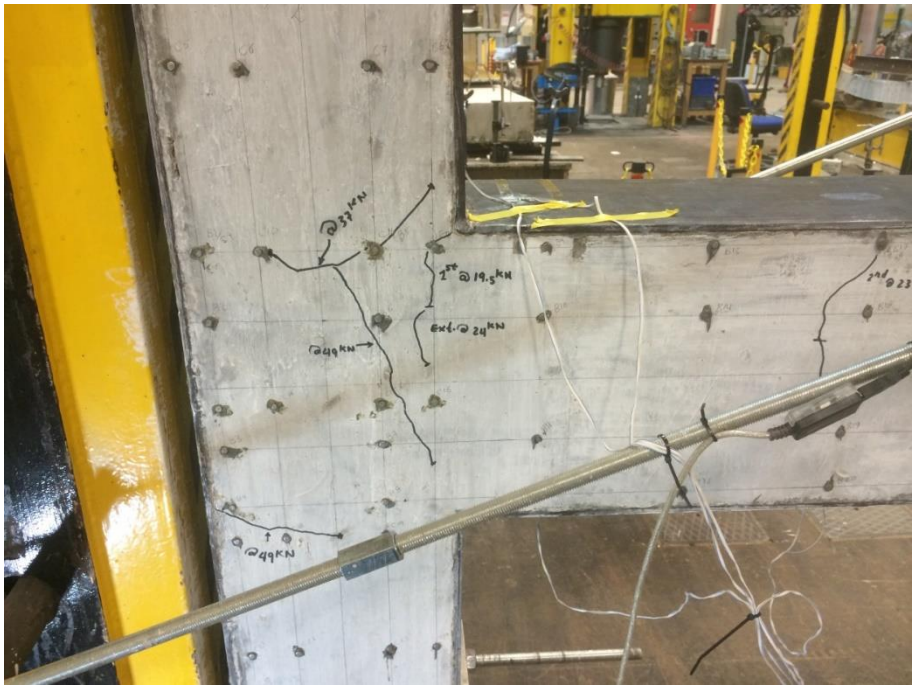

Photo 5-9: Cracking of SCS joint with SFC – experiment

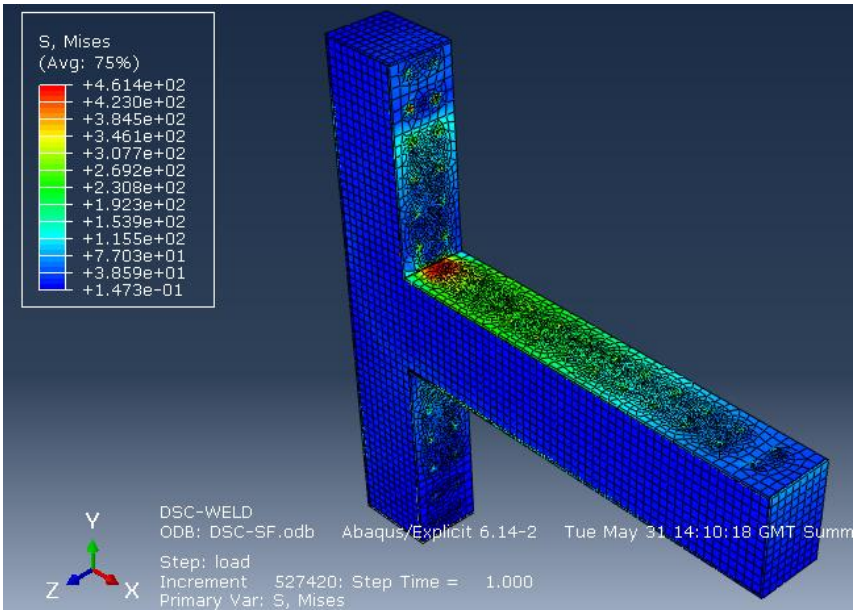

Photo 5-10: Von Mises stress distribution SCS – SF

5.7 Validation of the DSC Joint with the HSC Model

High-strength concrete is used in casting a double skin composite joint and, as in the double skin composite joint with steel fibres, the high-strength concrete is used in the junction of the beam column and is extended to 300 mm in the beam and in the column. Figure 5-20 shows a comparison

between the load deflection from the experimental test and the curve predicted using ABAQUS.

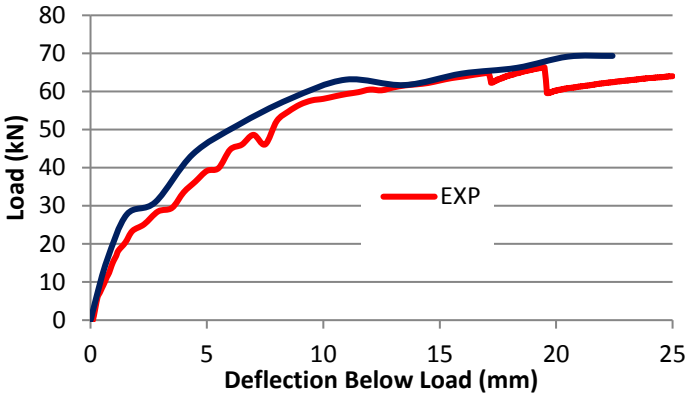

Figure 5-20: SCS with HSC Load – Deflection comparison

The finite element load-deflection curve agrees well with the experimental load deflection in the elastic and in the final range, which can be attributed to the cracking process in the intermediate region.

The maximum predicted load is higher than the experimentally measured load by 10.7% and they can be considered to be in good agreement.

In the steel plate strains presented in Figure 5-21, it can be seen that the precision of the model's strains is in good agreement with the strain gauge at 400 mm from the column face and before failure of the welding of the studs in the column.

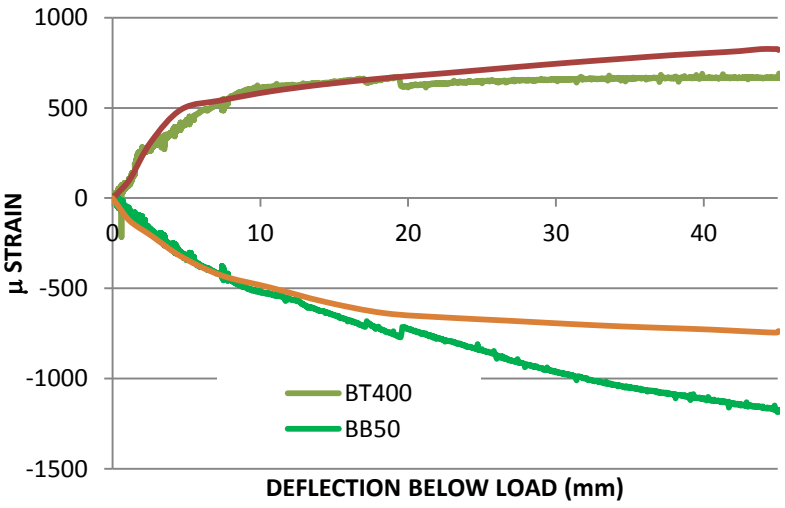

Figure 5-21: SCS joint with HSC steel plate strains

Photo 5-11and Photo 5-12 show the crack distribution in the finite element model and in the experimental test and it is obvious that ABAQUS has the ability to produce a precise cracking pattern.

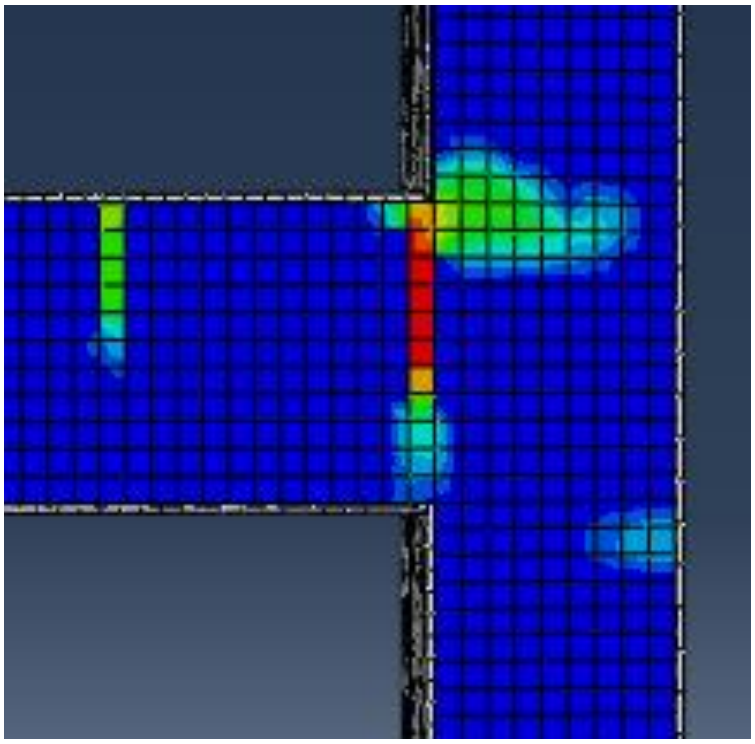

Photo 5-11: Cracking in the SCS with HSC - ABAQUS

Photo 5-12: Cracking in the DSC with HSC – test

5.8 Validation of the DSC Joint with NC under the Cyclic Load Model

The 3D model used in modelling the DSC beam-column joint with a normal concrete core and subjected to monotonic loading was used to model the specimen under the cyclic load. The C3D8R element was used to model the concrete core, stud connectors and steel plates. The three-dimensional truss element with two nodes (T3D2) was used to represent the longitudinal reinforcing bars as well as the transverse reinforcement.

The Concrete Damage Plasticity (CDP) model was used for concrete as it is designed to model concrete under monotonic and cyclic loading. One of the important aspects in the CDP model is the compression stiffness recovery, which can be directly defined as using stiffness recovery factors. This behaviour corresponded to crack closure when the load reversed its direction from tension to compression. Using a smooth amplitude, the load was applied in a reverse manner according to experimental history data. An explicit solution was used to perform the current analysis as it presents accurate results and needs a short amount of time, as is shown in the previous analyses of joints subjected to monotonic loading.

Figure 5-22 presents a comparison between the load-deflection curves obtained using ABAQUS and the load deflection from the experimental test. It can be said that the finite element model shows high stiffness compared to the tested specimen. This response reflects the effect of the constraints introduced by assuming a full bond between the steel and the concrete.

In terms of the maximum carried load, it is obvious that the accuracy of the predicted maximum loads is 95% or more in all three cycles. It was difficult to fully study the other parameters that might have an effect on the accuracy of the results because of time ABAQUS takes to run, where the three cycles presented in Figure 5-22 took approximately 44 hours to complete using the EXPLICIT solution.

No more modelling or parametric studies will be presented in this thesis about modelling the cyclic behaviour because of the time needed, and the author

believes that the base for developing the model has been introduced and can be modified and extended to perform such a study.

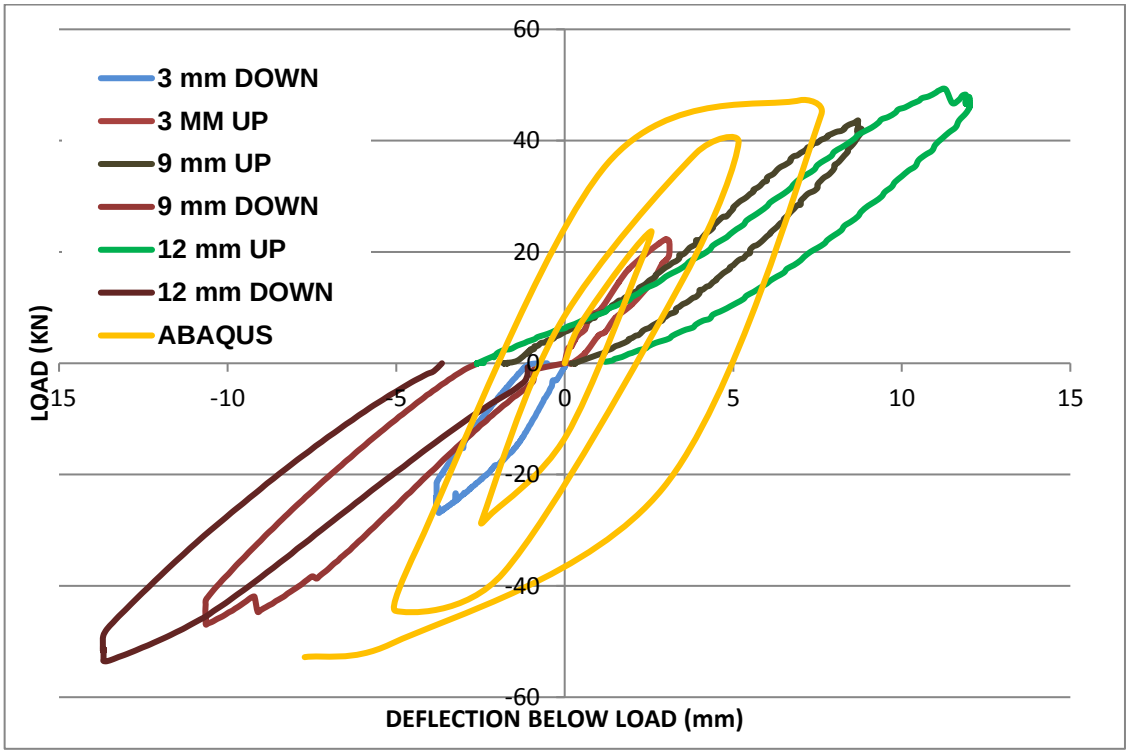

Figure 5-22: DSC under cyclic load – comparison

5.9 Summary

This chapter has presented a detailed description of the modelling of the reinforced concrete joint and of the double skin composite joint using the general finite element package ABAQUS 6.10.

The double skin composite joint was cast using three concrete types, plain concrete, steel fibre concrete, and high-strength concrete. Mesh sensitivity, element types, and solution techniques were studied in order to decide the most suitable model based on the accuracy and solution time.

A large number of previous studies were consulted in order to support the chosen method of simulation and material properties' definition.

The Concrete Damage Plasticity Model was used to model the concrete and the elastic-perfectly plastic model was used for steel parts. A three-dimensional solid element with eight nodes and reduced integration (C3D8R) was chosen to discretise the concrete, steel plate, and stud connectors. The

three-dimensional truss element with two nodes (T3D2) was used to discretise the steel reinforcing bars and was EMBEDDED in the concrete.

Good agreement was observed between the finite element solution and the experimental tests, which reflects the ability of ABAQUS to simulate the composite structural members with different materials.

In Chapter seven the following parameters will be used to perform the parametric study on the double skin composite joint:

1- Concrete compressive strength
2- Shear stud spacing to plate thickness ratio
3- Shear stud diameter to plate thickness ratio
4- Effect of column's axial load

Chapter 6 Applying Existing Analytical Methods

6.1 Introduction

It was concluded in Chapter two that all the available studies about steel-concrete-steel structural members had been performed on beams, columns, shear walls, and slabs. However, in some of the previous studies, an analytical analysis was used to determine the flexural strength, shear capacity and deflections. A design guide for the steel-concrete-steel beams and columns was presented by Narayanan et al. (1994) based on different parts of Eurocodes.

In this chapter, the previous proposed analytical analyses based on Figure 6-1 shown below are presented and used directly or by introducing some modifications to account for the differences. Flexural strength, cracking moment and the joint's shear strength are calculated and compared with experimental results and the finite element modelling.

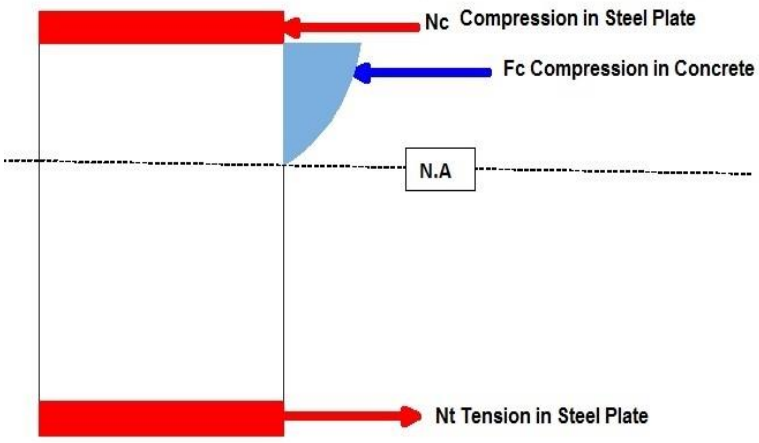

Figure 6-1: SCS forces' distribution

6.2 Previous Studies

6.2.1 Flexural Strength

For members subjected to bending only, Wright et al. (1991b) suggested the following equation to calculate the compression force in the concrete (F_c) :

$$N_{cu} = 0.45 f_{cu} b(0.9x) \quad (6\text{-}1)$$

Where:

f_{cu}: is the compressive cube strength,

b: is the section width, and

x: is the neutral axis depth.

The above equation was based on the concrete stress-strain relationship of BS8110, using a safety factor of 1.5 for concrete, a stress block of depth 0.9d and by ignoring the concrete in the tension zone.

The force in the top plate (N_c) and in the bottom plate (N_t) forces in the steel plates can be calculated using the following equations, respectively.

$$N_c = 0.93 \sigma_y b t_t \quad (6\text{-}2)$$

$$N_t = 0.93 \sigma_y b t_c \quad (6\text{-}3)$$

Where:

σ_y: is the yield stress of the plate,

b: is the width of the steel plate,

t_c and t_t are the thickness of the top plate and the thickness of the bottom plate respectively.

Equations 6-1 to 6-3 are applied to the fully composite sections. To account for the slip which might occur between the plate and the concrete, the following equations are proposed to calculate the forces in the steel plates:

$$N_c = 0.8 n_t P_d \quad (6\text{-}4)$$

$$N_t = 0.5 n_b P_d \tag{6-5}$$

Where n_c and n_t are the number of stud connectors welded to the top and bottom plates, respectively and P_d is the shear strength of the stud connector. The reduction factors of 0.8 and 0.5 are taken from BS5400 and BS5950 part-3.

Roberts et al. (1996) used plastic analysis to calculate the ultimate bending moment strength (M_{Rd}), as follows:

$$N_{cuRd} = 0.675 f_{cu} b(0.9x)/\gamma_c \tag{6-6}$$

$$\begin{aligned} N_{cRd} &\le A_{sc} f_{ysc}/\gamma_a \\ &\le n_c P_{cRd} \end{aligned} \tag{6-7}$$

$$\begin{aligned} N_{tRd} &\le A_{st} f_{yst}/\gamma_a \\ &\le n_t P_{tRd} \end{aligned} \tag{6-8}$$

$$\begin{aligned} N_{rRd} &\le A_r f_{ysr}/\gamma_a \\ &\le L_r \phi_r f_{rb} \end{aligned} \tag{6-9}$$

$$x = \frac{(N_{tRd} + N_{rRd} - N_{cRd})\gamma_c}{0.6075 f_{cu} b} \tag{6-10}$$

$$\begin{aligned} M_{Rd} = {} & N_{tRd}(h_c + t_c/2 + t_t/2) + N_{rRd}(h_r + t_c/2) \\ & - N_{cu}(0.45x + t_c/2) \end{aligned} \tag{6-11}$$

Where N_{cuRd}, N_{cRd} and N_{tRd} are the concrete compression force, steel plate compression force and steel plate tension force, respectively. X is the location of the neutral axis measured from the inner face of the compression plate. γ_c, A_{sc}, A_{st}, are factors for concrete which has a value of 1.5, area of steel plate in compression, and area of steel plate in tension. P_{cRd}, P_{tRd}, *and* N_{rRd} are the design shear strength of the shear connectors welded to the compression plate, tension plate and tensile force in the added steel reinforcement, respectively.

Liew and Sohel (2010) used plastic analysis to find the flexural capacity of the double skin composite beam assuming that the stress block of concrete in

compression has a depth of 0.9x as x represented the depth of the neutral axis measured from the inner face of the compression plate, as shown in Figure 6-1, and by ignoring the tensile strength of the concrete in the tension zone.

The compression force in the concrete (N_{cu}) was defined as:

$$N_{cu} = 0.85 f_{ck} b (0.9x)/\gamma_c \tag{6-12}$$

Where f_{ck} is the compressive cylinder strength of the concrete, b is the section width, and γ_c is the concrete safety factor, which has a value of 1.5.

Using the equilibrium of the horizontal forces:

$$N_t = N_c + 0.85 f_{ck} b (0.9x)/\gamma_c \tag{6-13}$$

In which N_t and N_c are the forces of the tension plate and compression plate, respectively.

$$x = 1.307 \gamma_c (N_t - N_c)/f_{ck} b \tag{6-14}$$

And the plastic moment (M_{pl}) was defined as:

$$M_{pl} = N_t \left(h_c + \frac{t_c}{2} + \frac{t_t}{2} \right) - \frac{0.765 f_{ck} b x}{\gamma_c} \left(0.45x + \frac{t_c}{2} \right) \tag{6-15}$$

Where t_c and t_t are the thickness of the compression and tension plates, respectively.

When the tension plate has the same thickness as the compression plate, and the neutral axis is moved to the maximum position that would cause the full yielding of the tension plate, and the concrete has fully cracked, the maximum plastic moment is defined as:

$$M_{pl} = N_t (h_c + t) = \sigma_y b t_t (h_c + t) \tag{6-16}$$

Where σ_y is the yield stress of the steel plate.

To account for the partial interaction effect, the following equation has been suggested to calculate the tensile force in the tension plate:

$$N_t = n_p(\kappa P_R) \tag{6-17}$$

Where κ is the reduction factor and P_R is the shear resistance of the stud connectors.

A transformed section was used by Dai and Liew (2010) to calculate the location of the neutral axis (x) and the resistance moment, as follows:

$$x = \alpha_E \left[\sqrt{(t_c + t_t)^2 + \frac{1}{\alpha_E}(t_t^2 + 2h_c t_t - t_c^2)} - (t_c + t_t) \right] \tag{6-18}$$

$$M = f_c b t_c \left(\frac{x}{3} + \frac{t_c}{2}\right) + f_t b t_t \left(h_c - \frac{x}{3} + \frac{t_t}{2}\right) \tag{6-19}$$

And in terms of tensile stress the moment can be written as:

$$M = f_t \left(\frac{x + t_c/2}{h_c - z + t_t/2}\right) b t_c \left(\frac{x}{3} + \frac{t_c}{2}\right) + f_t b t_t \left(h_c - \frac{x}{3} + \frac{t_t}{2}\right) \tag{6-20}$$

To take into account the effect of the partial interaction, the moment equation is introduced as:

$$M = nP_{Rk}\left[\left(\frac{x + t_c/2}{h_c - x + t_t/2}\right)\left(\frac{t_c}{t_t}\right)\left(\frac{x}{3} + \frac{t_c}{2}\right) + \left(h_c - \frac{x}{3} + \frac{t_t}{2}\right)\right] \tag{6-21}$$

Where, α_E is the modular ratio (E_s/E_c).

6.2.2 Shear Resistance

The shear forces in the stud connectors proposed by Roberts et al. (1996) are calculated as:

For the studs welded to the compression plate:

$$P_{cRd} = 0.8P_{Rk}/\gamma_v \tag{6-22}$$

For the studs welded to the tension plate:

$$P_{tRd} = 0.6P_{Rk}/\gamma_v \quad (6\text{-}23)$$

Where P_{cRd} and P_{tRd} are the shear force, P_{Rk} and γ_v are the characteristics of the shear strength and the safety factor of 1.25, respectively.

P_{Rk} can be calculated as:

$$P_{Rk} = 0.29\alpha d^2 (f_{ck} E_{cm})^{0.5} \quad (6\text{-}24)$$

$$\alpha = 0.2(h_s/d + 1) \quad for \ 3 \le h_s/d \le 4$$
$$\alpha = 1.0 \quad for \ h_s/d > 4 \quad (6\text{-}25)$$

The transverse shear resistance was defined to be a combination of the concrete shear strength and the studs that overlapped or had a length through the concrete depth, while the shear resistance of the steel plates was ignored because of their secondary role in providing shear strength. The design shear strength (τ_{Rd}) was defined according to the following equation:

$$\tau_{Rd} = \frac{f_{ck}}{20\gamma_c} + \frac{0.5 n_o A_s f_u}{b S_t \gamma_a} \quad (6\text{-}26)$$

$$V = V_c + V_s \quad (6\text{-}27)$$

Where A_s is the area of shear studs spaced at S_t and with an ultimate tensile strength of f_u and n_o is the number of studs across the width.

Liew and Sohel (2009) used an equation from EC2 (Eurocode2, 2004) to calculate the shear strength provided by NWC and LWC, as follows:

$$V_c = \left[C_c k_c \eta_1 (100\rho_1 f_{ck})^{1/3}\right] b h_c \quad (6\text{-}28)$$

$$k_c = 1 + \sqrt{200/h_c} \ \le 2.0 \quad (6\text{-}29)$$

$C_c = 0.18/\gamma_c \quad for\ NWC$

$C_c = 0.15/\gamma_c \quad for\ LWC$

$$n_1 = 0.4 + 0.6\rho/2200 \ \le 1.0 \quad (6\text{-}30)$$

Where ρ is concrete density.

For concrete with steel fibres, the equation presented by Majdzadeh et al. (2006) was used to estimate the fibrous concrete contribution, as follows:

$$V_c = \left[C_c k_c \eta_1 (100\rho_1 f_{ck})^{1/3} + k_f \tau_{f,FRC}\right] b h_c \quad (6\text{-}31)$$

For hooked-end steel fibres, $k_f = 0.216$, $t_{f,FRC} = 4.23V_f$

Using the method presented in the design guide for Bi-Steel constructions, Bowerman, Gough and King (1999), and Xie, Foundoukos and Chapman (2007b) calculated the transverse shear resistance of double skin composite beams as follows:

$$\tau_{uC} = 0.0525 f_{ck}^{2/3} \eta (1.2 + 0.4\rho) \quad (6\text{-}32)$$

$$\tau_{uS} = 0.9 k_T \frac{A_{sw} f_{yB}}{b s_x} \quad (6\text{-}33)$$

$$\rho = 100\, t_t / h_c \qquad \leq 2.0 \quad (6\text{-}34)$$

$$\eta = (1.6 - h_c/1000) \qquad \geq 1.0 \quad (6\text{-}35)$$

$$k_T = 2.5 \frac{f_{yP}}{f_{yB}} \left(\frac{t}{d}\right)^{1.25} \qquad t/d \leq 0.48 \; and \; f_{yP} \leq 355 N/mm2 \quad (6\text{-}36)$$

$$A_{sw} = \frac{\pi d^2 b}{4 s_y} \quad (6\text{-}37)$$

6.2.3 Deflection

Assuming a fully composite section, Roberts et al. (1996) suggested the following reduction factors (k_t and k_c) for tension plate width and for compression plate width as:

$$k_t = \frac{K_{st} n_t}{K_{st} n_t + 2 b t_t E_s / L} \quad (6\text{-}38)$$

$$k_c = \frac{K_{sc} n_c}{K_{sc} n_c + 2 b t_c E_s / L} \quad (6\text{-}39)$$

Where K_{st} and K_{ct} are the stiffness of the studs that were found experimentally using a push-out test to be 10000 N/mm for studs of 6 mm and 100 in diameter. n_t and n_c are the number of studs welded to the tension plate and compression plate over half the length of the beam (L).

The modified plates' widths are used in the transformed cracked section to calculate the section properties to be used in the deflection calculation.

6.3 Analysis of the Double Skin Composite Joint

6.3.1 Geometric and Material Properties

Material properties of three of the tested joints are represented in Table 6-1 below and the general details of the double skin composite joint and loading arrangement are shown in Figure 6-2.

Table 6-1: Material properties

Property	Symbol	Value	Unit
Concrete cube compressive strength (Plain Concrete)	f_{cu}	*43.24*	N/mm^2
Concrete cylinder compressive strength (Plain Concrete)	f_{ck}	*32.47*	N/mm^2
Concrete cube compressive strength (SFRC-Vf= 1%)	f_{cu}	*41.21*	N/mm^2
Concrete cylinder compressive strength (SFRC-Vf= 1%)	f_{ck}	*30.96*	N/mm^2
Concrete cube compressive strength (HSC)	f_{cu}	*93.96*	N/mm^2
Concrete cylinder compressive strength (HSC)	f_{ck}	*92.57*	N/mm^2
12 mm reinforcing bars' tensile yield strength	f_{ysr}	*503*	N/mm^2
8 mm link yield tensile strength	f_{yv}	*598*	N/mm^2
10 mm stud yield tensile strength	f_{ys}	*450*	N/mm^2

8 mm steel plate yield tensile strength	f_{yp}	258	N/mm^2
Tension steel plate thickness	t_t	8	mm
Compression steel plate thickness	t_c	8	mm
Beam concrete core height	h_{cb}	284	mm
Column concrete core height	h_{cc}	234	mm
Width – beam and column	B	200	mm
Beam span between point load in the column face	L	1150	mm
Volume fraction of the steel fibres	V_f	0.01	-
Number of studs across the width	n_o	2	-

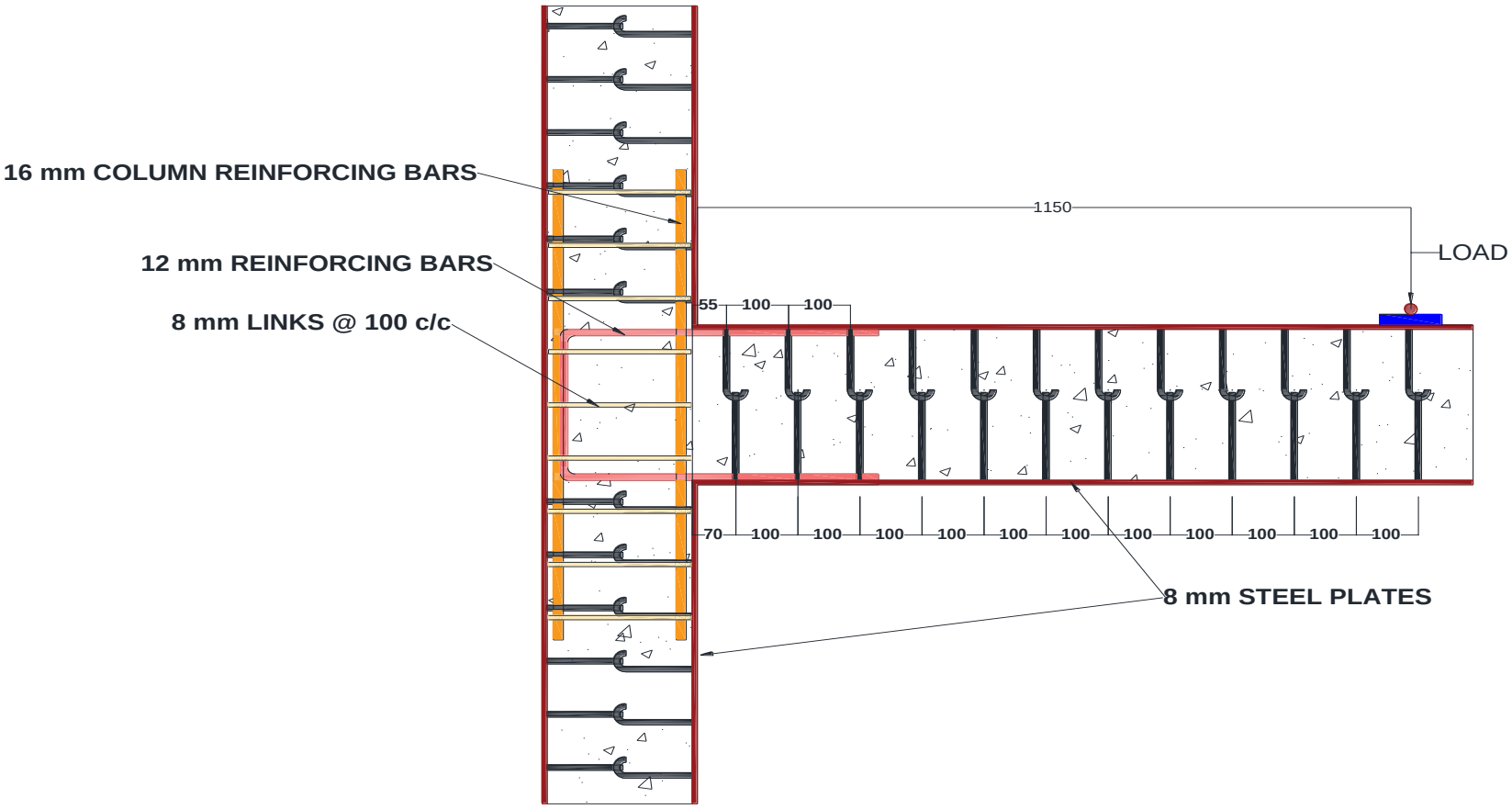

Figure 6-2: SCS joint and loading details

6.3.2 Flexural Strength

The equations presented in the previous sections can be applied to a double skin composite section when the section has no changes in its geometry or continuity. However, in the proposed arrangement of the double skin composite joint, the critical section of the beam has different properties because of the welded bars used to provide anchorage for the tension plate of the beam, as is seen in Figure 6-3. Comparing the maximum force that can be resisted by the steel plate (254x8x200 = 406.4 kN) section with the maximum force of the welded bars (3x113x504 = 170 kN) shows that the behaviour will be controlled by the yielding of the welded steel bars.

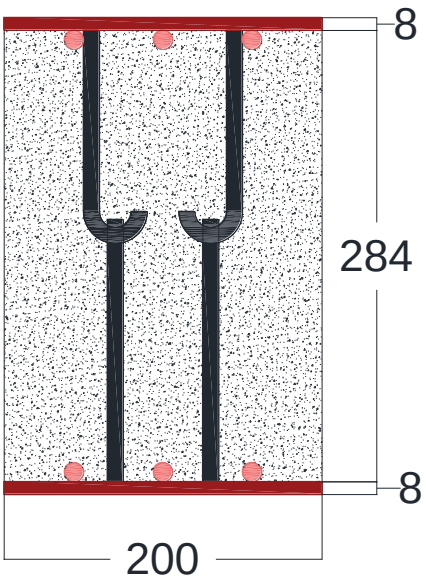

Figure 6-3: Beam cross-section

Since the section used in the present study has a tension steel plate of thickness equal to the compression steel plate, it can be considered as under-reinforced concrete (Liew and Sohel, 2010). All the tested specimens showed severe cracking before reaching the ultimate load capacity, which confirmed the observations reported by McKinley and Boswell (2002). The extensive cracking corresponds to the movement of the neutral axis towards the compression face of concrete (i.e. x= 0 in eq. 6.15), but the yield stress in the equation should belong to welded steel bars instead of steel plate yield stress and the lever arm should be modified to account for the location of the welded bars. Also, due to the continuity provided to the beam's tension plate by

welding it to the column plate, another source for the tensile resistance will be available from the face plate of the column, as shown in Figure 6-4.

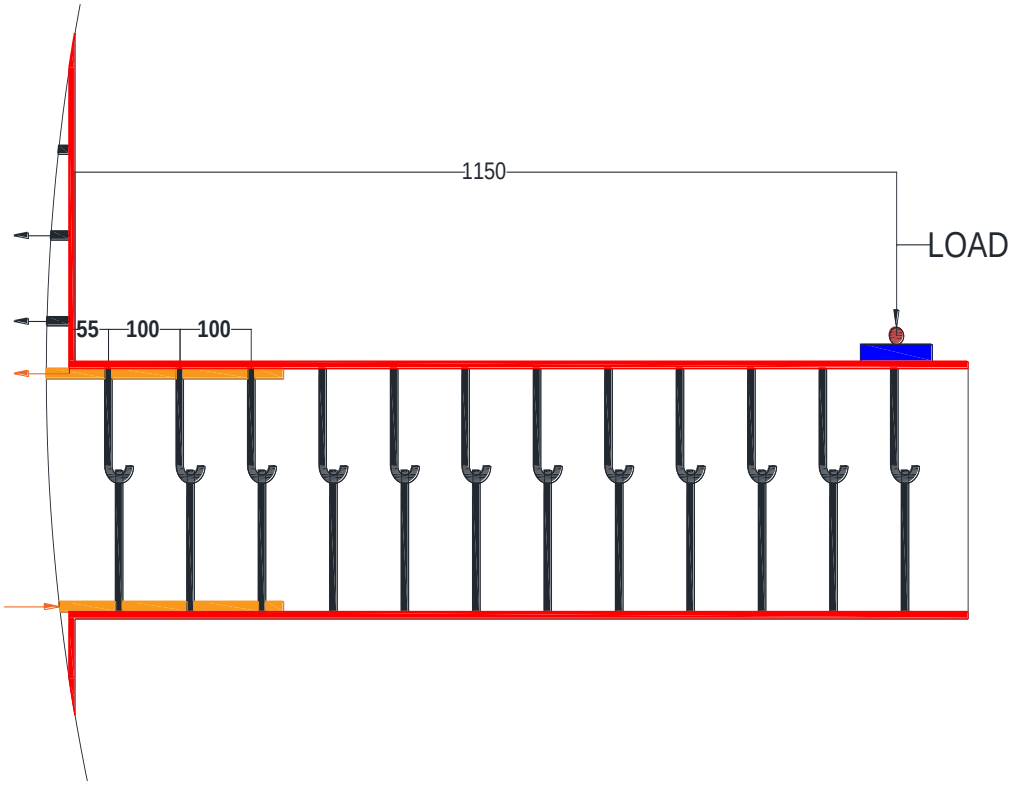

Figure 6-4: Beam's critical section in the SCS joint

The contribution of the column's plate transfers to the concrete through stud connectors welded to this plate. The studs welded to the column's plate, especially in the first row, have a crucial role in relation to the stress and strain of the welded bars because of the restraint that they provide. When the first row of studs failed, it was followed by rupture of the welded bars. Ultimate moment capacity was calculated based on the yielding of the welded steel bars and was based on this yielding as well as on the yielding of the first row of the column's studs. A comparison between the maximum experimentally measured load and the calculated load according to the latter assumptions showed that all the measured loads were higher than the calculated load, as shown in Table 6-2. This confirms that the tension resistance is provided by the column's steel plate through more than one row of studs.

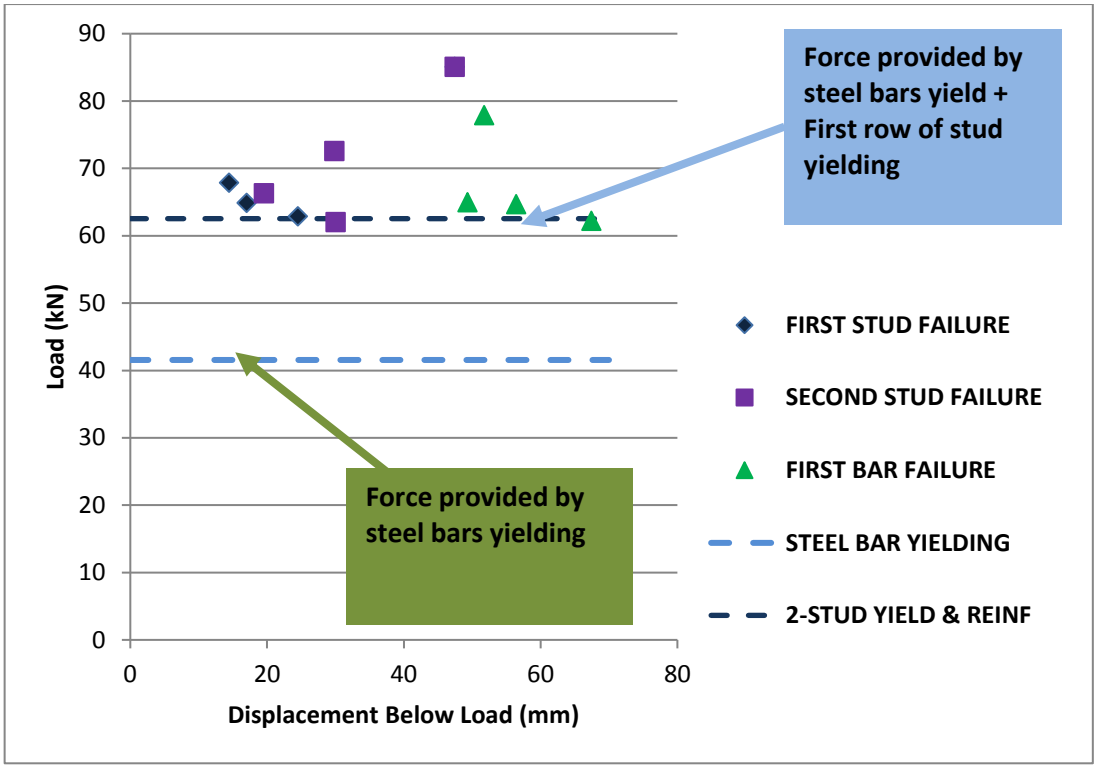

Figure 6-5: Maximum load comparison

Table 6-2: Test results for maximum load and corresponding displacement

JOINT	First Stud Failure		Second Stud Failure		First Bar Failure	
	Displ. (mm)	Load	Displ. (mm)	Load	Displ. (mm)	Load
DSC- Welded bars -NC-1	24.5	62.9	30	62.05	67.4	62.2
DSC- Welded bars -NC-2	14.4	67.9	29.8	72.6	49.3	65
DSC-SF-1%	47.4	85.1	47.4	85.1	51.7	77.9
DSC-HSC	17	64.9	19.5	66.3	56.4	64.7

6.3.3 Cracking Moment

One of the essential parameters of reinforced concrete is the cracking moment, which represents the beginning of changes in the section from full stiffness to reduced stiffness with the loading progression.

The cracking moment was calculated using the uncracked section and the following formula:

$$M_{cr,c} = \frac{f_r I_g}{y_t} \tag{6-40}$$

Where f_r is the modulus of rupture, which can be calculated using the following approaches:

a- According to ACI recommendations (ACI, Committee , American Concrete Institute, International Organization for Standardization 2008):

$$f_r = 0.62\lambda\sqrt{f_{ck}} \tag{6-41}$$

Where λ=1 for NWC.

b- According to EC2 (Eurocode2, 2004):

$$\begin{aligned} f_r &= 0.3 f_{ck}^{2/3} && when \ \leq C\,50/60 \\ f_r &= 2.12\ln\left(1+(f_{cm}/10)\right) && when \ > C\,50/60 \\ f_{cm} &= f_{ck} + 8\ (MPa) \end{aligned} \tag{6-42}$$

In the double skin composite joint, the critical section is the beam column interface position which contains three reinforcing bars welded to the plate, which means that the steel bars are located at the extreme tension and compression edges. It can be said that the steel bars will have the same strains as the concrete up to the initiation of the cracking stage. The steel will resist cracking by an amount of $M_{cr,\,s}$, which can be calculated as follows:

$$M_{cr,s} = A_s f_s (h_b - t_t - d_b) \tag{6-43}$$

Where f_s is the stress in the steel at cracking, which can be calculated based on the cracking strain of the concrete $\varepsilon_{c,cr}$..:

$$\varepsilon_s = \varepsilon_{c,cr} = \frac{f_r}{E_c} \tag{6-44}$$

$$f_s = E_s \varepsilon_s \tag{6-45}$$

Table 6.3 shows a comparison between the cracking moment measured experimentally and the cracking moment based on equations 6-40 to 6-45.

Table 6-3: Comparison between cracking moments

JOINT	Test	ACI-318	EC2	ABAQUS	% Ratio		
	$M_{cr,\ EXP}$ (kN.m)	$M_{cr,\ ACI}$ (kN.m)	$M_{cr,\ EC2}$ (kN.m)	$M_{cr,\ ABAQUS}$ (kN.m)	$\frac{M_{cr,ACI}}{M_{cr,EXP}}$	$\frac{M_{cr,EC2}}{M_{cr,EXP}}$	$\frac{M_{cr,FEA}}{M_{cr,EXP}}$
DSC-Original Design	10.33	9.57	9.6	-	92.6	92.9	-
DSC- Welded bars -NC-1	14.95	11.97	10.35	15.98	80	69	93.7
DSC-HSC	26.45	22.14	19.04	30.2	83.7	72	1.14

It is obvious that ACI 318 and EC2 (Eurocode2, 2004) have estimated the cracking moment of the composite joint without anchorage bars, while there is a difference of about 30% between the joint containing welded bars as an anchorage tool and the joint without welded bars. The increase of the cracking moment in the composite joint containing welded bars can be attributed to the restraint and confinement provided by the welded bars and the steel skin plates. Since the proposed methods to calculate the modulus of rupture do not take into account the effect of the restraining and confining, they will produce a lower estimated cracking stress.

6.3.4 Shear Capacity of the Joint

Hamil (2000) presented a simple method to calculate the ultimate joint shear capacity, as follows:

The shear in the joint is calculated from the overall equilibrium of the beam-column joint as:

$$V_j = T_b - V_{col} \tag{6-46}$$

Where Tb is the tensile force in the tension reinforcement:

$$T_b = A_s f_y \tag{6-47}$$

The shear in the column can be calculated based on the ultimate bending capacity of the beam:

$$V_{col} = \frac{M_{b,ult}}{L_c} \tag{6-48}$$

Hamil recommended using the available code methods to calculate the ultimate moment capacity $M_{b,ult}$ as BS8110 and Eurocode2 (2004). Also, he recommended ignoring the safety factors used in the codes to find $M_{b,ult}$.

After finding the shear force in the joint, the shear stress can be calculated as:

$$v_j = \frac{V_j}{b_e h_c} \tag{6-49}$$

The calculated shear stress should be compared with the ultimate shear capacity ($v_{c,ult}$) of the concrete of the joint to decide upon the requirement for shear reinforcement in the joint.

$$v_{c,ult} = \alpha\beta\sqrt{f_{ck}} \tag{6-50}$$

Where α is a reduction factor to account for the effect of the beam's reinforcement anchorage method:

$\alpha = 1 \; for \; bent \; down \; reinforcement \; and$

$\alpha = 0.85 \; for \; U - detailing$

B is a reduction factor and accounts for the effect of the joint aspect ratio, as follows:

$$\beta = 0.25\left(5.4 - \frac{h_b}{h_c}\right) \quad for \; 1.4 < \frac{h_b}{h_c} < 2.0$$

$$\beta = 1.0 \quad for \quad \frac{h_b}{h_c} < 1.4 \tag{6-51}$$

ACI-A presents recommendations for the reinforced concrete beam-column joint based on its type and it classifies the beam-column joint into two types, Type 1 and Type 2. Type 1 is defined as the connection of members that are not designed for seismic requirements and these members are not subjected to substantial inelastic deformations. Type 2 is a connection of members that are designed to withstand reversed deformations in the inelastic range.

For shear considerations, ACI-ASCE gives the nominal shear strength of the joint as:

$$v_{j,n} = 0.083\gamma_{352}\sqrt{f_{ck}} \quad (6\text{-}52)$$

Where γ_{352} i is a factor that depends on the location of the joint and it has a value of 15 for the exterior joints.

A recent by Vollum and Parker (2008) proposed a strut and tie model to analyse and design external joints. The model can be summarised as follows:

The joint's shear strength is given by the following equation:

$$V_j = b_e k v' f_{cd}(x - y) \quad (6\text{-}53)$$

Where b_e is the effective width of the joint and, according to EC2 (Eurocode2, 2004), k = 0.6, v' is defined as in equation 6-44 and f_{cd} is defined as in equation 6-45:

$$v' = 1 - \frac{f_{ck}}{250} \quad (6\text{-}54)$$

X and y are defined in Figure 6-6.

$$f_{cd} = \alpha_{cc}\frac{f_{ck}}{\gamma_c} \quad (6\text{-}55)$$

Where EC2 (Eurocode2, 2004) recommends $\alpha_{cc} = 1$, and $\gamma_c = 1.5$.

The shear strength of the joint is related to the flexural capacity of the beam through the definition of the node dimensions (x and y) according to the following iterative procedures listed below:

1- Find ΔT

$$\Delta T = 0.5(-b + \sqrt{b^2 - 4c} \quad (6\text{-}56)$$

$$b = 0.5(2d_c - h_c)vf_{cd}b_e \quad (6\text{-}57)$$

$$v = kv' \quad (6\text{-}58)$$

$$c = -0.25T_{syd}(h^* - z)vf_{cd}b_e \quad (6\text{-}59)$$

$$T_{syd} = A_{sw}f_{yd} \quad (6\text{-}60)$$

Where A_{sw} is the area of shear reinforcement in the joint and f_{yd} is the design yield stress in the shear reinforcement.

$$h^* = d_b + 0.5x - 2y$$

$$It\ is\ recommended\ to\ assume\ that\ h^* = d_b\ in\ the\ first\ iteration. \quad (6\text{-}61)$$

$$z = T_{syd}/(b_e v f_{cd}) \quad (6\text{-}62)$$

2- Calculate $M_{col} + \Delta M$

$$M_{col} = 0.125 b_e h_c^2 v f_{cd} \quad (6\text{-}63)$$

$$\Delta M = (2d_c - h_c)\Delta T \quad 6\text{-}64)$$

3- Find M_b using equation 6-55 in the first iteration and using equation 6-56 in the remaining iterations:

$$M_b = 2(M_b + \Delta M)/(1 - (1 + 0.5h_c/L_b)\, d_b/L_c) \quad (6\text{-}65)$$

$$M_b = 2(M_b + \Delta M)/(1 - (1 + 0.5h_c/L_b)\, (d_b + 0.5x - y)/L_c) \quad (6\text{-}66)$$

4- Find x and y:

$$x = d_b \left(1 - \sqrt{(1 - 2M_b/(b_e d_b^2 v f_{cd}))}\right) \quad \leq 0.5h_b \quad (6\text{-}67)$$

$$y = M_b\, (1 + 0.5h_c/L_b)/(L_c b_e v f_{cd}) \quad (6\text{-}68)$$

5- Using the calculated values of *x* and *y*, *h** can be recalculated and then ΔT.

Steps 2 to 5 are repeated until M_b is converged.

The shear calculations in the double skin composite joints have some implications due to the presence of the steel plates, which add another component for shear resistance and another enhancement to the shear resistance from the confinement provided by these plates.

A conservative shear check can be presented by ignoring the effect of the skin plates and treating the joint as a reinforced concrete joint. The three methods

presented by Vollum and Parker (2008), Hamil (2000) and ACI-ASCE 352R ACI-ASCE (Joint Committee 352-2002) are used to calculate the shear strength of the double skin composite joint.

A comparison between the maximum shear stress developed in the joint, calculated using the maximum load carried by the joint, and the maximum shear capacity of the joint is presented in Table 6-4. It is obvious that the maximum experimental shear stress is lower than the shear capacity, which means that all the compared joints failed by flexural strength at the maximum load, and this was observed experimentally and discussed in Chapter four. In the tested joints there were shear cracks in the joint during loading but the carried load increased up to the failure of the joint in flexural strength, which agreed with the statement: *"Previous research has shown that a joint can withstand a further significant increase in load after initial shear cracking"* (Hamil, 2000).

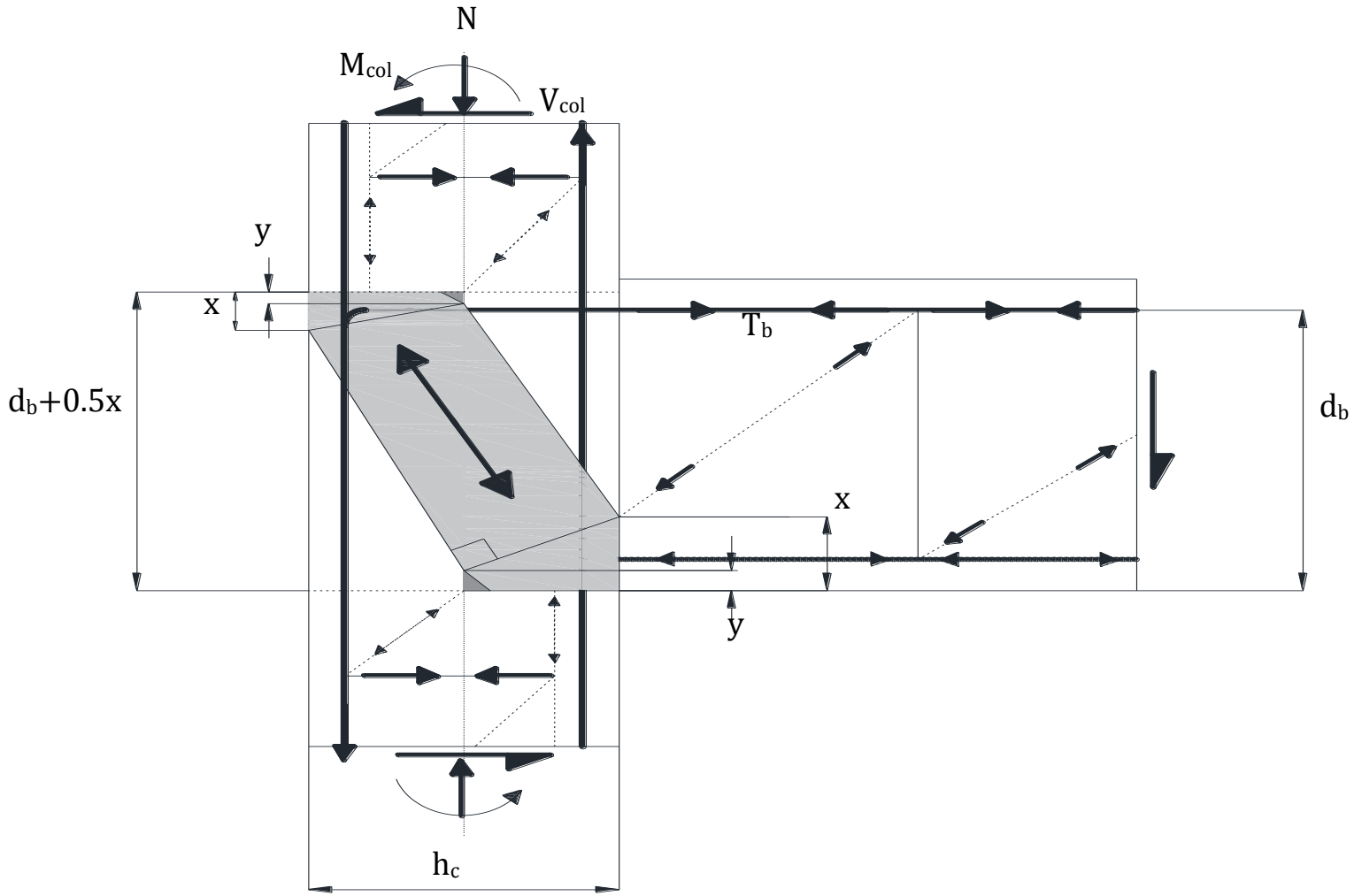

Figure 6-6: Strut and tie model (Vollum and Parker, 2008)

Table 6-4: Shear capacity of the joint

JOINT	Experimental		% Ratio		
	$P_{max,EXP}$ (kN)	$V_{max,EXP}$ (N/mm^2)	$\frac{v_{max,EXP}}{v_{max,VOLLUM}}$	$\frac{v_{max,EXP}}{v_{max,ACI}}$	$\frac{v_{max,EXP}}{v_{max,HAMIL}}$
DSC- Welded bars -NC-1	**103.9**	**2.08**	**37.9**	**43.0**	**34.5**
DSC- Welded bars -NC-1	**93.49**	**1.87**	**35.0**	**39.2**	**31.5**
DSC-SF 1%	**79.90**	**1.60**	**19.0**	**33.8**	**27.2**
DSC-HSC	**98.48**	**1.97**	**21.5**	**24.1**	**19.4**

6.4 Summary

This chapter has presented the previously proposed analytical formulas for the steel-concrete-steel constructions and formulas used to analyse the reinforced concrete joints. Flexural strength, cracking moment, and the joint's shear strength were calculated and compared with experimental results and the finite element modelling. Analytical results showed good correlation compared to the experimental results and the finite element analysis.

The flexural capacity of the beam was calculated at the face of the column. The presented analysis revealed that the welded reinforcing bars as well as the shear studs welded to the top front steel plate of the column share the tensile stresses. The comparison between the experimental results and the analytical values showed that the presented analysis produced a low estimation because there was more than one row of shear studs at work at the same time.

The cracking moment was estimated by taking into account the effect of steel bars that were welded to the steel plates, and the ACI code and EC2 (Eurocode2, 2004) code recommendations were used to estimate the cracking moment. Good estimations for the cracking moment of the joint that did not contain welded bars were provided, while both codes presented non-accurate results for the cracking moment.

Shear stress developed in the joint was compared against shear stress calculated by three methods and all three methods showed good agreement with the experimental failure observed.

Chapter 7 Parametric Study

7.1 Introduction

The model presented in Chapter five is used herein to perform a parametric study in order to investigate the effect of the following parameters on the behaviour of double skin composite beam-column joints:

- Concrete Compressive Strength
- Stud Spacing to Steel Plate Thickness Ratio
- Stud Diameter to Plate Thickness Ratio
- Effect of column's axial load

For the purpose of this study, only the outlined parameters are investigated; other parameters such as varying boundary conditions and beam section depth are not covered. The basis for this investigation is to achieve one of the objectives of the thesis: to study how some basic parameters influence the DSC joint.

The concrete compressive strength was chosen to compare the FE results with experimental observations presented in Chapter four which showed that there were no significant effects on the ultimate joint load but that its shear resistance was enhanced. The stud spacing to steel plate ratio plays a dominant role in the composite action of the DSC constructions and it is important to identify the minimum limit for the S/t ratio for practical considerations using the proposed model. The stud diameter to steel plate thickness ratio principally controls the failure mechanism of the DSC constructions, as presented in Chapter two of this thesis; therefore, the limits of this ratio can be produced using the proposed model. Finally, the column's axial load has a substantial effect on the behaviour of the beam-column joints and hence it is chosen to study the changes in the cracking mechanism and location.

In this chapter, in order to produce more general ideas about the behaviour of the DSC joint, the material properties will be taken from the existing codes that are available for the designers rather than using data from specific experimental tests which cannot be applied to other types of material.

The material properties for the current investigation were taken from EN 1992-2 (2005). By using this method, more general conclusions can be drawn compared to the author's tested materials.

7.2 Further Validation for the Model

The model was validated in Chapter five using the experimental results presented in Chapter four; another validation is presented in this section. The behaviour of the double skin composite beam-column joint containing a core consisting of HSC was presented in Chapter four and its modelling was presented in Chapter five. This joint was modelled using the parameters measured experimentally and showed good correlation with the experimental results. The same joint was modelled using the parameters taken from EC2 (Eurocode2, 2004) for a concrete of grade $F_{CK}90$ where this type of concrete has close properties to the HSC tested in the experimental programme.

Figure 7.1 shows a comparison between the experimental result and the modelling using ABAQUS. One of the curves was obtained using the parameters of concrete taken from EC2 (Eurocode2, 2004) and the second curve was obtained using parameters measured experimentally. In both the modelling cases, the maximum load deviated from the experimental results by approximately 10% and the behaviour during the loading stages showed good similarity.

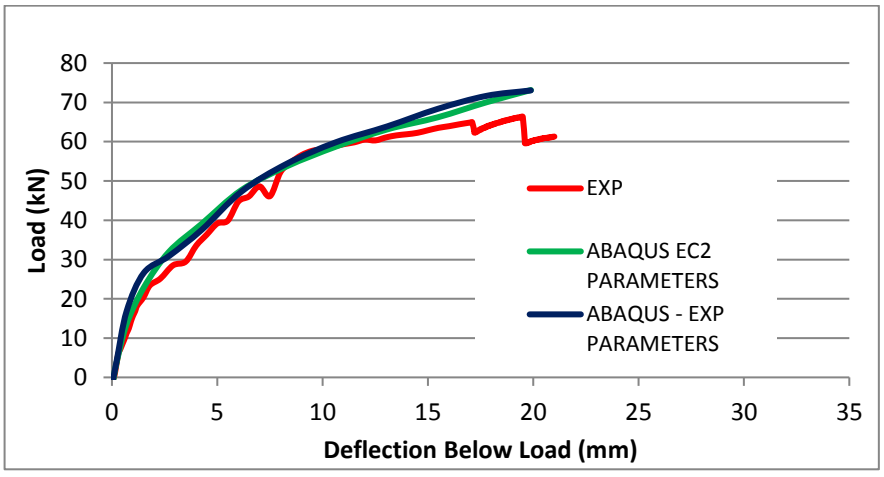

Figure 7-1: Load-deflection curve of HSC validated using EC2 and experiments

7.3 Concrete Compressive Strength

Three different concrete compressive strengths were chosen to be the concrete core of the original design of the double skin composite joint, i.e. 8 mm steel skin plates, 10 mm studs spaced at 100 mm, and welded bars to provide anchorage for the plates. The load and support conditions were maintained while the compressive strength of the concrete was treated as a variable parameter. For the purpose of this study, three grades of concrete were assessed. The chosen compressive strengths were $C25\ N/mm^2$ to represent the most commonly used compressive strength in the researcher's home country (Iraq), $C40\ N/mm^2$ to represent the most common compressive strength in the UK and a HSC of $C90\ N/mm^2$.

Figure 7-2 shows the effect of changing concrete properties on the behaviour of the double skin composite joint. When the compressive strength increased by 60% (from C25 to C40), the maximum carried load increased by 13% (from 60 kN to 68 kN). Increasing the compressive strength by 260% (from C25 to C90) increased the maximum load by 33% (from 60 kN to 80 kN). Considering the maximum strength, it can be concluded that increasing the concrete's compressive strength improves the joint ultimate load. Although this result contradicts the experimental results, the author believes it can be achieved by introducing bolted studs for the first row of column studs, as they controlled the joint capacity due to welding failure. Moreover, the shear cracks in the core region decreased significantly by using HSC, as can be seen in Photo 5.11, which reflects the role of increasing compression in improving shear resistance.

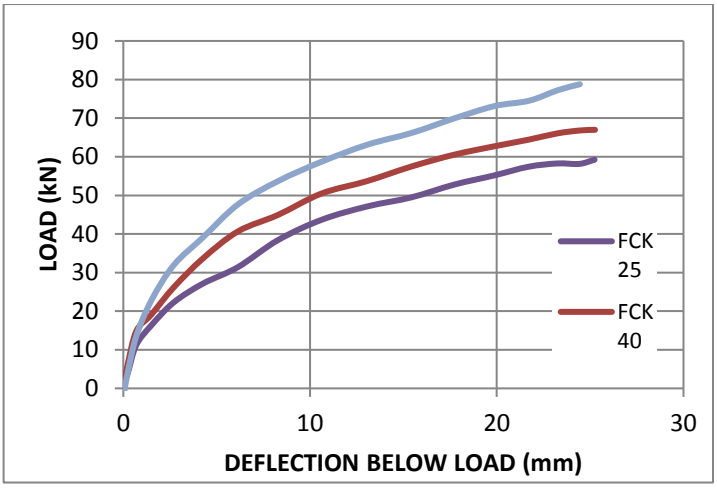

Figure 7-2: Load-deflection curve for three different concrete compressive strengths

Table 7-1 presents a comparison between the load carried at different deflection stages, taking maximum load and maximum deflection of C25 as a reference to calculate the ratios. It can be seen that C40 gives a 13% rise on C25 while C90 gives about a 30% rise on C25 in all stages. From a serviceability point of view, it is obvious that the increasing compressive strength has a pronounced effect in improving the deflection response (approximately 100% of ultimate load compared to 40% of maximum deflection). This behaviour was identified during the experimental tests on the SCS beam-column joints with a HSC core, as presented in section 4.3.1.

Table 7-1: Effect of concrete type on load-deflection response

Def. Ratio	40% (10 mm)		60% (15 mm)		80% (20 mm)		100% (25 mm)	
Concrete	Load	Ratio	Load	Ratio	Load	Ratio	Load	Ratio
C25	42	70%	49	82%	55	92%	60	100%
C40	50	83%	57	95%	63	105%	68	113%
C90	58	97%	66	110%	74	123%	80	133%

7.4 Influence of Stud Spacing to Plate Thickness Ratio (s/t)

According to Wright et al. (1991b), the stud spacing to steel plate thickness ratio is recommended to be taken at 40 or less. In this section, a comparison between three different ratios is presented. Figures 7.3 and 7.4 show the load-deflection behaviour for a range of spacing to thickness ratios varying from

12.5 to 100. It can be said that the variation in the maximum carried load is highly affected by increasing the ratio beyond 50, which can be attributed to the buckling of the plate under compression. Furthermore, failure of the concrete in shear is due to the lack of shear reinforcement in the beam. Also, the ductility of the double skin composite joint is decreased significantly by increasing the s/t ratio because of the early failure.

The above findings coincide well with the reported behaviour of the beams as presented in Chapter two.

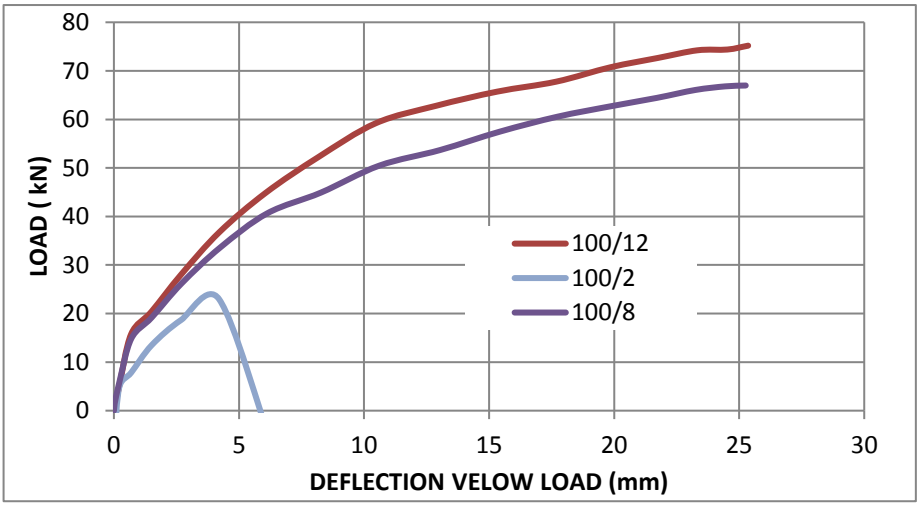

Figure 7-3: Effect of stud spacing to plate thickness ratio (s=100mm)

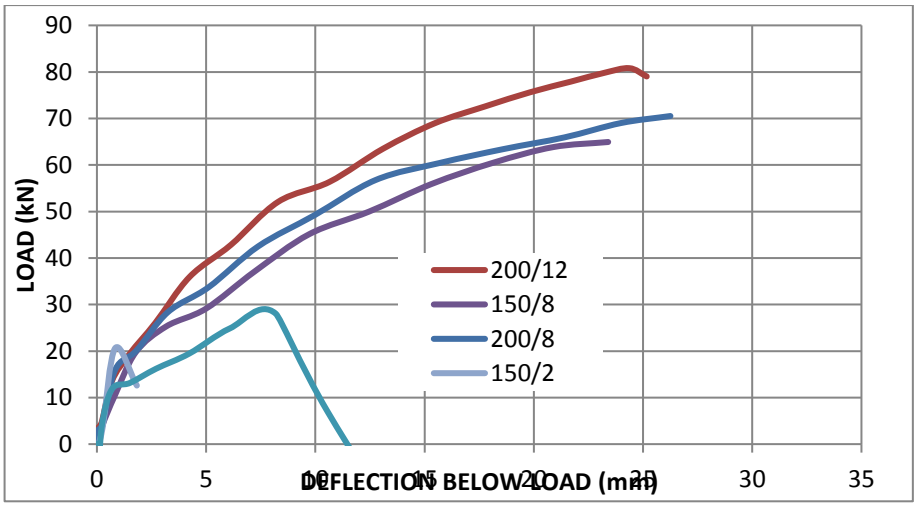

Figure 7-4: Effect of stud spacing to plate thickness ratio- different (t)

7.5 Influence of Stud Diameter to Plate thickness ratio

The diameter of the plate thickness ratio (d/t) has a great effect on the failure mechanisms of the beams, as presented in Chapter two. The recommended values for this ratio are 2 for the studs welded to the plate under compression and 2.5 for the plate under compression.

A range of d/t ratio from 1.5 to 5 is presented in Figure 7-5 through the load-deflection response. It is obvious that increasing the d/t ratio increases the ultimate load capacity. A 22% increase in load capacity was observed when the (d/t) ratio increased from 1.25 to 2.375 at constant steel plate thickness. The increase in load capacity can be attributed to the contribution of shear studs in resisting the flexural stresses in the beam at the critical section, as presented in Chapter six, section 6.3.2. Moreover, when increasing the d/t ratio from 1.25 to 1.58 and the steel plate thickness from 10 mm to 12 mm, the peak load increased by 30%. This increment in the peak load shows the effect of the steel plate in resisting the flexural stresses caused by the restraint of the beam plate by the column face plate.

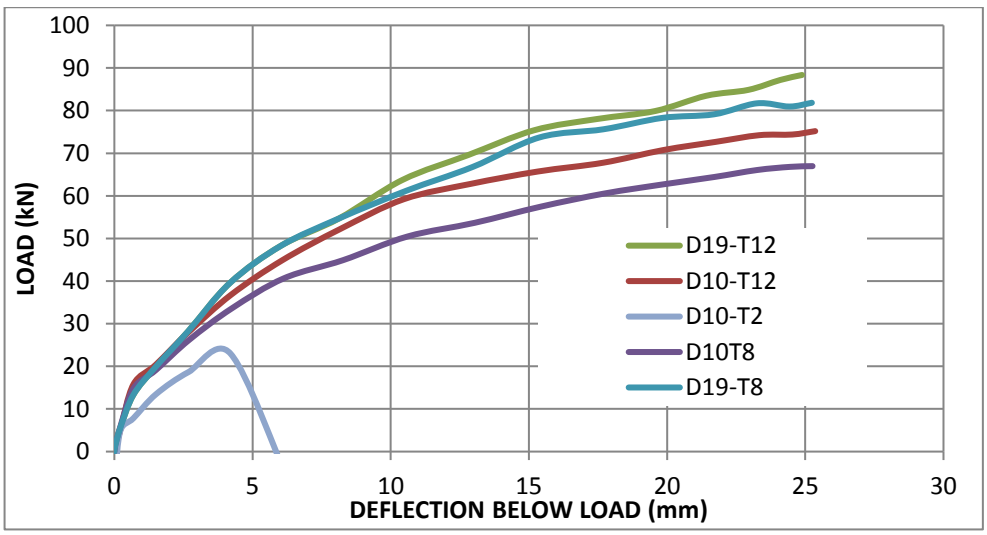

Figure 7-5 Effect of stud diameter to plate thickness ratio

7.6 Effect of Column's Axial Load

The column's axial load provides additional confinement to the concrete in the column region and therefore plays an important role in changing the crack development and pattern of the joint (Park and Paulay, 1975; Ichinose, 1991; Kumar and Shamim, 1999).

Figure 7-6 shows the cracking pattern for the DSC beam-column joint containing the HSC core analysed using the model presented in Chapter five. The axial compression load on the column varied between 0 to 1000 kN; the chosen load range represents the cases between no axial load and maximum load that can be carried by the column according to the SCS design guide (Narayanan et al., 1994). It can be seen that the cracking pattern changed significantly as the axial load increased. This means that the axial load will enhance the beam-column joint response due its role in moving the location of the plastic hinge away from the column face, and prevent the failure of the joint because of the extensive cracking in the joint region, as reported by Scott (1996) for the conventional RC beam-column joint.

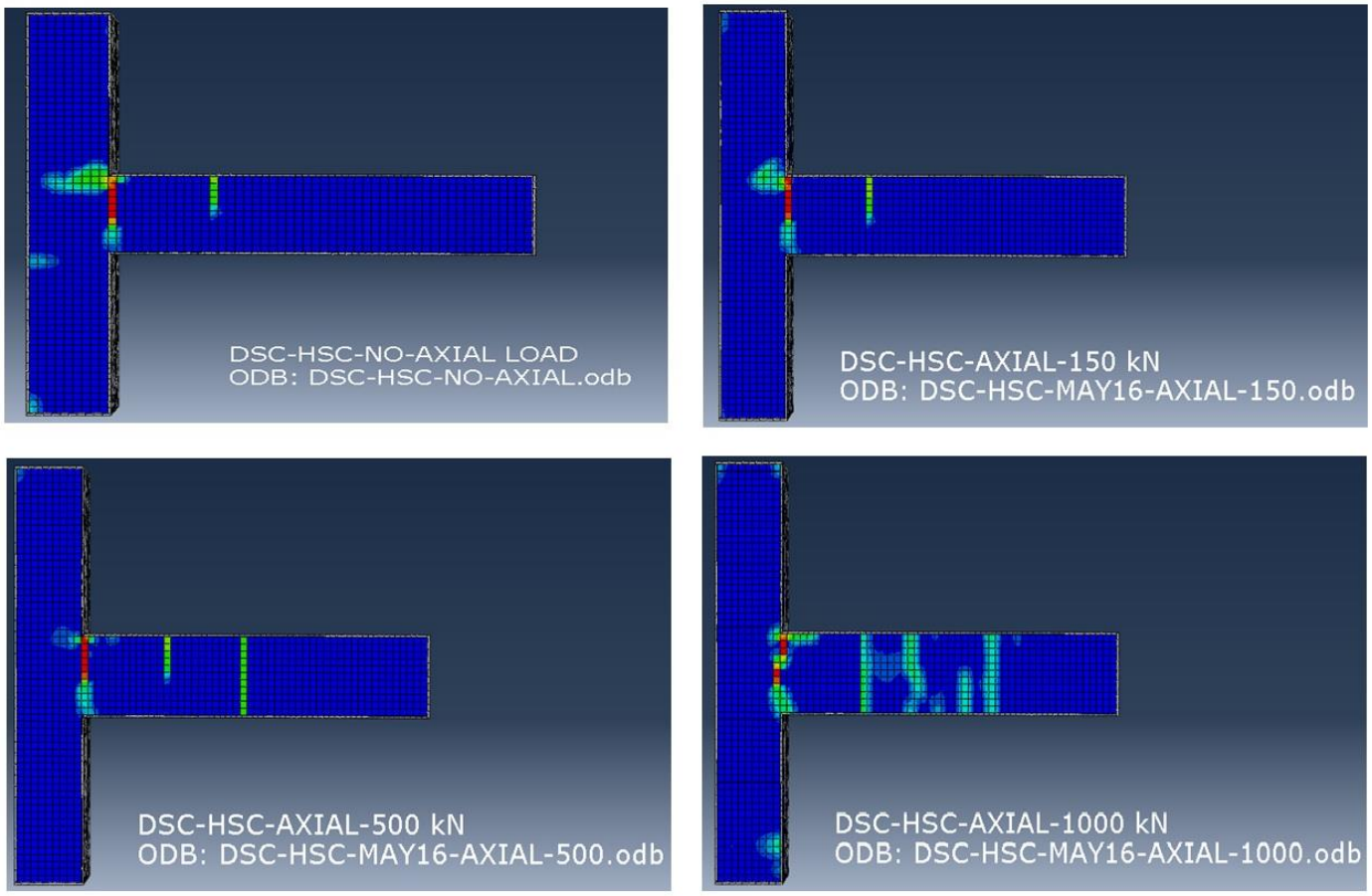

Figure 7-6: Effect of column axial load on the cracking of the SCS beam-column joint

In the present study, all the tested specimens were tested under no column load to investigate the behaviour of the beam-column joint using the most critical conditions (Kumar and Shamim, 1999). Therefore, the behaviour of the SCS beam-column joint obtained from ABAQUS cannot be compared to the experimental results.

Figure 7-7 shows the effect of axial load on the load-deflection response of the SCS beam-column joints. It is obvious that the low column load has an insignificant effect on the initial stiffness and the maximum carried load. On the other hand, 50% of the maximum theoretical column's load greatly affected the response of the joint, both in terms of the stiffness and the maximum carried load.

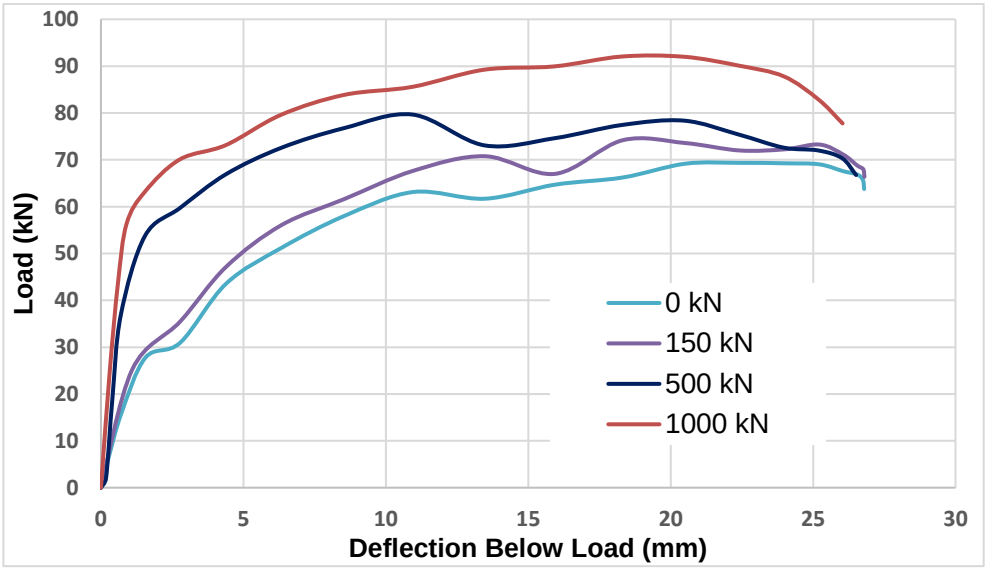

Figure 7-7: Effect of column's axial load on the joint behaviour

7.7 Summary

This chapter has presented a limited parametric study to study the effect of certain parameters: concrete compressive strength, stud spacing to plate thickness ratio, and stud diameter to plate thickness ratio.

The material properties used in the modelling to perform the parametric study were taken from EC2 (Eurocode2, 2004) rather than using specific test measurements, so the generated results can be considered more general.

The finite element model was validated against experimental data to ensure that it adequately replicated the experimental investigation.

The outcomes of this chapter can be listed as follows:

- The concrete compressive strength has an insignificant effect on the behaviour of double skin composite joints.
- The stud spacing to steel plate thickness ratio has a significant effect on the ductility and the maximum load.
- As with the stud spacing to plate thickness ratio, the stud diameter to steel plate ratio showed a significant effect on the maximum load.

Finally, the author is aware that some other parameters should have been studied in this chapter, such as beam's reinforcement, reinforcement in the column, etc. These parameters have not been studied due to time limitations.

Chapter 8
Conclusions and Recommendations for Further Studies

8.1 Introduction

The current study was set out to present the double skin composite beam-column joint as a new structural element which can be used as an alternative to conventional reinforced concrete.

The advantages of the proposed DSC beam-column joint can be summarised as follows:

- The speed of construction is quicker because it needs fewer details than do the RC joints.
- The proposed joint will enable the usage of DSC construction in one frame, i.e. the beams and columns' frame.
- The simplicity of the proposed joint means that skilled labourers are not required, because it includes very basic welding processes and concrete casting.

On the other hand, the following drawbacks persist with using such a system:

- It is a completely new system and it needs more tests and research to examine its structural performance.
- The initial cost of the system is relatively high.
- The design guide for the DSC system was first presented in 1999 and has not been updated.

The basic form of the joint was tested to assess its structural performance and to introduce the most suitable and efficient solution for the deficiencies in the primary design. Three methods to strengthen the basic design of the joint were introduced and tested experimentally: adding normal reinforcing bars to the connection zone, i.e. to the beam and to the column; welding bars to the steel plates of the beam and keeping the same previous reinforcement in the column; and extending the plates of the beam to meet the back plate of the column. Based on the best structural performance and simplicity of

manufacturing and rough estimation of the cost, a joint with welded bars was chosen for use in further tests.

The concrete strength effect was studied using High-Strength Concrete (HSC) and the effect of steel fibres and the behaviour of the joint under quasi-static load were assessed. Following the experimental programme, a finite element modelling was presented using ABAQUS CAE 6.10 to produce a numerical model which was validated against the experimental results. Three variables were studied using the validated model to highlight their effect on the behaviour of the double skin composite joint.

8.2 Conclusions

The conclusions drawn from the present are divided into two sub-sections:

- Conclusions drawn from the experimental programme.
- Conclusions drawn from the finite element modelling, and the parametric study.

8.2.1 Conclusions Drawn from the Experimental Programme

1. The double skin composite beam-column joint can be strengthened to be used as an alternative to the conventional beam-column joint. As can be seen in the test results for the joint with steel fibres and the joint with HSC, the failure occurred (plastic hinge formed) in the beam away from the column face.
2. Based on the structural performance and secondary consideration regarding the cost of the strengthening method, the DSC joint containing bars welded to the steel plates of the beam can be considered the most efficient solution.
3. The recommended stud spacing to steel plate thickness ratio (s/t) and stud diameter to steel plate thickness ratio (d/t) are used as a guide to produce the initial design of the DSC joint. An s/t of 12.5 and d/t of 1.25 used in the present study showed efficient behaviour against the buckling of the steel plate under compression and against the slip.
4. Increasing concrete compressive strength significantly improves joint shear resistance.

5. The DSC joint containing steel fibre showed the best performance regarding the integrity of the concrete during loading up to failure (this behaviour was reported in the previous studies on the beams and slabs). The crucial improvement was the improvement in the maximum load capacity and the location of the plastic hinge.
6. In the DSC joint tested under a quasi-static load, the width (area under consecutive cycles curve) increased, which indicates that the increase in the energy dissipated due to the crack development and growth.
7. The most important elements that affected the response and failure of the composite joint were the welded stud strength and plate tensile strength.
8. The cracking and the width of cracks drew attention to the serviceability requirements that need to be assessed precisely.

8.2.2 Conclusions Drawn from the Finite Element Modelling

1. The general finite element package ABAQUS CAE can be used to model the reinforced concrete beam-column joint and DSC joint efficiently and produces accurate results.
2. The Concrete Damage Plasticity Model (CDPM), which is incorporated in ABAQUS, was successfully used to model the concrete behaviour.
3. All concrete types used in the current study (NC, SFC, HSC) were modelled using CDPM and it can be said that the results are sufficiently accurate.
4. The three-dimensional continuum element (C3D8R) of the first degree with reduced integration was used successfully in the modelling of the concrete and the steel parts.
5. The predicted first crack location, cracking load, and cracking pattern were in good agreement with experimental tests.

8.3 Recommendations for Further Studies

The following further studies are recommended:

1- An experimental study to investigate the effect of the column load on the behaviour of the DSC joint.

2- Investigation into the effect of casting position on the behaviour of the DSC joint as the interaction degree will be affected.
3- Experimental investigation on the fire resistance of the DSC joint.
4- Investigation into the serviceability requirements, i.e. cracking width and distribution, vibration, creep and shrinkage effect on the system.
5- Investigating, experimentally, the welded bar area on anchorage efficiency.
6- Perform a parametric study using the presented model to investigate the effect of variation of each element of the DSC joint on its response.
7- An extension for the current model can be introduced by using a cohesive element to simulate the interaction between the concrete and the shear studs, which will provide more accurate results.
8- Application of optimisation theories to achieve optimum design and optimum construction method. Hence, the developed FE model can be used to perform the analysis and pass the results to another program (which can be written using MATLAB) which performs the optimisation process and return the results to ABAQUS in a loop until the optimum results are obtained.
9- FEA of the DSC joint can be subjected to cyclic loading and parametric study to study its behaviour precisely and identify the controlling parameters of its response under such loading.

References

Abbas, A.A., Mohsin, S.M.S. and Cotsovos, D.M. 2014. Seismic response of steel fibre reinforced concrete beam–column joints. *Engineering Structures.* **59**, pp.261-283.

ACI-ASCE. Joint Committee 352-2002. *Recommendations for Design of Beam-Column Connections in Monolithic Reinforced Concrete Structures (ACI 352R-02).* American Concrete Institute Farmington Hills, Michigan.

ACI. Committee , American Concrete Institute, International Organization for Standardization 2008. 0870312642. *Building code requirements for structural concrete (ACI 318-08) and commentary.* American Concrete Institute.

Aïtcin, P.C. 2011. *High performance concrete.* CRC Press.

AWS. 2006. *D1.1/D1.1M-Structural Welding Code-Steel.* American Welding Society.

Barros, J.A. and Figueiras, J.A. 1999. Flexural behavior of SFRC: testing and modeling. *Journal of Materials in Civil Engineering.* **11**(4), pp.331-339.

Barth, K.E. and Wu, H. 2006. Efficient nonlinear finite element modeling of slab on steel stringer bridges. *Finite Elements in Analysis and Design.* **42**(14), pp.1304-1313.

Bentur, A. and Mindess, S. 2006. *Fibre reinforced cementitious composites.* CRC Press.

Bischoff, P.H. 2003. Tension stiffening and cracking of steel fiber-reinforced concrete. *Journal of materials in civil engineering.* **15**(2), pp.174-182.

Bousselham, A. 2009. State of research on seismic retrofit of RC beam-column joints with externally bonded FRP. *Journal of Composites for Construction.* **14**(1), pp.49-61.

Bowerman, H., Coyle, N. and Chapman, J. 2002. An innovative steel/concrete construction system. *Structural Engineer.* **80**(20), pp.33-38.

Bowerman, H. and Pryer, J. 1997. Bi-Steel: A new steel-concrete-steel composite construction system for cores and superframes. In: *Conquest of vertical space in the 21st century. International conference*, pp.169-177.

Campione, G. 2015. Analytical prediction of load deflection curves of external steel fibers R/C beam–column joints under monotonic loading. *Engineering Structures.* **83**, pp.86-98.

Carreira, D.J. and Chu, K.-H. 1985. Stress-strain relationship for plain concrete in compression. In: *ACI Journal proceedings*: ACI.

CEB. CEP-FIP Model Code 1993. *Comite Euro-International du Beton.*

Chen, G., Teng, J. and Chen, J. 2010. Finite-element modeling of intermediate crack debonding in FRP-plated RC beams. *Journal of Composites for Construction.* **15**(3), pp.339-353.

Clubley, S.K., Moy, S.S.J. and Xiao, R.Y. 2003. Shear strength of steel–concrete–steel composite panels. Part I—testing and numerical modelling. *Journal of Constructional Steel Research.* **59**(6), pp.781-794.

Coronado, C.A. and Lopez, M.M. 2006. Sensitivity analysis of reinforced concrete beams strengthened with FRP laminates. *Cement and Concrete Composites.* **28**(1), pp.102-114.

Dai, X. and Liew, J.R. 2010. Fatigue performance of lightweight steel–concrete–steel sandwich systems. *Journal of Constructional Steel Research.* **66**(2), pp.256-276.

Dogan, O. and Roberts, T. 2010. Comparing experimental deformations of steel-concrete-steel sandwich beams with full and partial interaction theories. *International Journal of the Physical Sciences.* **5**(10), pp.1544-1557.

Dogan, O. and Roberts, T. 2012. Fatigue performance and stiffness variation of stud connectors in steel–concrete–steel sandwich systems. *Journal of Constructional Steel Research.* **70**, pp.86-92.

EN. BS 196-2 2013. *Method of testing cement. Chemical analysis of cement.*

EN. BS 1008 2002. *Mixing Water for Concrete. Specification for Sampling, Testing and Assessing the Suitability of Water.*

EN. BS 12390-3 2011. *Testing hardened concrete. Part 3.*

EN. BS 12390-5 2009. *Testing Hardened Concrete: Flexural Strength of Test Specimens.* British Standards Institution.

Eom, T.-S., Park, H.-G., Lee, C.-H., Kim, J.-H. and Chang, I.-H. 2009. Behavior of double skin composite wall subjected to in-plane cyclic loading. *Journal of Structural Engineering.* **135**(10), pp.1239-1249.

Eurocode2. 2004. *Design of Concrete Structures: Part 1-1: General Rules and Rules for Buildings.* British Standards Institution.

Eurocode3. 1993. Design of steel structures, Part 1.1: General rules and rules for buildings. *DD ENV.*

Ezeldin, A.S. and Balaguru, P.N. 1992. Normal-and high-strength fiber-reinforced concrete under compression. *Journal of Materials in Civil Engineering.* **4**(4), pp.415-429.

Foundoukos, N. and Chapman, J.C. 2008. Finite element analysis of steel–concrete–steel sandwich beams. *Journal of Constructional Steel Research.* **64**(9), pp.947-961.

Foundoukos, N., Xie, M. and Chapman, J.C. 2007. Fatigue tests on steel–concrete–steel sandwich components and beams. *Journal of Constructional Steel Research.* **63**(7), pp.922-940.

Hamil, S.J. 2000. *Reinforced concrete beam-column connection behaviour*. thesis, University of Durham.

Hordijk, D.A. 1991. *Local approach to fatigue of concrete.* TU Delft, Delft University of Technology.

Ichinose, T. 1991. Interaction Between Bond at Beam Bars and Shear Reinforcement in R/C Interior Joints. *Special Publication.* **123**, pp.379-400.

ISO6892-1:2009. 2009. *Metallic materials – tensile testing – Part 1: Method of test at room temperature.*

.

Jo, B.-W., Shon, Y.-H. and Kim, Y.-J. 2001. The evalution of elastic modulus for steel fiber reinforced concrete. *Russian journal of nondestructive testing.* **37**(2), pp.152-161.

Johnson, R. 1981. Loss of interaction in short-span composite beams and plates. *Journal of Constructional Steel Research.* **1**(2), pp.11-16.

Johnson, R.P. 2008. *Composite structures of steel and concrete: beams, slabs, columns, and frames for buildings.* John Wiley & Sons.

Kadarningsih, R., Satyarno, I. and Triwiyono, A. 2014. Proposals of beam column joint reinforcement in reinforced concrete moment resisting frame: A literature review study. *Procedia Engineering.* **95**, pp.158-171.

Kim, J. and LaFave, J.M. 2007. Key influence parameters for the joint shear behaviour of reinforced concrete (RC) beam–column connections. *Engineering Structures.* **29**(10), pp.2523-2539.

Kumar, V. and Shamim, M. 1999. Influence of beam reinforcement on exterior beam–column joints. *Journal of Structural Engineering.* **26**(2), pp.123-127.

Lee, J. and Fenves, G.L. 1998. Plastic-damage model for cyclic loading of concrete structures. *Journal of Engineering Mechanics.* **124**(8), pp.892-900.

Leekitwattana, M., Boyd, S. and Shenoi, R. 2010. An alternative design of steel-concrete-steel sandwich beam.

Li, Q. and Ansari, F. 2000. High-strength concrete in uniaxial tension. *ACI Materials Journal.* **97**(1).

Li, W., Li, Q.-n. and Jiang, W.-s. 2012. Parameter study on composite frames consisting of steel beams and reinforced concrete columns. *Journal of Constructional Steel Research.* **77**, pp.145-162.

Liang, Q.Q., Uy, B., Wright, H.D. and Bradford, M.A. 2003. Local and post-local buckling of double skin composite panels. *Proceedings of the Institution of Civil Engineers-Structures and Buildings.* **156**(2), pp.111-119.

Liang, Q.Q., Uy, B., Wright, H.D. and Bradford, M.A. 2004. Local buckling of steel plates in double skin composite panels under biaxial compression and shear. *Journal of Structural Engineering.* **130**(3), pp.443-451.

Liang, X.-w., Wang, Y.-j., Tao, Y. and Deng, M.-k. 2016. Seismic performance of fiber-reinforced concrete interior beam-column joints. *Engineering Structures.* **126**, pp.432-445.

Liew, J. and Sohel, K. 2010. Structural Performance of Steel-Concrete-Steel Sandwich Composite Structures. *Advances in Structural Engineering.* **13**(3), pp.453-470.

Liew, J.Y.R. and Sohel, K.M.A. 2009. Lightweight steel–concrete–steel sandwich system with J-hook connectors. *Engineering Structures.* **31**(5), pp.1166-1178.

Liew, J.Y.R., Sohel, K.M.A. and Koh, C.G. 2009. Impact tests on steel–concrete–steel sandwich beams with lightweight concrete core. *Engineering Structures.* **31**(9), pp.2045-2059.

Lok, T.-S. and Pei, J.-S. 1998. Flexural behavior of steel fiber reinforced concrete. *Journal of Materials in Civil Engineering.* **10**(2), pp.86-97.

Lok, T. and Xiao, J. 1999. Flexural strength assessment of steel fiber reinforced concrete. *Journal of Materials in Civil Engineering.* **11**(3), pp.188-196.

Lubliner, J., Oliver, J., Oller, S. and Onate, E. 1989. A plastic-damage model for concrete. *International Journal of Solids and Structures.* **25**(3), pp.299-326.

Majdzadeh, F., Soleimani, S.M. and Banthia, N. 2006. Shear strength of reinforced concrete beams with a fiber concrete matrix. *Canadian Journal of Civil Engineering.* **33**(6), pp.726-734.

McKinley, B. 1999. *Large deformation structural performance of double skin composite construction using British Steel's' Bi-Steel'*. thesis, City University.

McKinley, B. and Boswell, L. 2002. Behaviour of double skin composite construction. *Journal of Constructional Steel Research.* **58**(10), pp.1347-1359.

Moy, S., Xiao, R. and Lillistone, D. 1998. Tests for British Steel on the shear strength of the studs used in the Bi-Steel system. *University of Southampton, Department of Civil and Environmental Engineering.*

Narayanan, R., Roberts, T.M. and Naji, F. 1994. *Design guide for steel-concrete-steel sandwich construction: volume 1; general principles and rules for basic elements.* Steel Construction Institute.

Narayanan, R., Wright, H., Francis, R. and Evans, H. 1987. Double-skin composite construction for submerged tube tunnels. *Steel Construction Today.* **1**(6), pp.185-189.

Nataraja, M., Dhang, N. and Gupta, A. 1999. Stress–strain curves for steel-fiber reinforced concrete under compression. *Cement and Concrete Composites.* **21**(5), pp.383-390.

Neville, A. 2011. *Properties of Concrete, Trans*. Atlantic Publications, Inc.

Nguyen, H.T. and Kim, S.E. 2009. Finite element modeling of push-out tests for large stud shear connectors. *Journal of Constructional Steel Research.* **65**(10), pp.1909-1920.

Oduyemi, T.O.S. and Wright, H.D. 1989. An experimental investigation into the behaviour of double-skin sandwich beams. *Journal of Constructional Steel Research.* **14**(3), pp.197-220.

Oehlers, D.J. and Bradford, M.A. 2013. *Composite Steel and Concrete Structures: Fundamental Behaviour: Fundamental Behaviour.* Elsevier.

Park, R. and Paulay, T. 1975. *Reinforced concrete structures.* John Wiley & Sons.

Pauletta, M., Di Luca, D. and Russo, G. 2015. Exterior beam column joints–shear strength model and design formula. *Engineering Structures.* **94**, pp.70-81.

Qian, K. and Li, B. 2011. Experimental and analytical assessment on RC interior beam-column subassemblages for progressive collapse. *Journal of Performance of Constructed Facilities.* **26**(5), pp.576-589.

Qureshi, J., Lam, D. and Ye, J. 2011. Effect of shear connector spacing and layout on the shear connector capacity in composite beams. *Journal of constructional steel research.* **67**(4), pp.706-719.

Rackham, J., Couchman, G.H. and Hicks, S. 2009. *Composite slabs and beams using steel decking: best practice for design and construction.* Metal Cladding & Roofing Manufacturers Association in partnership with the Steel Construction Institute.

Ricci, P., De Risi, M.T., Verderame, G.M. and Manfredi, G. 2016. Experimental tests of unreinforced exterior beam–column joints with plain bars. *Engineering Structures.* **118**, pp.178-194.

Roberts, T. 1985. Finite difference analysis of composite beams with partial interaction. *Computers & Structures.* **21**(3), pp.469-473.

Roberts, T. and Dogan, O. 1998. Fatigue of welded stud shear connectors in steel–concrete–steel sandwich beams. *Journal of Constructional Steel Research.* **45**(3), pp.301-320.

Roberts, T., Edwards, D. and Narayanan, R. 1996. Testing and analysis of steel-concrete-steel sandwich beams. *Journal of Constructional Steel Research.* **38**(3), pp.257-279.

Saenz, L.P. 1964. Discussion of equation for the stress-strain curve of concrete by Desayi and Krishnan. *ACI Journal.* **61**(9), pp.1229-1235.

Scott, R.H. 1996. Intrinsic mechanisms in reinforced concrete beam-column connection behavior. *ACI Structural Journal.* **93**(3), pp.336-346.

Shakya, K., Watanabe, K., Matsumoto, K. and Niwa, J. 2012. Application of steel fibers in beam–column joints of rigid-framed railway bridges to reduce longitudinal and shear rebars. *Construction and Building Materials.* **27**(1), pp.482-489.

Shanmugam, N., Kumar, G. and Thevendran, V. 2002. Finite element modelling of double skin composite slabs. *Finite Elements in Analysis and Design.* **38**(7), pp.579-599.

Sharma, A., Eligehausen, R. and Reddy, G. 2011. A new model to simulate joint shear behavior of poorly detailed beam–column connections in RC structures under seismic loads, Part I: Exterior joints. *Engineering Structures.* **33**(3), pp.1034-1051.

Simulia. 2010. ABAQUS 6.10-2, Users' manual. *Providence, RI, USA: HKS Inc.*

Sohel, K., Liew, J., Alwis, W. and Paramasivam, P. 2003. Experimental investigation of low-velocity impact characteristics of steel-concrete-steel sandwich beams. *Steel & Composite Structures.* **3**(4), pp.289-306.

Sohel, K.M.A. and Richard Liew, J.Y. 2011. Steel–Concrete–Steel sandwich slabs with lightweight core — Static performance. *Engineering Structures.* **33**(3), pp.981-992.

Solomon, S., Smith, D. and Cusens, A. 1976. Flexural tests of steel-concrete-steel sandwiches. *Magazine of Concrete Research.* **28**(94), pp.13-20.

Soroushian, P. and Lee, C. 1989. Constitutive modeling of steel fiber reinforced concrete under direct tension and compression. *Elsevier Applied Science.* pp.363-377.

Subedi, N. 2003. Double skin steel/concrete composite beam elements: experimental testing. *Structural Engineer.* **81**(21), pp.30-35.

Subedi, N. and Coyle, N. 2002a. Advances in steel-concrete-steel composite design. In: *Concrete floors and slabs. Proceedings of the international seminar held at the University of Dundee, Scotland, UK on 5-6 September 2002*.

Subedi, N. and Coyle, N. 2002b. Improving the strength of fully composite steel-concrete-steel beam elements by increased surface roughness—an experimental study. *Engineering Structures.* **24**(10), pp.1349-1355.

Tadepalli, P., Mo, Y., Hsu, T. and Vogel, J. 2009. Mechanical properties of steel fiber reinforced concrete beams. In: *Proceedings of the 2009 Structures Congress: Don't Mess with Structural Engineers, ASCE, Reston, VA, USA*, pp.1039-1048.

Thomas, M. 2013. *Supplementary cementing materials in concrete.* CRC Press.

Tomlinson, M. and Tomlinson, A. 1990. 17. Shell composite construction for shallow draft immersed tube tunnels. In: *Immersed Tunnel Techniques: Proceedings of the Conference*: Thomas Telford, p.209.

Vollum, R. and Parker, D. 2008. External beam–column joints: design to Eurocode 2. *Magazine of Concrete Research.* **60**(7), pp.511-521.

Wee, T., Chin, M. and Mansur, M. 1996. Stress-strain relationship of high-strength concrete in compression. *Journal of Materials in Civil Engineering.* **8**(2), pp.70-76.

Wright, H. and Oduyemi, T. 1991. Partial interaction analysis of double skin composite beams. *Journal of Constructional Steel Research.* **19**(4), pp.253-283.

Wright, H., Oduyemi, T. and Evans, H. 1991a. The experimental behaviour of double skin composite elements. *Journal of Constructional Steel Research.* **19**(2), pp.97-110.

Wright, H.D., Oduyemi, T.O.S. and Evans, H.R. 1991b. The design of double skin composite elements. *Journal of Constructional Steel Research.* **19**(2), pp.111-132.

Xie, M. and Chapman, J.C. 2006. Developments in sandwich construction. *Journal of Constructional Steel Research.* **62**(11), pp.1123-1133.

Xie, M., Foundoukos, N. and Chapman, J. 2007. Static tests on steel–concrete–steel sandwich beams. *Journal of Constructional Steel Research.* **63**(6), pp.735-750.

Xie, M., Foundoukos, N. and Chapman, J.C. 2005. Experimental and numerical investigation on the shear behaviour of friction-welded bar–plate connections embedded in concrete. *Journal of Constructional Steel Research.* **61**(5), pp.625-649.

Yan, J.-B. 2014. Finite element analysis on steel–concrete–steel sandwich beams. *Materials and Structures.* pp.1-23.

Yan, J.-B., Liew, J.R., Zhang, M.-H. and Sohel, K. 2014. Experimental and analytical study on ultimate strength behavior of steel–concrete–steel sandwich composite beam structures. *Materials and Structures.* pp.1-22.

Zhao, X.-L. and Han, L.-H. 2006. Double skin composite construction. *Progress in Structural Engineering and Materials.* **8**(3), pp.93-102.